arXiv:1006.3538v1 [astro-ph.CO] 17 Jun 2010

The Chemical Evolution of the Ursa Minor Dwarf Spheroidal Galaxy[1]

Judith G. Cohen[2] and Wenjin Huang[3]

ABSTRACT

We present an abundance analysis based on high resolution spectra of 10 stars selected to span the full range in metallicity in the Ursa Minor dwarf spheroidal galaxy. We find [Fe/H] for the sample stars ranges from -1.35 to -3.10 dex. Combining our sample with previously published work for a total of 16 luminous UMi giants, we establish the trends of abundance ratios [X/Fe] as functions of [Fe/H] for 15 elements. In key cases, particularly for the α-elements, these trends resemble those for stars in the outer part of the Galactic halo, especially at the lowest metallicities probed. The neutron capture elements show a r-process distribution over the full range of Fe-metallicity reached in this dSph galaxy. This suggests that the duration of star formation in the UMi dSph was shorter than in other dSph galaxies. The derived ages for a larger sample of UMi stars with more uncertain metallicities also suggest a population dominated by uniformly old ($\sim$13 Gyr) stars, with a hint of an age-metallicity relationship.

In comparing our results for UMi, our earlier work in Draco, and published studies of more metal-rich dSph Galactic satellites, there appears to be a pattern of moving from a chemical inventory for dSph giants with [Fe/H] $\lesssim -2$ dex which is very similar to that of stars in the outer part of the Galactic halo (enhanced α/Fe relative to the Sun, coupled with subsolar [X/Fe] for the heavy neutron capture elements and r-process domination), switching to subsolar α-elements and super-solar s-process dominated neutron capture elements for the highest [Fe/H] dSph stars. The combination of low star formation rates over a varying and sometimes extended duration that produced the stellar populations in the local dSph galaxies with [Fe/H] > -1.5 dex leads to a chemical inventory wildly discrepant from that of any component of the Milky Way.

We note the presence of two UMi giants with [Fe/H] < -3.0 dex in our sample, and reaffirm that the inner Galactic halo could have been formed by early accretion of Galactic satellite galaxies and dissolution of young globular clusters, while the outer halo could have formed from those satellite galaxies accreted somewhat later.

Subject headings: galaxies: individual (UMi), galaxies: abundances, galaxies: dwarf

---

[1] Based on observations obtained at the W.M. Keck Observatory, which is operated jointly by the California Institute of Technology, the University of California and the National Aeronautics and Space Administration

[2] Palomar Observatory, Mail Stop 105-24, California Institute of Technology, Pasadena, California 91125 (jlc@astro.caltech.edu)

[2] Palomar Observatory, current address: University of Washington, Astronomy, Box 351580, Seattle, Washington, 98195 (hwenjin@astro.washington.edu)

1. Introduction

The Ursa Minor (UMi) dwarf spheroidal (dSph) galaxy is a satellite of the Milky Way at a distance of about 70 kpc (Mighell & Burke 1999). It is the least luminous of the 8 classical dSph satellites, with $L_V = 3{\times}10^5\ L_\odot$ (Grebel, Gallagher & Harbeck 2003). Cudworth, Olszewski, & Schommer (1986) provide a proper motion survey and photometry for this galaxy down to the level of the horizontal branch. With $\sim$450 members, they found that the stellar population of the UMi dSph resembles that of an old metal-poor Galactic globular cluster with a steep red giant branch (RGB) and a blue horizontal branch. The HST imaging study of Mighell & Burke (1999) confirms this simple star formation history for UMi, suggesting a single major burst of star formation about 14 Gyr ago that lasted less than 2 Gyr. The photometric survey by Bellazzini et al (2002) established a mean abundance [Fe/H] -1.8 dex with a spread of $\sim$0.5 dex within UMi, assuming all stars are of a similar age. There is no evidence for multiple main sequences nor any sign of ongoing star formation. Very low upper limits were established in UMi for neutral hydrogen gas by Young (2000) and for ionized H by Gallagher et al (2003).

Many radial velocity surveys (see, e.g. Cudworth, Olszewski, & Schommer 1986; Palma et al. 2003) of large samples of stars have been carried out to determine membership and measure the stellar velocity dispersion as a function of radius in UMi, while Walker et al (2008) highlights the very large v_r datasets that can be assembled today for such galaxies. The observed σ_v in UMi, as is also true for Draco, is unexpectedly high, given the low luminosity of the system, and remains flat to large radii, which according to Peñarrubia, McConnachie & Navarro (2008) (see also the references therein) requires the presence of large amounts of dark matter. These studies generally ignore the issue of potential ongoing tidal disruption affecting the internal kinematics of the Milky Way satellite. Piatek *et al.* (2001) (see also Bellazzini et al 2002; Palma et al. 2003) review the evidence for substructure in UMi, which might be an argument for tidal effects..

There is great current interest in the detailed properties of satellites of the Galaxy in light of our greatly improved hierarchical cold dark matter cosmological models, which gave rise to the the missing satellite problem (Klypin et al 1999). This is only enhanced by the discovery that the dSph galaxies appear to be dark matter dominated systems, unlike globular clusters of similar total stellar mass. With the advent of efficient high dispersion spectrographs, large area CCD detectors, and 10-m class telescopes, studying stars in at least the nearer Galactic satellites at high spectral dispersion has become feasible.

High resolution spectroscopy was obtained for 6 UMi giants by Shetrone, Côté & Sargent (2001), and for three (including two duplicates from the earlier work) by Sadakane et al. (2004), one of which was reexamined in an attempt to detect the radioactive actinide thorium by Aoki *et al.* (2008). In this paper we present detailed abundance analyses of a sample of 10 luminous UMi stars near the RGB tip, which more than doubles the sample of UMi stars from the earlier works. Our goal is understanding the chemical evolution of UMi, and how this and other dSph galaxies may be related to the population of Galactic halo field stars and to Galactic globular clusters. The sample is presented in §2 where the procedure for determining their stellar parameters is described. The next section describes the observations, while §4 gives some details of the abundance analysis. We compare our results to those for Galactic halo field stars in §5, apply our toy model for abundance ratios in §5.1, and discuss the age-metallicity relation in UMi in §5.3. A discussion of the predictions of nucleosynthesis and chemical evolution models as applied to UMi and to Draco is given in §6. We speculate on the role the dSph satellite galaxies might have played the formation of the Galactic halo in §6.1. A brief summary concludes the paper.

This paper is a sequel to our earlier study of the chemical evolution of the Draco dSph (Cohen & Huang 2009) (henceforth C09). The techniques used are similar and the reader is urged to consult our earlier work for additional details as necessary.

2. Stellar Sample and Stellar Parameters

Our sample in the UMi dSph galaxy contains 10 stars; details are given in Table 1. It was selected from Table 3.6 of Winnick (2003) to include stars which are known radial velocity members of this satellite to the Galaxy at or near the RGB tip spanning the full range in color and in metallicity, and not previously observed at high spectral resolution. Winnick measured the infrared Ca triplet in moderate resolution spectra of a sample of UMi stars chosen from earlier radial velocity surveys, excluding known carbon stars (see, e.g. Shetrone, Bolte & Stetson 1998). Details of her calibration with metallicity and related issues were discussed in the appendix to C09.

We adopt the procedures described in Cohen *et al.* (2002) and used in all subsequent work by the first author published to date to determine the stellar parameters for our sample of luminous UMi giants. Our T_{eff} determinations are based on the broad band colors $V-I$, $V-J$ and $V-K$ and the predicted colors from the model grid of Houdashelt, Bell & Sweigart (2000). The optical photometry is from the SDSS (York *et al.* 2000) using the transformation equations of Smith et al. (2002). The IR photometry is taken from 2MASS (Skrutskie *et al.* 1997; Cutri *et al.* 2003), and is transformed from the 2MASS system to the Johnson-Bessell system using the results of Carpenter (2001). The galactic extinction is from the map of Schlegel, Finkbeiner & Davis (1998); E$(B-V)$ does not exceed 0.03 mag for any star in the UMi sample.

We derive surface gravities by combining these T_{eff} with bolometric corrections from the model grid, the observed V corrected for reddening, an assumed stellar mass of 0.8 $M_{\odot}$, and the distance to the UMi dSph galaxy. We use the [Fe/H] values of Winnick (2003) from the infrared Ca triplet as an initial guess. We iterate as necessary given the metallicity we derive here through analysis of our high resolution spectra[1].

The resulting stellar parameters, which have been derived with no reference to the spectra themselves, are given in the second and third columns of Table 2, as are the heliocentric radial velocities. The random uncertainties in the adopted T_{eff} from photometric errors are 100 K. This ignores systematic errors which may be present. The adopted uncertainties in $\log(g)$ based on the uncertainties in T_{eff}, the stellar mass, and the distance to UMi are 0.2 dex.

---

[1] This was also the procedure used for the Draco HIRES sample; the description of the procedure for determinations of $\log(g)$ given in C09 is not correct.

Fig. 1 shows our sample of 10 luminous giants in UMi in a plot of $g' - i'$ versus g' corrected for interstellar reddening; the previously studied sample of 6 giants from Shetrone, Côté & Sargent (2001) and by Sadakane et al. (2004) is shown as well. Members of UMi from the list of Winnick (2003) were cross indexed with the SDSS photometry (York *et al.* 2000) from DR7 (Abazajian *et al.* 2009) and are also displayed. Superposed in this figure are isochrones from the Dartmouth Stellar Evolution Database (Dotter *et al.* 2008) for [Fe/H] -2.5 dex with $[\alpha/\mathrm{Fe}] = +0.2$ dex (solid lines) and for [Fe/H] -1.5 dex with $[\alpha/\mathrm{Fe}]$ Solar (dashed lines) for ages 9 and 12.5 Gyr.

Our HIRES sample of luminous UMi giants was selected to span the full range in metallicity as inferred from the Ca triplet indices by Winnick (2003). Fig. 1 shows it does cover the full range in $g' - i'$ color of the upper RGB of UMi members. The luminosity of the brightest UMi giants is in good agreement with that predicted from the isochrones for the RGB tip as a function of metallicity in the g', i' colors. The deduced ages will be described later in §5.3.

3. Observations

The UMi stars in our sample were observed with HIRES-R (Vogt *et al.* 1994) at the Keck I telescope during three runs, in June 2008, Aug. 2009, and Feb. 2010. Sky conditions were good during all of these runs. An earlier run in 2005 was assigned for this purpose, but no usable spectra could be obtained at that time. The instrument configuration yielded complete spectral coverage in a single exposure from 3810 to 6700 Å, and extends to 8350 Å with small gaps between orders. The slit width was 1.1 arcsec ($\lambda/\Delta\lambda = 35,000$) for all exposures. The total exposure times for each star are given in Table 1; the exposures were broken up into 1800 or 2400 sec segments to expedite removal of cosmic rays. The signal-to-noise ratios (S/N) per spectral resolution element at 5800 Å in the continuum near the center of the echelle order are given in the last column of this table; they range from 80 to 100, but the S/N drops towards the bluer part of the spectra, becoming poor (less than 40) at the bluest end of these spectra. This S/N calculation utilizes only Poisson statistics, ignoring issues of cosmic ray removal, night sky subtraction, flattening, etc.

The processing of the spectra was done with MAKEE[2] and Figaro (Shortridge 1993) scripts, and follows closely that described by Cohen *et al.* (2006). The equivalent widths were measured as described in Cohen *et al.* (2004). Due to the lower S/N in the blue, lines bluer than 4400 Å were ignored if the species had sufficient other detected lines. Lines with $W_\lambda > 175$ mÅ were discarded except for two lines from the Mg triplet, the Na D lines and Ba II lines in some of the stars; for these key elements no or only a few weaker features could be detected in most of the stars. Table 3 lists the atomic parameters adopted for each line and their equivalent widths measured in the spectra of each of the UMi dSph stars.

---

[2] MAKEE was developed by T.A. Barlow specifically for reduction of Keck HIRES data. It is freely available on the world wide web at the Keck Observatory home page, http:
www2.keck.hawaii.edu/inst/hires/data_reduction.html.

UMi N37, 33533, and 41065 show strong emission in the blue wing of Hα in their spectrum; the first two also show weaker emission in the red wing of this line. UMi COS233 (COS ID numbers are from Cudworth, Olszewski, & Schommer 1986) and JI2 show weak emission in the blue wing of Hα, with no emission detected in the red wing. No other anomalies were noted from visual inspection of the spectra.

4. Analysis

The analysis is identical to that of Cohen *et al.* (2008) and earlier references therein. In particular we use the model stellar atmosphere grid of Kurucz (1993) and a current version of the LTE spectral synthesis program MOOG (Sneden 1973), which treats scattering as LTE absorption.

Our analysis assumes classical plane parallel stellar atmospheres and LTE, both for atomic and for molecular features. We adopt a Solar Fe abundance of $\log[\epsilon(\mathrm{Fe})] = 7.45$ dex based on our solar spectrum analysis, see also Asplund, Grevesse & Sauval (2005). This value is somewhat lower (by up to 0.10 dex) than that used by many groups, which leads directly to our [Fe/H] values for a given star being somewhat higher and to our abundance ratios [X/Fe] being somewhat lower than those which would be inferred by most other teams. Our gf values are generally taken from Version 3.1.0 of the NIST Atomic Spectra Database (phsics.nist.gov/PhysRefData/ASD/index.html, NIST Standard Reference Database 78). A comparison of $\log gf$ values for Fe we adopt with those of the First Stars Project at the VLT (Cayrel et al 2004) was given in Cohen *et al.* (2008), and shows excellent agreement for both Fe I and Fe II. Corrections for hyperfine structure for Sc II, V I, Mn I, Co I, Cu I, Ba II, and Eu II were used when necessary: the majority of the HFS patterns were adopted from Prochaska et al (2000).

Our abundances for C are from the 4320 Å region of the G band of CH, where the absorption is less than in the main part of the G band at 4300 Å. O abundances are primarily from the forbidden line at 6363 Å; the radial velocity of UMi often shifts the 6300 Å [O I] line to overlap the strong terrestrial atmospheric line at 6295.2 Å, making it not usable. Our nominal Solar C and O abundances are 8.59 and 8.83 dex respectively. See C09 for further comments on the molecular abundances.

Since the UMi stars are rather faint for 2MASS, the uncertainties in the K_s magnitudes are fairly large, ranging up to 0.09 mag. We therefore feel free to slightly adjust T_{eff} and $\log(g)$ after the first pass through the analysis to improve the ionization equilibrium and slope of the abundances determined from the set of Fe I lines as a function of χ (the excitation potential of the lower level).

These spectroscopic stellar parameters are given in the fourth and fifth column of Table 2 and are the ones used subsequently. With these values we were able to achieve good ionization equilibrium for Ti and Fe as well reasonable excitation equilibrium of Fe I. Table 4 gives the slope of a linear fit to the abundances determined from the set of Fe I lines as a function of χ, W_λ, and λ, which are most sensitive to T_{eff}, v_t, and the wavelength dependence of any problems in establishing the correct location of the continuum (perhaps arising from the more severe crowding towards bluer wavelengths) or of a missing major source of continuous opacity, respectively. There are $\sim$ 75 to 190 Fe I lines detected in each star, with χ ranging from 0 to $\sim$4.5 eV. The only slope which is large enough to be of concern and which tends to have the most significant correlation coefficient is that with χ ($\mid cc(\chi) \mid \; > \; 0.4$ for some of the sample giants), which depends largely on T_{eff}. In our final adopted solutions, the Fe I slope as a function of χ tends to be slightly negative, with values ranging from -0.02 to -0.11 dex/eV, with small $\mid cc(\chi) \mid$ for the most negative values. This slope decreases by $\sim$0.1 dex/eV/(ΔT_{eff}= +250 K). A decrease in T_{eff} of a maximum of 125 K, consistent with our adopted T_{eff} uncertainty, would make all these slopes consistent with zero, and would decrease the [Fe/H] derived from Fe I lines by $\sim$0.2 dex, but would ruin the ionization equilibrium of Ti.

One potential concern is the possibility of non-LTE in Fe affecting the ionization equilibrium. This is discussed in detail in C09. The slightly negative Fe I slope with excitation potential mentioned above may be a sign that overionization of Fe is occurring. If this were the case, we would have been driven to adopt a higher T_{eff} than the actual value; our derived [Fe/H] values would be too high as indicated above, but the deduced abundance ratios would not be significantly affected by such a decrease in T_{eff}. With this in mind, we adopt asymmetrical uncertainties for T_{eff} of +100 K, -150 K. Since we have been able to achieve satisfactory ionization equilibrium for Fe and for Ti and at the same time reasonably good excitation equilibrium for Fe with a single value of T_{eff} which differs from that set solely from broad band photometry by 50 K or less for more than half of the UMi giants, we regard our choices for stellar parameters as satisfactory. Ideally, of course, one would like to have a full non-LTE 3D analysis including both convection and spherical (as distinct from plane parallel) layers for all species, but at the present time this is not practical.

Our derived abundances for the 10 UMi luminous giants are given in Tables 5a and 5b. The sensitivity of the absolute and relative abundances for each species detected to small changes in T_{eff}, log(g), microturbulent velocity, and assumed [Fe/H] for the stellar atmosphere model are similar to those we calculated for Draco; see Tables 5 and 6 of C09. The only non-LTE correction we have made is to the Al abundance when the 3961 Å resonance line of Al I was used; in many cases this was the only feature of Al that could be detected. We adopt a correction of +0.60 dex based on the calculations of Baumüller & Gehren (1996, 1997).

We compare the [Ca/H] derived by Winnick (2003) based on her infrared Ca triplet indices with our values from HIRES spectra. The result for UMi and for Draco from C09 is shown in Fig. 2. We find (for UMi only) that [Ca/H](HIRES) $= -0.21 + 0.98 \times$ [Ca/H](Winnick/CaT] with σ around the linear fit of only 0.13 dex.

5. Comparison with Galactic Halo Field Stars

We compare the behavior of abundance ratios within UMi to those of Galactic halo field stars in detail. The sample of UMi stars with detailed abundance analyses based on high dispersion spectra is now 16, including the 10 we present here. Shetrone, Côté & Sargent (2001) presented an analysis for 6 UMi members; there is no overlap with our sample. We ignore their star K, which they state is a carbon star. Better spectra taken with HDS at the Subaru telescope were analyzed by Sadakane et al. (2004) for three stars, two of which were included in Shetrone, Côté & Sargent (2001). In view of the much higher S/N of the Sadakane et al. (2004) spectra, we adopt their abundances for these two stars[3].

We proceed by examining a series of plots (Figs. 3 to 17) in which we show the UMi sample, both our 10 stars (indicated by large filled circles) and the 6 observed previously from Shetrone, Côté & Sargent (2001) (denoted by small open circles, and less accurate than subsequent UMi studies), with the more accurate Sadakane et al. (2004) abundances indicated by large open circles. These figures also display current results for Galactic halo stars, but see also the seminal early review of McWilliam (1997). The main halo survey included is the 0Z project led by J. Cohen to datamine the Hamburg/ESO Survey for extremely metal-poor stars in the Galactic halo. Many of the most metal-poor candidates from this work have been observed with HIRES at the Keck Observatory and analyzed in a manner very similar to the present study as described in Cohen *et al.* (2004) and Cohen *et al.* (2008), with the difference that most of the spectra for the 0Z project were taken further towards the blue than those of the dSph stars, a move necessary because of the low density of lines in the red in spectra of such low metallicity stars. Only the giants in the metal-rich end of the 0Z project database, much of which is not yet published (J. Cohen, N. Christlieb et al, in preparation), is shown in these figures. A number of other halo field star surveys, the most important of which at the lower metallicities probed here is the First Stars Project (Cayrel et al 2004), are shown, including those stars from McWilliam *et al.* (1995) not re-observed by Cayrel et al (2004).

It should be noted that these Galactic halo field star surveys are dominated by inner halo stars with $R_{GC} < 20$ kpc adopting the inner/outer halo boundary set by Carollo et al (2007). If one redefines this boundary to lie at a somewhat smaller R_{GC}, then many of the 0Z giants are in the outer halo. Much smaller samples of probable outer halo dwarfs in the local neighborhood have been isolated from their kinematics, and their chemical inventory analyzed in detail in several previous studies, in particular by Nissen & Schuster (1997, 2010) and by Stephens (1999). Roederer (2008) has compiled a sample of halo stars with parallaxes to isolate outer halo stars. These studies collectively find a small deficit in [Mg/Fe] in outer halo stars as compared to inner halo ones shown by the dotted and dashed lines in Fig. 6, accompanied by slightly subsolar [Na/Fe] and [Ni/Fe].

We will see that the differences in the chemical inventory between Galactic halo field stars and the UMi sample, which may be a function of Fe-metallicity, are small, not larger than ∼0.3 dex in most cases. This means that some care is required to ensure that all the abundances from the various sources are homogeneous. While we have not done a full check of this, we have taken a few steps the first of which is to adjust each survey to our set of Solar abundances, particularly to our adopted value of [Fe/H], whenever possible. Specific cases where there are clear problems related to issues of homogeneity between the various analyses are noted individually below.

---

[3] Our spectra have S/N considerably higher than those of Shetrone, Côté & Sargent (2001), and perhaps slightly lower than those of Sadakane et al. (2004).

Overall the abundance relations we find here for the UMi augmented sample are more clearly defined with less scatter than we found earlier for Draco. In part this is a consequence of the (small) difference in distance, with UMi being somewhat closer, hence having somewhat brighter stars near the RGB tip, resulting in better spectra. But we wonder if part of this is also a result of the more extended epoch of star formation in Draco than in UMi, resulting in a more complex chemical evolution with stronger spatial variations within the Draco dSph.

The trend of [C/Fe] versus [Fe/H] is shown in Fig. 3, based for the majority of these stars on the strength of the G band of CH. The solid lines represent the mean behavior of thick disk dwarfs from the survey by Reddy, Lambert & Allende Prieto (2006). The C abundance in luminous giants is lowered substantially from an initial [C/Fe] $\approx$ 0.0 dex due to intrinsic nucleosynthesis (the CN cycle of H burning) followed by dredge-up to the stellar surface of processed material within which C has burned to N (see e.g. Cohen, Briley & Stetson 2005). The C abundances in most of the luminous UMi giants studied here are abnormally low, presumably due to mixing; their initial C abundances cannot be determined. Note that in Fig. 3 and those that follow the asymmetric uncertainties we adopted in §2 are shown for [Fe/H], but not for abundance ratios [X/Fe]; for the latter the larger uncertainty is plotted.

It is quite difficult to measure O abundances in metal-poor giants. The set of features that can be used is very limited and each has problems. This has resulted in considerable controversy about O abundances in metal-poor stars in recent years, see e.g. the discussion in Melendez et al (2004). The forbidden OI lines at 6300 and 6363 Å line are very weak, and the 7770 Å triplet, which has substantial non-LTE effects, is not detectable. [O/Fe] ratios for the UMi giants and for a compilation of surveys in the literature are shown in Fig. 4.

The arrow in Fig. 4 indicates the probable correction for 1D to 3D effects required for luminous giants given by Cayrel et al (2004), which has not been implemented, but which would bring the plateau in [O/Fe] down to a mean level of ∼+0.5 dex. The lines are linear fits from Ramirez, Allende Prieto & Lambert (2007) to their samples of thick disk and halo dwarfs (solid line) and to thin disk dwarfs (dashed line). They use only the 7770 Å triplet, with appropriate non-LTE corrections; these lines become detectable in dwarf stars but are considerably weaker in giants. The net result is that the UMi giants appear low in [O/Fe] when compared to samples of field halo giants which rely on the same 6363 Å forbidden line.

Fig. 5 shows that the UMi giants clearly have [Na/Fe] somewhat lower than the Galactic halo field stars over the entire metallicity range spanned within UMi, a trend seen at intermediate metallicities for outer halo local dwarfs by Nissen & Schuster (2010). There is a very large range in [Na/Fe] among the highest Fe-metallicity stars in UMi. Spite et al (2005) found that Na/Fe ratios vary by a factor of $\sim$5 from star to star among very metal-poor luminous RGB stars, which they interpret as as a result of deep mixing. The figure suggests that there is a separation of $\sim$0.2 dex for [Na/Fe] at a fixed [Fe/H] between the two large surveys of very metal-poor halo field stars, i.e. the First Stars Survey led by R. Cayrel and the 0Z Survey led by J. Cohen. Andrievsky *et al.* (2007) have demonstrated that non-LTE effects in [Na/Fe] based solely on the NaD lines are substantial and depend on the luminosity and T_{eff} of the star. Hence part of the origin of this difference for [Na/Fe] may arise from a difference in mean sample luminosity between these two surveys of halo field stars; see C09 for additional discussion.

Fig. 6 shows the important hydrostatic α-element Mg, another element with only a few accessible features in our UMi spectra. The published values from Cayrel et al (2004) for the First Stars project have been increased by 0.15 dex following Bonifacio *et al.* (2009). We find that [Mg/Fe] is constant to within the uncertainties at the super-solar value of $\sim$0.35 dex, consistent with that typical of outer halo Galactic giants found by Roederer (2008), at all Fe-metallicities among the UMi giants. The highest [Fe/H] UMi giant, COS171, has [Mg/Fe] 0.5 dex lower than the three other stars of similar [Fe/H]. It is a low outlier for this and for many other species and is discussed in §5.4.

The behavior of the explosive α-element Si is shown in Fig. 7 with the mean relation for thick disk stars from Reddy, Lambert & Allende Prieto (2006) indicated. The figure shows good agreement between the 0Z and First Stars Project abundance ratios for this element. The lowest Fe-metallicity UMi giants show [Si/Fe] consistent with that of Galactic halo stars, but this ratio falls steadily with increasing [Fe/H] in UMi, while it remains constant among the halo stars. The Solar ratio of [Si/Fe] is reached at [Fe/H] ~ -1.6 dex, far more metal-poor than is typical of Galactic populations.

The explosive α-element Ca also has problems with inconsistencies between the two large surveys of very metal-poor halo stars, the First Stars Project and the 0Z Project; this issue is discussed in C09. No detectable difference between the inner and outer halo was found by Roederer (2008) or Ishigaki, Chiba & Aoki (2010), so the mean distance of the halo sample is not relevant. Ignoring the low outlier COS171, [Ca/Fe] is $+0.1\pm0.1$ dex for all the UMi giants. If the 0Z measurements of [Ca/Fe] are adopted, then the luminous UMi giants have [Ca/Fe] comparable to, or only slightly lower than, those of Galactic halo stars over the full range of [Fe/H] found in UMi.

Figs. 9 and 10 show the behavior for Sc and the explosive α-element Ti respectively. The mean relation for thick disk stars from Reddy, Lambert & Allende Prieto (2006) is shown for the latter. In both cases there is good agreement between the abundance ratios deduced by the 0Z Project and the First Stars Project. [Sc/Fe] is slightly sub-solar and below the Galactic halo field giants over the full range of [Fe/H]. For the explosive α-element Ti the metal-rich UMi stars are slightly above the solar value, but fall below the halo field. [Ti/Fe] at the extremely metal-poor end of the

UMi sample may be closer to the halo field, but the value is uncertain there.

In UMi it is the explosive α-element Si which shows the strongest divergence from the Galactic halo field as a function of increasing [Fe/H]. The hydrostatic element [Mg/Fe] behaves fairly close to the outer halo trends of Roederer (2008). The small range in [Mg/Fe] seen among the UMi giants is in contrast to Draco (see C09), where there is a stronger decrease as [Fe/H] increases. The latter might be expected for a more extended epoch of star formation since Mg, unlike Ca or Si, is produced only in SNII, while Ca and Si are produced in both SNII and SNIa (Woosley & Weaver 1995). However, given the postulated very short duration of star formation within UMi, the SNIa never had time to contribute for any element in this dSph, while in Draco, star formation lasted long enough for some SNIa contribution.

There are several elements which probably have metallicity dependent yields, related to the value of the neutron excess, such that at low metallicity, the yield is reduced, as appears to be the case for the UMi stars. This includes Na, Sc, Mn (see e.g. Cescutti et al 2008), Ni, and Zn; their production is discussed in Arnett (1971) (see also Clayton 2003) for Na, Woosley & Weaver (1995) and Limongi & Chieffi (2003) for Sc, Woosley & Weaver (1995) and Ohkubo, Umeda, Nomoto & Yoshida (2006) for Ni, and Timmes, Woosley & Weaver (1995) for Zn. Stronger odd-even effects are found for lower metallicity and, in the case of Sc, for lower mass progenitors (Limongi & Chieffi 2003). Thus a relative absence of the higher mass SNII with $M > 35 M_{\odot}$ might give rise to the low [Sc/Fe] in the UMi and in the Draco sample.

[Cr/Fe] (Fig. 11) and [Mn/Fe] (Fig. 12) for the UMi giants overlaps the lower edge of the distribution for Galactic halo field stars. Both of these abundance ratios decline rapidly as [Fe/H] decreases in Galactic halo field stars. A known problem discussed in Cohen *et al.* (2004) requires that the Mn abundance derived from the 4030 resonance triplet lines be increased by 0.2 dex. These are the strongest Mn I lines in the optical and the only ones accessible for extremely metal-poor stars. The offset has been applied to the two most metal-poor UMi giants, where these were the only Mn features detected. Bergemann & Gehren (2008) suggest that the non-LTE corrections for Mn in very metal poor giants are large and positive, and will flatten the [Mn/Fe] ratio to a constant value of about -0.1 dex for [Fe/H] < -1.5 dex. Since all the stars used here are luminous giants, the non-LTE effects will presumably be of comparable size for every star of a fixed [Fe/H], and hence will not significantly affect statements regarding relative differences between the UMi giants and the Galactic halo giants.

Fig. 13 displays the [Co/Fe] ratios which for Galactic halo stars rise rapidly from near the Solar ratio as [Fe/H] decreases below -2 dex. Co was only detected in one of the two EMP stars in our UMi sample, but at higher [Fe/H], it is slightly subsolar, perhaps somewhat lower than the halo stars. However, there is only one Co I line with equivalent width exceeding 20 mÅ in most of these stars, which is at 4121 Å, uncomfortably far in the blue. Given the paucity of suitable lines, any conclusion regarding the behavior of [Co/Fe] in UMi is still uncertain. The large positive non-LTE corrections suggested by Bergemann, Pickering & Gehren (2010) further complicate the situation.

The nickel abundance relative to Fe (Fig. 14) appears to fall below that of the halo field (which has [Ni/Fe] at the Solar ratio over the entire range of Fe-metallicity) among the higher metallicity UMi stars. Nissen & Schuster (2010) suggest that in the outer halo [Ni/Fe] is slightly subsolar. The [Ni/Fe] ratios for the lowest metallicity UMi stars overlap in Fig. 14 those of Galactic field halo stars.

The Galactic halo field samples from the 0Z Project and the First Stars Project overlap well for the abundance ratio [Zn/Fe]. Among field halo stars, [Zn/Fe] is close to the Solar ratio but rises rapidly below [Fe/H] ~ -2 dex, as shown most recently for halo dwarfs by Nissen et al (2008). In the UMi giants, [Zn/Fe] behaves similarly to the Ni abundance ratio for intermediate metallicities; the UMi stars fall below those in the Galactic halo and below the Solar ratio in this regime of [Fe/H]. At the lowest metallicities, [Zn/Fe] for the UMi giants appears to rise above the Solar value.

The Galactic halo field samples from the 0Z Project and the First Stars Project (data for Sr and Ba is from Francois et al 2007) overlap well for the abundance ratio [Sr/Fe] versus Fe-metallicity shown in Fig. 16. The Sr II lines used are the resonance lines at 4077 and 4215 Å; they are uncomfortably far in the blue for the UMi spectra, where the S/N is rather low. The limited detections of these lines for the UMi giants, including those with [Fe/H] < -3 dex, suggests that [Sr/Fe] is approximately constant at -0.1 dex. This is in good agreement with the behavior of the bulk of the halo field star samples. Fig. 17 shows the abundance ratios [Ba/Fe], with the mean for the Galactic thick disk from Reddy, Lambert & Allende Prieto (2006) indicated as a solid line. The UMi giants follow the lower envelope of the halo field stars. The data for Eu and other heavy neutron capture elements is discussed in §5.2.

5.1. The Toy Model Fits of C09 Applied To the UMi Abundances

The 10 UMi giants in our sample have [Fe/H] between -1.35 and -3.10 dex. To provide a context for the understanding of our results we apply to the UMi sample the toy model fits for the behavior of abundance ratios [X/Fe] vs [Fe/H] developed for our sample in the Draco dSph described in detail in C09. This toy model was guided by the behavior of abundance ratios in Galactic populations, the thin disk, thick disk, and Galactic halo field stars since the same nucleosynthetic processes are involved, although they may contribute different relative fractions to the chemical inventory in different environments.

Our toy model fits offer important clues for the importance of various nucleosynthesis processes in the UMi and the Draco dSph galaxies as compared to in the Galactic thick disk and halo stellar populations. The parameters of the toy model depend on the nucleosynthetic yields for the production channels for each of the elements X and Fe, the IMF, the rate of star formation, accretion, loss of gas via galactic winds, interaction between the dSph and the Milky Way via tides, ram pressure stripping, etc. as will be discussed in §6.

The toy model sets [Fe/H](A) as the mean for the lowest metallicity stars in the UMi sample, and A(X) is the mean of [X/Fe] for the same stars. [Fe/H](B) is the mean [Fe/H] for the highest metallicity stars, and B(X), a value of [X/Fe], is defined similarly. The toy model represents such relationships as a plateau in [X/Fe] at the value [X/Fe](low) over the range [Fe/H](A) to [Fe/H](low,X) and another plateau at a value of [X/Fe](high), from [Fe/H](high,X) to [Fe/H](B). A straight line connects the two plateaus. Thus our model has four variables whose values are determined directly from the dataset of [X/Fe] as a function of [Fe/H], with two additional fit parameters. We solve for the two free parameters in this toy model [Fe/H](low,X) and [Fe/H](high,X) by minimizing the variance around the fit. The resulting parameters are given in Table 6.

We apply this toy model to to 11 elements for which sufficient accurate data is available for UMi members. We use the augmented sample of UMi giants, ignoring the outlier COS171 which is discussed in detail in §5.4, leaving a sample of 15 UMi stars. We use the two lowest metallicity stars in the UMi sample to determine the plateau values A(X) and [Fe/H](A). At the high metallicity end, we use three highest metallicity UMi stars, each of which has [Fe/H] $-1.6{\pm}0.1$ dex obtained from a high quality spectrum, to determine the plateau values B(X) and [Fe/H](B). In solving for the two fit parameters, weights are halved for the 3 stars with lower accuracy spectra, which are those from Shetrone, Côté & Sargent (2001) not reobserved with the Subaru/HDS by Sadakane et al. (2004). The resulting parameters for each element are listed in Table 6 and the fits are shown when available in Figs. 5 to 17.

The uncertainties in A(X) and in B(X) are approximately those of σ[X/Fe] for a single UMi star from our sample. These values are given in Tables 5 and 6 of C09. Thus, for example, for [Mg/Fe] they are ±0.14 dex. A(Mg) is only 0.13 dex larger than B(Mg), so the decline in [Mg/Fe] as [Fe/H] increases in the UMi sample is not statistically significant. The decrease in [Na/Fe], [Si/Fe], and [Zn/Fe], and the increase in [Cr/Fe], [Mn/Fe] and [Ba/Fe] as [Fe/H] increases are statistically significant. Even when the change between the low and high metallicity abundance ratio is clearly statistically significant, the values for the knees of the distribution, [Fe/H](low) and [Fe/H](high) are quite uncertain due to the small sample of UMi giants coupled with the uncertainty of the individual [X/Fe] determinations for each UMi giant.

To overcome the large uncertainties in the location of the knees of the fits, we have combined several elements, assuming that at least some elements, if not all, share the same values of [Fe/H](low,X) and [Fe/H](high,X). This dramatically increases the number of data points in the fit and lowers the uncertainties for the final derived parameters.

The [Fe/H](low/high,X) parameter space of interest is limited to a triangular area in the [Fe/H](low,X)-vs-[Fe/H](high,X) plane because [Fe/H](low,X) $\leq$ [Fe/H](high,X). In this area, $100{\times}100/2$ sampling points are uniformly distributed. For each sampling point (i.e. a pair of [Fe/H](low,X) and [Fe/H](high,X)), we calculate the χ^2 residual for each element using the already determined values of A(X) and B(x) for each element. Then we add up the residuals for all of the elements used in the combined fit. The summation is the χ^2 residual at that sampling point. We apply this procedure to all sampling points in the triangular area, and obtain the residual χ^2 valley for the combined elements. The lowest position of the valley gives us the best fit parameters, as is shown in Fig. 18. Three such combined fits were calculated; the results are given as the last entries in Table 6.

We estimate the uncertainties for the best combined fit results as follows. We set $\chi^2_{\rm min}$ to the minimum value of all χ^2 we calculated within the triangular region of interest in the [Fe/H](low,X)-vs-[Fe/H](high,X) plane. Then the "equal-altitude" contour line with $\chi^2 - \chi^2_{\rm min} = \chi^2_{\rm min}/(N-3)$ roughly defines the 1-σ range of the fitting results, and that with $\chi^2 - \chi^2_{\rm min} = 4\chi^2_{\rm min}/(N-3)$ roughly defines the 2-σ range, where N is the number of data points used in the fit procedure. N in a combined fit is dramatically larger than in a single-element fit. Each data point from Shetrone, Côté & Sargent (2001) is counted as 0.5 in N, and their χ^2 contribution is also weighted by a factor of 0.5. The derived [Fe/H](high,X) for each of the three combined fits is identical to within the uncertainties with [Fe/H](B), suggesting we did not detect any plateau in [Fe/H] at the high metallicity end of the UMi sample.

5.2. The Heavy Neutron Capture Elements

Just as the relative contribution of SNIa as compared to SNII to the chemical inventory of the ISM provides a timescale, so too does that of the r versus the s-process for heavy neutron capture elements. The s-process, reviewed in Busso, Gallino & Wasserburg (1999), occurs primarily in intermediate mass AGB stars. The site of the r-process is less clear, but is suspected to be in SNII during the formation of a neutron star (Qian & Wasserburg 2007).

Here we emphasize the difference in behavior for these elements between the UMi and Draco dSph galaxies and the galactic halo field stars. Unlike Draco, [Sr/Fe] (Fig. 16) remains high (approximately at the solar ratio) over the full range of [Fe/H] in UMi, while it falls for the lowest [Fe/H] stars in Draco. The former behavior is that of the mean for the halo field, while the latter is that of the low extreme of the Galactic halo field population. The behavior of [Ba/Fe], though, is similar in the two dSph galaxies, and lies at the low extreme of the range shown by halo field stars at low metallicity. Thus far, no star with [Ba/Fe] as low as the outlier Draco 119 (Fulbright, Rich & Castro 2004) has been found in UMi. The low outlier in UMi (COS171) is low for its rather high Fe-metallicity for all the neutron capture elements; it is ~0.8 dex low for [Ba, La, Ce, Nd, and Eu/Fe].

But the most important difference between the behavior of UMi and Draco for these elements is shown in the upper panel of Fig. 19, which displays the abundance ratio of the elements diagnostic for the s-process (Ba) and the r-process (Eu). The solar r-process ratio shown in the top panel is taken from Simmerer et al (2004); the solar ratio is a mixture of r and s-process material, while the pure s-process ratio for [Ba/Eu] lies above the top of the figure. Unlike Draco, even at the highest metallicities reached in UMi, there is still no sign of a contribution from the s-process, while in Draco there is. Another symptom of this is seen in the lower panel of this figure, where the [Eu/Fe] ratios are very high for the highest [Fe/H] giants in UMi, while in C09 they appear to drop towards solar for the higher metallicity Draco giants. The exceptions in the lower panel are the outlier UMi COS171 and UMi 28104, which is strongly depleted in the neutron capture elements in the second (Ba) peak, as is shown in Fig. 17, but note that both stars follow the rest of the UMi sample, displaying the r-process ratio, in the upper panel of Fig. 19.

The UMi giants are slightly brighter than the Draco giants, and this helps in the secure detection of the many neutron-capture elements with only a few weak lines, including La, Ce, and Nd, among the stars at the metal-rich end of the UMi sample. The ratios among these elements also support the conclusion that the neutron capture elements in UMi originate entirely in the r-process, as was suggested earlier by Sadakane et al. (2004). As one expects in such a case, [Nd/Fe] shows an enhancement which is roughly 0.5 dex smaller than that of [Eu/Fe], consistent with the description of Nd as having roughly equal contributions in the Sun from each of the r and s-process, while for Eu, the r-process dominates.

Simmerer et al (2004) suggest that in the Galactic halo, signs of the s-process begin only at [Fe/H] > -2.6 dex, and a mean [Eu/La] ratio halfway between the pure r-process value and the Solar ratio is reached only at [Fe/H] ~ -1.4 dex. The survey of cool metal-poor local dwarfs of Mashonkina et al (2003) reaches the halfway point in [Eu/Ba] from pure r-process to the Solar mixture only at [Fe/H] ~ -0.5 dex. Thus the result from Fig. 19 is clear; the UMi distribution is close to that of the Galactic halo, while in Draco, the s-process becomes important at a Fe-metallicity significantly lower than is characteristic of the Galactic halo.

The relative population of the first and second peaks in neutron capture heavy element abundances is shown in Fig. 20 using Y vs Ba. In the lowest metallicity UMi stars, one sees primarily the very low fraction of Ba compared to a normal fraction of Y, while in the somewhat higher metallicity UMi stars, [Ba/Fe] approaches the solar value, and [Y/Ba] becomes slightly subsolar, and well below the value typical of the halo field[4]. Clearly for the lowest metallicity UMi giants, production of additional Sr and Y[5] by some additional mechanism such as the "weak r-process" or the "lighter element primary process" introduced by Travaglio et al (2003) is required.

5.3. Age – Metallicity Relation for UMi

A very useful diagnostic of the star formation rate as a function of time is the age – metallicity relationship. We construct this for UMi using [Fe/H] values obtained from detailed abundance analyses for the augmented sample in UMi including results from Shetrone, Côté & Sargent (2001) and from Sadakane et al. (2004). [Ca/H] from Winnick (2003) for the remaining members of UMi she observed at moderate dispersion was transformed into [Ca/H](HIRES) using using the linear fit given in §4. SDSS photometry from DR7 (Abazajian *et al.* 2009) for these stars is combined with the isochrones of Dotter *et al.* (2008). We adopt a relation between [α/Fe] and [Fe/H] based on our results described above. Given [Fe/H], [α/Fe], the colors, the distance of UMi and the adopted reddening, we can determine the age of each UMi giant.

---

[4] The equivalent figure of C09, Fig. 19, shows [Ba/Sr] as a function of [Fe/H]. The Draco data are correctly plotted, but a mistake was made in the location of the r and s-process ratios in that figure. They should both be very close to the Solar ratio.

[5] The Zr abundances for the UMi sample are quite uncertain.

We do this for each star with $M_{i'} < -2.0$ mag. The isochrones along the RGB for lower luminosity stars converge too much in the (g' – i') color to attempt this. The results are shown in Fig. 21. Stars which are slightly redder than the reddest isochrone for the appropriate metallicity are assigned ages of 14 Gyr. The (large) uncertainty is these ages is discussed in C09.

The median age for the 40 UMi giants is 14 Gyr, which is considerably higher than the median we found in C09 for Draco luminous giants. In the mean, the UMi stars are of a uniform old age, in good agreement with the CMD analysis of HST images by Dolphin (2002) and more recently by Orban et al (2008). There is a hint of an age-metallicity relation, with the highest metallicity stars being $\sim$ 3 Gyr younger on average than the bulk of the UMi stellar population.

5.4. Outliers in UMi and in Draco

As noted above, our UMi sample contains one outlier, COS171. This star seems depleted in everything except Fe, or perhaps received a substantial amount of pure Fe ejecta in addition to a more normal mix. In hindsight, Draco XI-2 may be a less extreme case (see C09). The Galactic halo contains a very small number of very peculiar stars (see, e.g. Cohen *et al.* 2008; Lai *et al.* 2009), but none of these known to the authors come close to matching the characteristics of COS171. The low α stars discussed by Ivans *et al.* (2003) show peculiarities only for the α and heavy neutron capture elements and are are much less depleted in these elements with respect to Fe than is COS171.

While COS171 is indeed unique within the Draco, the UMi, and Galactic halo samples of stars with detailed abundance analyses, it is highly reminiscent of the more extremely depleted stars in Fornax analyzed by Letarte (2007), but COS171 has a somewhat lower [Fe/H]. This analogy holds through the Fe-peak, but not for the heavy neutron capture elements. Somehow this star shares many of the characteristics of stars in a galaxy that has experienced extended star formation over at least 5 Gyr (Orban et al 2008) with a mean [Fe/H] much higher than that of Draco or UMi. It is interesting to note that its estimated age (see §5.3) is 9.4 Gyr, considerably younger than that of the vast majority of the UMi stellar population, but the errors on this age are quite large.

The only outlier in the Draco sample discussed in C09, Draco 119 (Fulbright, Rich & Castro 2004), has a very different behavior; it is normal for most elements, and is a low outlier only for the neutron capture elements beyond the Fe-peak. Given the low star formation rate in these low-metallicity dSph galaxies and the extremely low fraction of the neutron capture elements even at Solar metallicity, a wide range in the abundances of these very rare heavy elements, as is seen in Galactic halo field stars at very low metallicity, should be expected.

6. Chemical Evolution of the UMI dSph Galaxy

In addition to our UMi analysis reported here and that of Draco in C09, as of today, there are only three other dSph galaxies with published detailed abundance analyses from high dispersion spectra for 14 or more stars to which we can compare our Draco results. These are the Sgr dSph (the main core, not the stream) (Monaco et al 2005; Sbordone et al 2007) and the Carina dSph galaxy, for which Koch et al (2008a) combines his analysis of 10 giants with 5 from the earlier study by Shetrone et al (2003). The extensive study of Fornax by Letarte (2007) is not directly relevant as the lowest metallicity stars in their Fornax sample barely overlap the highest metallicity giants in UMi or Draco.

In comparing our results for UMi, our earlier work in Draco (C09), and published studies of more metal-rich dSph Galactic satellites, there appears to be a pattern of moving from a chemical inventory for dSph giants with [Fe/H] $\lesssim -2$ dex which is very similar to that of stars in the outer part of the Galactic halo (enhanced α/Fe relative to the Sun, coupled with subsolar [X/Fe] for the heavy neutron capture elements and r-process domination), switching to subsolar α-elements and super-solar s-process dominated neutron capture elements for the highest [Fe/H] dSph stars. The combination of low star formation rates over a varying and sometimes extended duration that produced the stellar populations in the local dSph galaxies with [Fe/H] > -1.5 dex leads to a chemical inventory wildly discrepant from that of any component of the Milky Way.

To demonstrate this in detail, we apply our toy model to the recent data for the Carina and the Sgr dSph galaxies. Fig. 22 for [Mg/Fe] and for [Ti/Fe] show the fits for these two galaxies, for UMi, and for Draco. The fits for the Milky Way thin and thick disk are also displayed. This figure clearly demonstrates the differences among the dSph satellites for [Mg/Fe] as a function of [Fe/H]. The UMi sample is constant to within the uncertainties at [Mg/Fe] $\sim +0.35$ dex. For the other dSph galaxies that relation begins high at low metallicity but [Mg/Fe] begins to decline at considerably lower [Fe/H] for higher metallicity star; the [Fe/H] at which this decline begins increases as the mean metallicity of the dSph increases. A similar situation occurs for [Ti/Fe], but with a smaller total range in this ratio, hence the differences in the trends for the various dSph galaxies are less certain. What definitely is changing between the various dSph galaxies is the Fe-metallicity range. Among the dSph satellites with suitable abundance data, the UMi and Draco systems have the the lowest mean [Fe/H] for their giants, Carina is intermediate, and Sgr is closest to the Milky Way.

The knee values [Fe/H](X,low) and [Fe/H](X,high), which represent the timescale (or, more correctly, the [Fe/H]) at which the relative contributions of processed ejecta into the ISM of the system from the various nucleosynthesis sites change significantly, are also changing for these two (and other) elements among the various dSph Galactic satellites. The Galactic thick and thin disk populations all approach [X/Fe] = 0 close to or at the Solar Fe-metallicity, i.e. B(X) and [Fe/H](high,X) ~ 0. But in UMi and in Draco, as is shown for UMi here in Table 6 and for Draco in Table 8 of C09, the approach toward Solar ratios for some elements begins at a considerably lower [Fe/H]. For example. [Fe/H](low,Si) is -0.5 dex for the Milky Way thick disk, -1.6 dex for UMi, and -2.0 dex for Draco. In addition, the relative contributions of the r vs the s-process to the production of heavy neutron capture elements varies a lot among the dSph galaxies, with UMi showing *no* detectable contribution from the s-process, believed to originate from intermediate mass AGB stars, consistent with its short epoch of star formation.

Recent models of chemical evolution for the disk, bulge, and halo of the Milky Way based on the precepts first established by Tinsley (1973) have been presented by several groups, including Timmes, Woosley & Weaver (1995), Kobayashi et al (2006), Prantzos (2008), and Matteucci (2008). These models generally assume complete and uniform mixing of the gas over the total volume considered at all times with the exception of the more sophisticated model of Marcolini et al (2006, 2008). Such models have been reasonably successful in reproducing the chemical evolution of the major components of the Milky Way overall, although failing in some (minor) details.

The evolution of the dSph galaxies differs in principle from that of the Milky Way or its halo. Their binding energies are lower, so the importance of gas loss may be higher, particularly in the case of material from SNII, for which the ejection velocity is significantly larger than the escape velocity. Furthermore since both UMi and Draco at present show no evidence for the presence of gas, gas loss via a galactic wind or through interactions between the dSph satellite and its host, the Milky Way, must have been important in the past. These galaxies also show the consequences of lower star formation efficiency which leads to slower star formation overall without the large initial burst that dominates nucleosynthesis in most of the Milky Way components. In a system where the star formation rate is slower and more constant with time, SNIa ejecta can become important contributors before [Fe/H] just from SNII builds up in the dSph interstellar medium to high values near ~ -1 dex. It is this time delay between the SNII and SNIa contributions that dominates discussion of the chemical evolution of dSph galaxies.

Lanfranchi & Matteucci (2004) suggest another mechanism for affecting the α/Fe ratios, namely the presence of a strong outflow, which reduces the amount of gas available for star formation. This in turn cuts off the production of α-elements in massive stars, while the SNIa rate, and the consequent production of Fe, continues unaffected. This too could cause the drop in [α/Fe] ratios common among the dSph galaxies. Separating the contribution of a slow star formation versus a strong outflow in the chemical history of a dSph is not easy from abundance ratios alone. It requires a knowledge of the metallicity distribution of the stars in the dSph, and ideally of the age-metallicity distribution as well. Lanfranchi & Matteucci (2004) claim that both effects are necessary to explain the characteristics of UMi and of Draco.

Matteucci (2008) reviews models for the chemical evolution of the dSph galactic satellites of the Milky Way that reproduce the behavior of the α-elements. Presumably the agreement at the lowest [Fe/H] values probed here, where the Galactic halo stars overlap the Draco giants, is a consequence of a chemical inventory to which only SNII contributed, but the trends in UMi are not as well reproduced. Lanfranchi & Matteucci (2004) present detailed models for the evolution of 6 of the dSph Milky Way satellites, including UMi and Draco, which try to reproduce not only the chemical evolution but also the total stellar mass and their individual star formation histories as derived from CMD studies. Their model for UMi has a very low star formation efficiency and the shortest duration of star formation (only 3 Gyr occurring immediately after the galaxy condensed) of these 6 dSph galaxies. To within the uncertainties of the measurements and the models, they succeed in reproducing the almost flat [Ca/Fe] relation with [Fe/H] of Fig. 8, but their relation shows a fairly steep decline in [Mg/Fe] vs [Fe/H] which is not seen in UMi (see Fig. 6).

There are a number of other problems when one compares detailed chemical evolution models to our data. Lanfranchi, Matteucci & Cescutti (2008), who address the production of heavy elements beyond the Fe peak in dSph galaxies, substantially underpredict the ratio [Y/Fe] for the most metal poor stars in UMi, and overpredict [Ba/Fe] for the same stars in both Draco and UMi. The Ba/Eu ratio is predicted satisfactorily for these UMi stars, but probably that is simply a result of the dominance of the r-process in their production. The cause of the relatively small difference in behavior of [Mg and Si/Fe] vs [Ca, and Ti/Fe] at the lowest metallicities in UMi and in Draco is not clear, particularly since Si is an explosive α-element while Mg is a hydrostatic one. How this behavior relates to the mass distribution of the SNII progenitors, given that one also needs to reproduce the odd-even effect at [Sc/Fe], is not obvious. Qualitatively similar differences in the behavior of the α-elements vs [Fe/H] are also seen in the Galactic bulge (Fulbright, McWilliam & Rich 2007), but again there are differences in detail as the separation between hydrostatic and explosive α-elements is cleaner there, i.e. [Si/Fe] behaves like [Ca/Fe] and [Ti/Fe] in the Galactic bulge, which does not appear to be the case for UMi.

Carigi, Hernandez & Gilmore (2002) presented a chemical evolution model for UMi which also requires a metal-rich wind. More sophisticated models for dSph galaxies are presented by Marcolini et al (2006) and by Salvadori, Ferrara & Schneider (2008), who use a hierarchical merger tree with a semi-analytical scheme galaxy formation. These more complex but more realistic models are rapidly improving but are not yet fully capable of following chemical evolution in detail.

6.1. Implications for the Formation of the Galactic Halo

Whether the Galactic halo could have been formed by accretion of satellite dwarf galaxies has become a question of great current interest; see e.g. Tolstoy et al (2003), Shetrone, Côté & Sargent (2001), among others. Due largely to technical advances and the construction of 8 to 10 m telescopes, the data now available for the Galactic satellite galaxies is a tremendous improvement over that of a decade ago both in terms of number of stars analyzed and in accuracy of the results. Recent efforts are summarized in the review by Geisler et al (2008). The very recent review of Tolstoy, Hill & Tosi (2009) focuses on their large ongoing project at the VLT to study dwarf galaxies (the DART project, Tolstoy et al 2003).

Our work in UMi and in Draco (see C09) and that published for the Carina and for the Sgr dSph galaxies show that abundance ratios among stars in dSph galaxies tend to overlap those of Galactic halo giants at the lowest Fe-metallicities probed. This is only to be expected, as the nucleosynthesis ejecta from SNII are to first order independent of metallicity. It is thus possible that the satellites were accreted early in their development. Their properties as we observe them today would then not be relevant to this issue. In each of these stellar populations, a minimum metallicity threshold for formation of low mass stars along the lines of that discussed by Bromm & Larson (2004) seems to exist.

Helmi et al (2006) claimed that early accretion of satellites as a way of forming the Galactic halo was still ruled out because of the metallicity distribution function (MDF) they deduce for four dSph galaxies. Given the MDF they used for the Galactic halo, they claimed that dSph galaxies would be expected to contain at least a few stars with [Fe/H] < -3.0 dex, while they had not to date detected any such stars in the four dSph galaxies in which they have extensive samples from the DART project[6].

However we found one such star in Draco (C09) and two more in UMi. Frebel, Kirby & Simon (2010) have found a star at [Fe/H] -3.8 dex in the Sculptor dSph galaxy. Aoki *et al.* (2009) have found a star at -3.10 dex in Sextans. Several more such stars have been found in the ultrafaint Milky Way satellites: Norris et al (2008) ([Fe/H] -3.7 dex in Bootes I), Simon *et al.* (2010) ([Fe/H] -3.2 dex in Leo IV), and Frebel *et al.* (2010) (two giants, at -3.10 and -3.23 dex in UMa II). A number of other stars found by Kirby et al (2008) and Kirby et al (2010) in various dSph galaxies are suspected to be below -3.0 dex, but most are too faint for high-dispersion spectroscopy. In addition Schörck et al (2009) recently completed a determination of the halo MDF based based on the Hamburg/ESO Survey which shows that completeness corrections are important in the MDF derived from the HES.

Collectively this very recent work serves to help reestablish the scenario for the formation of the Galactic halo via accretion of satellite galaxies as viable. The material now in the inner halo of the Galaxy had to have been accreted early in the star formation history of the dSph galaxies, giving time for orbital mixing to eliminate traces of discrete stellar streams, while satellite galaxies accreted somewhat later could contribute to populating the outer halo, which shares many of the abundance anomalies of the dSph galaxies. Dissolved globular clusters had to disperse fairly quickly before the ubiquitous light element correlations among O, Na, Mg and Al developed, as these are not seen among halo field stars.

---

[6] Starkenburg *et al.* (2010) very recently retracted these claims.

7. Summary

We present a detailed abundance analysis based on high resolution spectra obtained with HIRES on the Keck I Telescope of 10 stars in the Ursa Minor dwarf spheroidal galaxy. The sample was selected to span the full range in metallicity inferred from Winnick (2003), who used moderate resolution spectroscopy for radial velocity members of this dSph galaxy found by earlier surveys. Her CaT indices of the strength of the near-infrared Ca triplet correlate well with [Ca/H] we derive from our detailed abundance analyses with differences from a linear fit of only $\sigma = 0.13$ dex.

We use classical plane-parallel (1D) LTE models from the Kurucz grid (Kurucz 1993) with a recent version of the stellar abundance code MOOG (Sneden 1973). [Fe/H] for our sample stars ranges from -1.35 to -3.10 dex. Combining our sample with previously published work of Shetrone, Côté & Sargent (2001) for 6 UMi giants[7], and an analysis based on higher S/N spectra of three UMi giants by Sadakane et al. (2004), two of which were already studied in the earlier work, gives a total of 16 luminous UMi giants with detailed abundance analyses.

We find that for the UMi sample [Mg/Fe] is constant to within the uncertainties with a value $\sim +0.35$ dex for all the stars[8], a trait shared by outer Galactic halo stars. The abundance ratios [Si/Fe], [Cr/Fe], [Ni/Fe], [Zn/Fe], and perhaps [Na/Fe] and [Co/Fe] for the UMi giants overlap those of Galactic halo giants at the lowest [Fe/H] probed, but for the higher Fe-metallicity UMi stars are significantly lower than those of Milky Way halo giants. For the explosive α-elements Ca and Ti the abundance ratios are also constant to within the uncertainties but are somewhat low over the full metallicity range of the UMi dSph stars compared to Galactic halo giants, being closer, but still perhaps slightly low, at the lowest Fe-metallicities. Nucleosynthetic yields sensitive to the neutron excess, hence to the initial metallicity of the SN progenitor (see, e.g. Timmes, Woosley & Weaver 1995), may be important in explaining the origin of differences between UMi giants and Galactic field stars for several of the abundance ratios studied here.

The heavy neutron capture elements in UMi giants have r-process ratios at all metallicities in UMi, consistent with the short duration of its star forming epoch inferred from CMDs (Orban et al 2008). The relative contribution of these heavy elements seems to increase as [Fe/H] increases for most of the UMi giants.

There are small, but real, differences between the trends of abundance ratios between UMi and those of Draco from our earlier study (see C09) which are discussed in detail in §5. There is one outlier in our UMi sample, which appears to have an excess of Fe, or a depletion of essentially all elements with respect to Fe. Similar behavior is seen among the most extreme of the Fornax dSph giants (Letarte 2007).

In comparing our results for UMi, our earlier work in Draco (C09), and published studies of more metal-rich dSph Galactic satellites, there appears to be a pattern of moving from a chemical inventory for dSph giants with [Fe/H] $\lesssim -2$ dex which is very similar to that of stars in the outer part of the Galactic halo (enhanced α/Fe relative to the Sun, coupled with subsolar [X/Fe] for the heavy neutron capture elements and r-process domination), switching to subsolar α-elements and super-solar s-process dominated neutron capture elements for the highest [Fe/H] dSph stars. The combination of low star formation rates over a varying and sometimes extended duration that produced the stellar populations in the local dSph galaxies with [Fe/H] > -1.5 dex leads to a chemical inventory wildly discrepant from those seen in any component of the Milky Way.

---

[7] We ignore one carbon star from Shetrone, Côté & Sargent (2001).

[8] The anomalous outlier UMi COS171 is ignored here. See §5.4.

The dominant uncertainty in these results is the possibility of differential non-LTE or 3D effects between the very cool luminous giants in our sample from the UMi and Draco dSph galaxies and the comparison halo field and globular cluster stars, which are somewhat hotter. With a 30-m telescope it will be possible to reach lower luminosity and somewhat hotter giants in the dSph satellites of the Milky Way where these issues will be less important.

In C09 we developed a toy model fit which we use to illuminate these trends, and to compare them with those of Galactic globular clusters and of giants from the Carina and Sgr dSph galaxies. Since there is good agreement in most cases for the abundance ratios at the lowest metallicity within a given sample and also the highest metallicities sampled, the fundamental contributors to their chemical inventory (SNII at the lowest metallicity and SNIa plus other sources at the highest [Fe/H]) behave in very similar ways in all these environments. We thus infer that the IMF for massive stars must be similar as well. The key differences lie in the [Fe/H] corresponding to the knee values, i.e. in the timescale (or, more correctly, the [Fe/H]) at which the relative contributions of processed ejecta into the ISM of the system from the various nucleosynthesis sites change significantly. The UMi and Draco systems, which have among the lowest luminosities for the classical dSph satellites of the Milky Way, have the lowest mean [Fe/H] for its giants, Sgr is intermediate, and the Carina dSph is closest to the Milky Way halo and the thick disk. Our new data will enable much more sophisticated modelling of the chemical evolution of Draco with more detail than our simple toy model can provide.

We note the presence of two luminous giants in our UMi sample with [Fe/H] < -3.0 dex. This combined with other recent evidence for a small number of extremely low metallicity stars in other dSph galaxies reaffirms that the inner Galactic halo could have largely been formed by early accretion and dissolution of Galactic satellite galaxies and by globular clusters which dissolved prior to the imprinting of an AGB signature, while the outer halo could have formed largely from those dSph galaxies accreted later.

The age–metallicity relationship established by combining photometry, spectroscopic metallicities, and isochrones suggests that the stellar population in UMi consists of old metal-poor stars. Unlike our previous result in C09 for Draco, there is no evidence for the presence of an intermediate age component in UMi. There is a hint of an age-metallicity relationship with the most metal-rich UMi stars being ~ 3 Gyr younger than the metal-poor old population.

The entire Keck/HIRES and LRIS user communities owes a huge debt to Jerry Nelson, Gerry Smith, Steve Vogt, and many other people who have worked to make the Keck Telescope and HIRES a reality and to operate and maintain the Keck Observatory. We are grateful to the W. M. Keck Foundation for the vision to fund the construction of the W. M. Keck Observatory. The authors wish to extend special thanks to those of Hawaiian ancestry on whose sacred mountain we are privileged to be guests. Without their generous hospitality, none of the observations presented herein would have been possible.

The authors are grateful to NSF grant AST-0507219 and grant AST-0908139 for partial support. This publication makes use of data from the Two Micron All-Sky Survey, which is a joint project of the University of Massachusetts and the Infrared Processing and Analysis Center, funded by the National Aeronautics and Space Administration and the National Science Foundation.

REFERENCES

Abazajian, K. N. *et al.*, 2009, ApJS, 182, 543

Andievsky, S. M., Spite, M., Korotin, S. A., Spite, F., Bonifacio, P., Cayrel, R., Hill, V. & Fracois, P., 2007 A&A, 464, 1081

Aoki, W., Honda, S., Sadakane, K. & Arimoto, N., 2007, PASJ, 59, L15

Aoki, W. *et al.*, 2009, A&A, 502, 569

Armandroff, T. E., Olszewski. E. W. & Pryor, C., 1995, AJ, 110, 2131

Arnett, D., 1971, ApJ, 166, 153

Asplund, M., Grevesse, N. & Sauval, A. J., 2005, Astronomical Society of the Pacific Conference Series, 336, 25

Baumüller, D. & Gehren, T., 1996, A&A, 307, 961

Baumüller, D. & Gehren, T., 1997, A&A, 325, 1088

Bellazzini, M., Ferraro, F. R., Origlia, L., Pancino, E., Monaco, L. & Oliva, E., 2002, AJ, 124, 3222

Bergemann, M. & Gehren, T., 2008, A&A, 492, 823

Bergemann, M., Pickering, J. C. & Gehren, T., 2010, MNRAS, 401, 1334

Bonifacio, P. *et al.*, 2009, A&A, 501, 519

Bromm, V. & Larson, R. B., 2004, ARAA, 42, 79

Busso, M., Gallino, R. & Wasserburg, G.J., 1999, ARA&A, 37, 239

Carigi, L, Hernandez, X. & Gilmore, G., 2002, MNRAS, 334, 117

Carpenter, J., 2001, AJ, 121, 2851

Carollo, D. et al, 2007, Nature, 450, 1020

Cayrel, R. et al, 2004, A&A, 416, 1117

Cescutti, G., Matteucci, F., Lanfranchi, G. A. & McWilliam, A., 2008, A&A,491, 401

Clayton, D., "Handbook of Isotopes in the Cosmos", 2003, Cambridge U. Press

Cohen, J. G., Christlieb, N., Beers, T. C., Gratton, R. G. & Carretta, E., 2002, AJ, 124, 470

Cohen, J. G., Christlieb, N., McWilliam, A., Shectman, S., Thompson, I., Wasserburg, G. J., Ivans, I., Dehn, Karlsson, T. & Melendez, J., 2004, ApJ, 612, 1107

Cohen, J. G. *et al.*, 2006, AJ, 132, 137

Cohen, J. G., Christlieb, N., McWilliam, A., Shectman, S., Thompson, I., Melendez, J., Wisotzki, L. & Reimers, D., 2008, ApJ, 672, 320

Cohen, J. G., Briley, M. M. & Stetson, P. B., 2005, AJ, 130, 1177

Cohen, J. G. & Huang, W., 2009, ApJ, 701, 1053 (C09)

Collet, R., Asplund, M. & Trampedach, R., 2007, A&A, 469, 687

Cudworth, K. M., Olszewski, E. W. & Schommer, R. A., 1986, AJ, 92, 766

Cutri, R. M. *et al.*, 2003, "Explanatory Supplement to the 2MASS All-Sky Data Release, http: www.ipac.caltech.edu/2mass/releases/allsky/doc/explsup.html

Dolphin, A. E., 2002, MNRAS, 332, 91

Dotter, A., Chaboyer, B., Jevremovic, D., Kotov, V., Baron, E. & Ferguson, J. W., 2008, ApJS, 178, 89

Francois, P. et al, 2007, A&A, 476, 935

Frebel, A., Simon, J. D., Geha, M. & Willman, B., 2010, ApJ, 708, 560

Frebel, A., Kirby, E. & Simon, J. D., 2010, Nature, 464, 72

Fulbright, J. P., 2000, AJ, 120, 1841

Fulbright, J., Rich, R. M. & Castro, S., 2004, ApJ, 612, 447

Fulbright, J. P., McWilliam, A. & Rich, R. M., 2007, ApJ, 661, 1152

Gallagher, J. S., Madsen, G. J., Reynolds, R. J., Grebel, E. K. & Smecker-Hane, T. A., 2003, ApJ, 588, 326

Geisler, D., Wallerstein, G., Smith, V. V. & Casetti-Dinescu, D. I., 2008, PASP, 119, 859

Gratton, R., Sneden, C. & Carretta, E., 2004, ARA&A, 42, 385

Grebel, E. K., Gallagher, J. S. & Harbeck, D., 2003, AJ, 125, 1926

Greggio, L., Renzini, A. & Daddi, E., 2008, MNRAS, 388, 829

Grevesse, N. & Sauval, A. J., 1998, Space Science Reviews, 85, 161

Helmi, A. et al, 2006, ApJ, 651, L121

Houdashelt, M. L., Bell, R. A. & Sweigart, A. V., 2000, AJ, 119, 1448

Ishigaki, M., Chiba, M. & Aoki, W., 2010, PASJ, in press

Ivans, I. I., Sneden, C., James, C. R., Preston, G. W., Fulbright, J. P., Hoflich, P. A., Carney, B. W. & Wheeler, J. C., 2003, ApJ, 592, 906

Iwamoto, K., Brachwitz, F., Nomoto, K., Kishimoto, N., Umeda, H., Hix, W. R. & Thieleman, F. K., 1999, ApJS, 125, 439

Johnson J., 2002, ApJS, 139, 219

Kirby, E. N., Simon, J. D., Geha, M., Guhathakurta, P. & Frebel, A., 2008, ApJ, 685, L43

Kirby, E N. *et al.*, 2010, in preparation

Klypin, A., Kravtsov, A. V., Valenzuela, O. & Prada, F., 1999, ApJ, 522, 82

Kobayashi, C., Umeda, H., Nomoto, K., Tominaga, N. & Ohkubo, T., 2003, ApJ, 653, 1145

Koch, A., Grebel, E. K., Gilmore, G. F., Wyse, R. F. G., Kleyna, J. T., Harbeck, D. R., Wilkinson, M. I. & Evans, N. W., AJ, 135, 1580

Koch, A., McWilliam, A., Grebel, E. K., Zucker, D. B. & Belokurov, V., 2008, ApJ, in press

Kurucz, R. L., 1993, ATLAS9 Stellar Atmosphere Programs and 2 km/s Grid, (Kurucz CD-ROM No. 13)

Lai, D. K., Rockosi, C. M., Bolte, M., Johnson, J. A., Beers,, T. C., Lee, Y. S., Allende Prieto, C. & Yanny, B., 2009, ApJ, 697, L63

Lanfranchi, G. A. & Matteucci, F., 2004, MNRAS, 351, 1338

Lanfranchi, G. A., Matteucci, F. & Cescutti, G., 2008, A&A, 481, 635

Letarte, B., 2007, PhD thesis, University of Groningen

Limongi, M. & Chieffi, A., 2003, ApJ, 592, 404

Marcolini, A., D'Ercole, A., Brighenti, F. & Recchi, S., 2006, MNRAS, 371, 643

Marcolini, A., D'Ercole, A., Battaglia, G. & Gibson, B. K., 2008, MNRAS, 386, 2173

Mashonkina, L. & Gehren, T., 2001, A&A, 376, 232

Mashonkina, L., Gehren, T., Travaglio, C. & Borkova, T., 2003, A&A, 397, 275

Matteucci, F., 2008, in "Chemical Evolution of the Milky Way and Its Satellites", in Saas-Fe Advance Course, "The Origin of the Galaxy and the Local Group", ed. E. Grebel & B. Moore

McWilliam, A., Preston, G. W., Sneden, C. & Shectman, S., 1995, AJ, 109, 2736

McWilliam, A., 1997, ARA&A, 35, 503

Melendez, J., Shchukina, N. G., Vasiljeva, I. E. & Ramirez, I., 2006, ApJ, 641, 1082

Mighell, K. J. & Burke, C. J., 1999, AJ, 118, 366

Mishenina, T. V., Kovtyukh, V. V., Soubiran, C., Travaglio, C. & Busso, M., 2002, A&A, 396, 189

Monaco, L. et al, 2005, A&A, 441, 141

Nissen, P. E. & Schuster, W. J.,1 997, A&A, 326, 751

Nissen, P. E. & Schuster, W. J., 2010, A&A, 511, 10

Nissen, P. E. et al 2000, A&A, 353, 722

Nissen, P. E., Primas, F., Asplund, M. & Lambert, D. L., 2002, A&A, 390, 325

Nissen, P. E., Ackerman, C., Asplund, M., Fabian, D., Kerber, F., Kaufl, H. U. & Pettini, M., 2008, A&A, 649, 319

Norris, J. E., Yong, D., Gilmore G. & Wyse, R. F. G. 2010, ApJ, 711, 350

Ohkubo, T., Umeda, H., Nomoto, K. & Yoshida, T., 2006, AIPC, 847, 458

Orban, C., Gnedin, O. Y., Weisz, D. R., Skillman, E. D., Dolphin, A. E. & Holtzman, J. A., 2008, AJ, 686, 1030

Palma, C., Majewski, S. R., Siegel, M. H., Patterson, R. J., Ostheimer, J. C. & Link, R., 2003, AJ, 125, 1352

Peñarrubia, J., McConnachie, A. W. & Navarro, J.,2008, ApJ, 672, 904

Piatek, S., Pryor, C., Bristow, P., Olszewski, E. W., Harris, H. C., Mateo, M., Minniti, D. & Tinney, C. G., 2005, AJ, 130, 95

Prantzos, N., 2008, in “Stellar Nucleosynthesis: 50 Years After B2FH”, 2008, ed. C. Charbonnel & J. P. Zahn, EAS Publications Series

Prochaska, J. X., Naumov, S. O., Carney, B. W., McWilliam, A. & Wolfe, A. M., 2000, AJ, 120, 2513

Qian, Y. Z. & Wasserburg, G J., 2007, Physics Reports, Review Section of Physics Letters, 442, 237

Ramirez, I., Allende Prieto, C. & Lambert, D. L., 2007, A&A, 465, 271

Reddy, B. E., Tomkin, J., Lambert, D. L., & Allende Prieto, C., 2003, MNRAS, 340, 304

Reddy, B. E., Lambert, D. L. & Allende Prieto, C., 2006, MNRAS, 367, 1329

Roederer, I. U., 2008, AJ, 137, 272

Sadakane, K., Arimoto, N., Ikuta, C., Aoki, W., Jablonka, P. & Tajitsu, A., 2004, PASJ, 56, 1041

Salvadori, S., Ferrara A. & Schneider, R., 2008, MNRAS, 371, 885

Sbordone, L., Bonifacio, P., Buonanno, R., Marconi, G., Monaco, L. & Zaggia, S., 2007, A&A, 465, 815

Schlegel, D., Finkbeiner, D. P. & Davis, M., 1998, ApJ, 500, 525

Schörck, T. et al, 2009, A&A, 507, 817

Shetrone, M. D., Bolte, M. & Stetson, P. B., 1998, AJ, 115, 1888

Shetrone, M. D., Côté, P. & Sargent, W. L. W., 2001, ApJ, 548, 592

Shetrone, M. D., Côté, P. & Stetson, P. B., 2001, PASP, 113, 1122

Shetrone, M. D. et al, 2003, AJ, 125, 684

Shortridge K. 1993, in *Astronomical Data Analysis Software and Systems II*, A.S.P. Conf. Ser., Vol 52, eds. R.J. Hannisch, R.J.V. Brissenden, & J. Barnes, 219

Simmerer, J., Sneden, C., Cowan, J. J., Collier, J., Woolf, V. M. & Lawler, J. E., 2004, ApJ, 617, 1091

Simon, J. D., Frebel, A., McWilliam, A., Kirby, E. N. & Thompson, I. B., 2010, ApJ(Astro-ph/1001.3137)

Skrutskie, M. F., Schneider, S.E., Stiening, R., Strom, S.E., Weinberg, M.D., Beichman, C., Chester, T. *et al.*, 1997, in *The Impact of Large Scale Near-IR Sky Surveys*, ed. F.Garzon *et al.* (Dordrecht: Kluwer), p. 187

Smith, J. A. *et al.*, 2002, AJ, 123, 2121

Sneden, C., 1973, Ph.D. thesis, Univ. of Texas

Spite, M. et al, 2005, A&A, 430, 655

Starkenburg, E. *et al.*, 2010, A&A, 513, A34

Stephens, A., 1999, AJ, 117, 1771

Timmes, F. X., Woosley, S. E. & Weaver, T. A., 1995, ApJS, 98, 617

Tinsley, B. M., 1973, ApJ, 186, 35

Tolstoy, E. et al, 2003, AJ, 125, 707

Tolstoy, E., Hill, V. & Tosi, M., ARAA, 47, 371

Travaglio, C., Gallino, R., Arnone, E., Cowan, J., Jordan, F. & Sneden, C., 2004, ApJ, 601, 864

Tsujimoto, T., 2006, A&A, 447, 81

Vogt, S. E. *et al.* 1994, SPIE, 2198, 362

Walker, M. G., Mateo, M., Olszewski, E. W., Gnedein, O. Y., Wang, W., Sen, B. & Woodroofe, M., 2007., ApJ, 667, L53

Winnick, R. A., 2003, PhD thesis, Yale University, "Metallicity Distributions in the Draco, Ursa Minor and Sculptor Dwarf Spheroidal Galaxies"

Woosley, S. E. & Weaver, T. A., 1995, ApJ, 101, 181

York, D. G., Adelman, J., Anderson Jr., J. E. *et al.*, 2000, AJ, 120, 1579

Young, L. M., 2000, AJ, 119, 188

This preprint was prepared with the AAS LaTeX macros v5.2.

Table 1. The Sample of Stars in the Ursa Minor dSph

ID[a]	Coords.[a] (J2000)		V[a] (mag)	I[a] (mag)	Date Obs.	Exp. Time (sec)	S/N[b]
COS171	15 08 04.97	+67 14 00.8	17.25	15.94	06/2008	7200	80
COS233	15 08 10.01	+67 17 24.5	16.93	15.61	06/2008	7200	95
JI2	15 10 27.11	+67 24 36.2	16.98	15.65	06/2008	7200	80
JI19	15 10 11.68	+67 08 28.8	17.26	16.07	06/2008	7200	80
N37	15 11 05.76	+67 13 15.3	17.07	15.71	06/2008	7200	95
27940	15 11 24.30	+67 33 50.2	16.81	15.41	09/2009	6000	85
28104	15 13 12.33	+67 33 20.6	16.86	15.50	02/2010	8100	105
33533	15 13 26.09	+67 16 22.7	16.90	15.62	06/2008	7200	100
36886	15 13 30.30	+67 06 37.3	17.01	15.76	02/2010	7400	80
41065	15 11 01.48	+66 52 54.5	16.71	15.35	09/2009	4900	85

[a] The star names, coordinates, and photometry are from Winnick (2003), with the original source of the latter two being Palma et al. (2003).

[b] S/N per spectral resolution element ($\lambda/\Delta\lambda = 35,000$) in the continuum at the center of the echelle order at 5800 Å.

Table 2. Stellar Parameters for the Ursa Minor Giants

ID	$T_{\rm eff}$ (K) (phot)	$\log(g)$ (dex) (phot)	$T_{\rm eff}$ (K) (spec)	$\log(g)$ (dex) (spec)	v_t (km s^{-1})	v_r (km s^{-1})
COS171	4290	0.80	4380	0.8	1.9	−256.2
COS233	4425	0.80	4425	0.8	2.2	−266.3
JI2	4415	0.80	4415	0.85	2.1	−254.7
JI19	4530	1.0	4450	0.8	3.0	−246.2
N37	4290	0.80	4390	0.8	1.8	−240.4
27940	4290	0.70	4290	0.7	2.2	−248.4
28104	4365	0.65	4365	0.65	2.3	−244.2
33533	4525	0.80	4450	0.85	3.0	−248.9
36886	4400	0.75	4400	0.75	2.6	−231.0
41065	4400	0.60	4350	0.6	2.6	−259.7

Table 3. Equivalent Widths for Ten Stars in the Ursa Minor dSph

λ Å	Ion	χ (eV)	log(gf) (dex)	33533 (mÅ)	JI19 (mÅ)	36886 (mÅ)	41065 (mÅ)	COS233 (mÅ)	28104 (mÅ)	27940 (mÅ)	JI2 (mÅ)	N37 (mÅ)	COS171 (mÅ)
6300.30	[O I]	0.00	−9.780	···	···	17.9	10.0	···	···	···	···	31.0	···
6363.78	[O I]	0.02	−10.300	···	···	···	8.0	8.1	8.8	10.0	8.5	8.1	12.6
7771.94	O	9.15	0.369	···	···	···	···	···	···	···	···	···	8.5
5682.63	Na I	2.10	−0.700	···	···	···	···	···	···	9.4	8.0	13.5	···
5688.19	Na I	2.10	−0.420	···	···	···	9.8	12.0	10.0	15.3	15.5	22.5	12.0
5889.95	Na I	0.00	0.110	150.3	161.3	224.4	225.6	236.1	269.7	300.9	240.5	255.0	218.1
5895.92	Na I	0.00	−0.190	121.7	134.4	189.5	207.7	210.7	220.4	259.6	214.8	225.4	205.1
4703.00	Mg I	4.34	−0.440	43.0	53.6	85.8	113.0	115.0	124.1	128.5	118.2	136.3	107.3
5172.70	Mg I	2.71	−0.380	187.0	185.6	257.7	283.5	304.0	338.3	348.6	···	···	···
5183.62	Mg I	2.72	−0.160	201.0	206.3	301.7	323.8	355.0	389.3	433.1	···	···	···
5528.40	Mg I	4.34	−0.480	38.4	56.5	97.7	117.0	128.0	142.5	154.0	143.0	155.0	140.0
5711.09	Mg I	4.34	−1.670	···	···	20.5	18.4	38.0	38.3	49.0	49.3	53.5	45.0
6318.72	Mg I	5.11	−2.100	···	···	···	···	···	···	···	7.0	8.0	···
7387.69	Mg I	5.75	−1.200	···	···	···	···	···	···	10.3	···	···	···
3961.52	Al I	0.00	−0.340	154.2	145.0	133.9	···	193.0	233.4	···	···	···	···
6696.02	Al I	3.14	−1.340	···	···	···	···	···	···	···	···	9.5	···
6698.67	Al I	3.14	−1.640	···	···	···	···	···	···	···	···	9.5	···
3905.53	Si I	1.91	−1.040	···	208.2	···	···	···	···	···	···	···	···
4102.94	Si I	1.91	−3.140	56.0	95.0	105.0	124.0	···	···	128.0	134.4	···	137.0
5421.18	Si I	5.62	−1.430	···	···	···	···	···	···	···	6.2	···	···
5665.55	Si I	4.92	−2.040	···	···	···	···	···	···	···	···	···	12.5
5690.43	Si I	4.93	−1.870	···	···	···	···	···	···	7.2	···	13.6	···
5701.10	Si I	4.93	−2.050	···	···	···	···	···	···	···	···	···	13.5
5772.15	Si I	5.08	−1.750	···	···	···	···	···	···	···	···	13.7	···
5948.54	Si I	5.08	−1.230	···	···	6.9	14.6	15.0	16.2	27.5	28.1	28.0	31.0
6145.02	Si I	5.61	−1.440	···	···	···	···	···	4.2	···	···	···	···
6155.13	Si I	5.62	−0.760	···	···	10.0	7.5	···	9.3	14.0	15.6	22.3	15.0
6237.32	Si I	5.62	−1.010	···	···	···	···	···	···	10.0	···	···	···
7003.57	Si I	5.96	−0.830	···	···	···	···	···	···	8.2	···	11.5	···
7005.89	Si I	5.98	−0.730	···	···	···	···	···	···	10.9	12.4	16.8	13.4
7034.90	Si I	5.87	−0.880	···	···	···	···	···	···	···	9.9	···	···
7405.77	Si I	5.61	−0.820	···	···	···	···	20.8	21.5	17.0	22.0	30.9	21.0
7415.95	Si I	5.61	−0.730	···	···	8.6	···	16.6	12.6	14.3	20.2	32.5	27.6
7423.50	Si I	5.62	−0.580	···	···	7.1	14.1	17.7	23.6	23.3	26.0	31.9	27.6
7698.97	K I	0.00	−0.168	12.8	29.6	76.3	79.4	105.5	108.8	133.3	116.4	138.3	130.0
4226.74	Ca I	0.00	0.244	···	213.9	···	···	···	···	···	···	···	···
4289.37	Ca I	1.88	−0.300	···	···	82.7	···	···	···	···	···	···	···
4318.66	Ca I	1.90	−0.210	···	···	···	···	···	95.4	···	···	···	115.4
4425.44	Ca I	1.88	−0.338	···	50.0	58.0	73.8	75.9	91.9	103.7	87.3	119.0	103.1
4435.69	Ca I	1.89	−0.520	11.9	···	···	···	···	···	···	···	···	···
4454.79	Ca I	1.90	0.260	46.2	64.8	96.6	113.2	···	123.3	···	···	···	···
4578.56	Ca I	2.52	−0.558	···	···	13.5	···	28.1	24.2	31.7	37.0	···	47.2
5512.99	Ca I	2.93	−0.300	···	···	12.4	···	27.6	19.0	36.5	33.1	42.9	40.7
5581.96	Ca I	2.52	−0.710	···	···	···	···	33.0	···	···	···	71.5	···
5588.75	Ca I	2.52	0.210	20.3	30.6	65.3	75.5	89.6	95.3	119.0	109.2	120.3	121.4

Table 3—Continued

λ Å	Ion	χ (eV)	log(gf) (dex)	33533 (mÅ)	JI19 (mÅ)	36886 (mÅ)	41065 (mÅ)	COS233 (mÅ)	28104 (mÅ)	27940 (mÅ)	JI2 (mÅ)	N37 (mÅ)	COS171 (mÅ)
5590.11	Ca I	2.52	−0.710	···	11.0	16.3	22.2	38.5	38.1	53.3	54.0	65.8	60.5
5594.46	Ca I	2.52	−0.050	18.5	25.0	52.0	62.8	78.4	84.7	116.0	104.0	···	···
5601.28	Ca I	2.52	−0.690	···	···	24.0	22.0	33.7	39.5	61.3	57.9	76.5	72.2
5857.45	Ca I	2.93	0.230	11.5	16.6	33.2	42.6	59.7	61.2	84.1	82.3	88.8	83.3
6161.30	Ca I	2.52	−1.030	···	···	···	12.9	12.5	17.4	26.8	22.6	38.9	29.5
6162.17	Ca I	1.90	−0.090	48.3	66.3	106.5	121.0	134.4	146.0	···	155.2	170.2	163.4
6166.44	Ca I	2.52	−0.900	···	···	···	11.4	13.5	16.5	23.9	27.0	41.1	41.2
6169.04	Ca I	2.52	−0.540	···	6.2	14.9	24.1	29.8	35.7	47.9	50.0	64.3	60.3
6169.56	Ca I	2.52	−0.270	···	11.3	27.0	34.5	46.0	52.9	67.3	64.7	81.6	78.0
6471.66	Ca I	2.52	−0.590	···	···	24.0	35.0	41.4	46.9	64.2	59.7	76.7	74.1
6493.78	Ca I	2.52	0.140	10.0	20.5	45.1	55.1	77.5	81.0	101.0	88.8	113.0	105.2
6499.65	Ca I	2.54	−0.590	···	···	16.5	···	31.1	35.0	50.2	43.1	62.8	63.0
6717.68	Ca I	2.71	−0.610	···	···	17.4	19.8	37.5	43.2	59.8	53.3	73.2	80.5
7148.15	Ca I	2.71	0.218	18.5	26.5	63.9	71.4	89.1	96.4	113.6	108.2	121.2	117.2
4246.82	Sc II	0.32	0.242	107.8	128.2	170.5	···	···	···	···	···	···	···
4314.08	Sc II	0.62	−0.100	···	105.0	142.6	···	···	···	···	···	···	···
4670.41	Sc II	1.36	−0.580	···	20.1	51.7	79.6	94.0	71.4	95.9	···	···	···
5526.79	Sc II	1.77	0.130	17.3	26.3	57.8	65.9	82.5	82.6	79.0	94.0	85.1	69.2
5657.90	Sc II	1.51	−0.500	10.2	17.6	49.0	53.0	74.6	73.7	86.5	77.0	82.3	70.0
5667.15	Sc II	1.50	−1.240	···	···	16.0	22.3	27.0	29.0	34.1	26.3	30.8	17.5
5669.04	Sc II	1.50	−1.120	···	···	16.2	20.9	35.5	33.2	40.5	36.2	44.5	24.3
5684.20	Sc II	1.51	−1.080	···	···	26.3	33.2	38.3	38.3	40.3	34.4	43.0	28.9
6245.64	Sc II	1.51	−1.130	···	···	26.0	24.7	43.5	35.0	42.2	38.8	51.6	29.2
6604.60	Sc II	1.36	−1.479	···	5.4	23.9	22.8	33.8	29.9	38.7	40.6	43.5	29.3
3924.53	Ti I	0.02	−0.940	···	···	···	···	70.8	···	···	···	···	···
3998.64	Ti I	0.05	−0.050	48.5	···	···	···	···	···	···	···	···	···
4512.74	Ti I	0.84	−0.480	···	···	18.2	39.9	41.0	50.2	68.0	68.6	81.2	62.5
4518.03	Ti I	0.83	−0.230	···	···	38.0	46.1	63.3	59.5	91.7	79.6	90.1	···
4533.25	Ti I	0.85	0.480	22.2	56.8	74.2	93.5	95.1	95.7	125.0	115.7	130.5	133.0
4534.78	Ti I	0.84	0.280	24.8	44.0	57.6	62.1	85.5	94.2	118.0	113.5	120.0	104.8
4548.77	Ti I	0.83	−0.350	···	···	22.0	50.4	47.3	55.3	75.9	···	83.9	69.2
4555.49	Ti I	0.85	−0.490	···	···	26.4	30.9	46.7	59.0	70.6	73.2	81.1	62.7
4681.92	Ti I	0.05	−1.070	12.5	27.7	64.1	72.1	90.9	98.9	129.4	119.9	132.0	116.7
4981.74	Ti I	0.85	0.500	37.1	54.2	87.4	110.9	104.0	117.5	151.8	136.7	149.4	134.0
4999.51	Ti I	0.83	0.250	24.2	43.1	73.3	81.3	106.5	106.9	137.5	131.8	152.5	118.2
5022.87	Ti I	0.83	−0.430	···	···	31.0	46.1	56.4	63.0	88.7	80.7	95.6	78.5
5039.96	Ti I	0.02	−1.130	18.0	34.1	53.3	87.5	92.5	96.0	123.1	113.3	126.0	108.5
5173.75	Ti I	0.00	−1.120	15.1	32.2	65.2	89.3	97.2	102.7	138.5	125.1	153.9	119.9
5210.39	Ti I	0.05	−0.880	20.7	43.8	81.8	101.3	115.0	119.0	151.2	129.0	150.0	129.2
5426.26	Ti I	0.02	−3.010	···	···	···	···	···	13.0	16.3	···	28.6	···
5471.20	Ti I	1.44	−1.390	···	···	···	···	···	···	···	···	7.8	···
5474.21	Ti I	1.46	−1.230	···	···	···	···	···	···	···	···	17.0	···
5490.15	Ti I	1.46	−0.933	···	···	···	···	6.9	10.6	···	10.3	20.7	···
5662.16	Ti I	2.32	−0.109	···	···	···	···	···	···	11.6	···	17.9	···
5866.45	Ti I	1.07	−0.840	···	···	13.3	15.3	27.8	29.8	53.6	47.5	74.0	48.3

Table 3—Continued

λ Å	Ion	χ (eV)	log(gf) (dex)	33533 (mÅ)	JI19 (mÅ)	36886 (mÅ)	41065 (mÅ)	COS233 (mÅ)	28104 (mÅ)	27940 (mÅ)	JI2 (mÅ)	N37 (mÅ)	COS171 (mÅ)
5922.11	Ti I	1.05	−1.470	···	···	···	···	5.9	6.6	19.3	9.7	26.3	14.8
5937.81	Ti I	1.07	−1.890	···	···	···	···	···	···	5.2	···	11.0	···
5941.75	Ti I	1.05	−1.520	···	···	···	···	···	7.7	15.2	···	26.6	14.4
5953.16	Ti I	1.89	−0.329	···	···	···	···	···	9.9	15.6	13.1	27.4	18.2
5965.83	Ti I	1.88	−0.409	···	···	···	···	9.7	9.6	21.0	13.5	26.0	···
5978.54	Ti I	1.87	−0.496	···	···	···	···	···	···	···	11.0	22.2	25.0
6064.63	Ti I	1.05	−1.940	···	···	···	···	···	4.2	13.8	···	13.6	···
6126.22	Ti I	1.07	−1.420	···	···	···	···	···	6.7	21.8	20.7	33.3	16.9
6258.10	Ti I	1.44	−0.355	···	···	7.2	19.0	24.3	26.1	49.0	46.6	65.7	42.1
6258.71	Ti I	1.46	−0.240	···	···	11.5	17.2	30.3	34.5	53.0	54.8	82.8	51.6
6261.10	Ti I	1.43	−0.479	···	···	8.3	17.1	21.2	25.6	40.4	36.2	56.9	32.2
6743.12	Ti I	0.90	−1.630	···	···	···	···	6.2	9.2	15.7	19.8	31.0	17.7
7344.69	Ti I	1.46	−0.992	···	···	···	···	···	···	14.7	···	···	···
3900.54	Ti II	1.13	−0.450	···	118.2	···	···	···	···	···	···	···	···
4012.39	Ti II	0.57	−1.610	···	99.8	···	···	···	···	···	···	···	···
4028.35	Ti II	1.89	−0.870	···	52.2	···	···	···	···	···	···	···	···
4312.86	Ti II	1.18	−1.160	···	108.7	···	···	···	···	···	···	···	···
4395.03	Ti II	1.08	−0.510	···	131.5	178.3	···	···	···	···	···	···	···
4399.77	Ti II	1.24	−1.290	72.6	85.6	116.8	126.8	129.9	···	···	···	···	113.1
4417.72	Ti II	1.16	−1.160	75.9	90.0	129.7	141.6	139.9	138.6	···	···	160.5	118.4
4443.81	Ti II	1.08	−0.700	106.0	127.7	152.6	170.0	158.1	175.5	···	164.8	···	143.4
4468.51	Ti II	1.13	−0.600	108.0	132.6	159.1	···	···	176.7	···	···	···	168.9
4501.28	Ti II	1.12	−0.760	115.0	112.8	146.5	165.3	159.9	172.2	···	182.1	···	166.0
4533.97	Ti II	1.24	−0.640	109.6	134.4	160.4	···	···	···	···	···	···	158.1
4563.77	Ti II	1.22	−0.820	102.7	122.6	134.9	139.8	153.9	156.3	···	173.0	165.8	159.0
4571.98	Ti II	1.57	−0.340	85.0	118.8	152.0	163.0	150.0	169.3	···	166.6	···	152.4
4583.41	Ti II	1.16	−2.870	···	···	37.0	36.8	38.4	44.9	46.4	53.5	60.3	47.8
4589.95	Ti II	1.24	−1.650	47.3	70.6	94.2	107.7	102.9	110.9	114.0	111.5	112.1	101.2
4657.20	Ti II	1.24	−2.320	21.0	22.4	57.9	69.2	73.6	78.1	100.5	91.4	···	···
4708.67	Ti II	1.24	−2.370	20.0	39.9	52.2	47.5	77.7	69.5	76.8	90.0	82.0	67.8
4762.78	Ti II	1.08	−2.710	···	···	39.6	···	···	···	···	···	···	···
4798.54	Ti II	1.08	−2.670	···	35.7	48.8	68.3	···	66.8	···	···	···	···
4865.62	Ti II	1.12	−2.810	···	28.3	38.0	55.6	64.7	57.9	65.4	59.0	71.8	52.0
4911.20	Ti II	3.12	−0.340	···	···	19.4	20.0	20.5	24.8	34.5	36.0	44.0	31.9
5185.91	Ti II	1.89	−1.460	16.6	31.9	59.5	69.6	70.5	72.2	86.4	79.3	91.0	74.7
4111.77	V I	0.30	0.408	···	···	49.8	···	69.5	76.8	98.0	101.3	···	80.5
5670.85	V I	1.08	−0.425	···	···	···	···	···	11.4	18.6	···	19.2	···
5703.57	V I	1.05	−0.212	···	···	···	···	10.4	8.2	31.2	16.6	24.0	12.6
6081.44	V I	1.05	−0.579	···	···	···	···	9.1	···	11.9	···	18.2	12.0
6090.22	V I	1.08	−0.062	···	···	···	6.5	16.4	14.4	13.0	21.3	32.6	16.3
6199.20	V I	0.29	−1.280	···	···	···	···	···	···	···	···	29.1	···
6243.10	V I	0.30	−0.978	···	···	10.1	12.3	···	18.3	40.0	30.3	57.7	26.1
6251.82	V I	0.29	−1.340	···	···	···	6.8	···	···	···	···	25.0	11.6
6274.64	V I	0.27	−1.670	···	···	···	···	···	···	···	···	14.9	8.0
6285.14	V I	0.28	−1.510	···	···	···	···	···	···	11.4	···	···	···

Table 3—Continued

λ Å	Ion	χ (eV)	log(gf) (dex)	33533 (mÅ)	JI19 (mÅ)	36886 (mÅ)	41065 (mÅ)	COS233 (mÅ)	28104 (mÅ)	27940 (mÅ)	JI2 (mÅ)	N37 (mÅ)	COS171 (mÅ)
4254.33	Cr I	0.00	−0.110	105.9	113.1	···	···	···	···	···	217.7	···	···
4274.79	Cr I	0.00	−0.230	93.0	93.4	···	···	···	···	···	···	···	···
4289.72	Cr I	0.00	−0.361	97.1	106.5	···	···	···	···	···	···	···	···
4545.96	Cr I	0.94	−1.380	···	···	31.0	38.5	60.2	50.2	90.6	79.3	114.8	106.0
4600.76	Cr I	1.00	−1.280	···	···	29.7	49.5	59.4	69.7	92.7	···	104.9	96.1
4616.13	Cr I	0.98	−1.210	···	···	31.9	56.0	68.3	71.3	103.1	101.9	106.1	113.0
4626.18	Cr I	0.97	−1.340	···	···	38.5	45.7	56.9	66.7	90.1	80.6	110.0	113.0
4652.17	Cr I	1.00	−1.030	15.0	19.0	48.6	69.7	75.7	80.3	108.4	103.0	116.7	111.0
4789.34	Cr I	2.54	−0.370	···	···	···	6.8	···	···	···	···	···	···
5206.04	Cr I	0.94	0.030	74.0	84.0	122.0	135.5	154.2	167.3	···	188.9	···	···
5298.28	Cr I	0.98	−1.170	···	···	51.3	···	···	90.1	···	···	···	···
5409.80	Cr I	1.03	−0.710	30.0	27.0	75.9	86.0	110.0	118.2	153.4	135.4	152.6	142.8
5783.09	Cr I	3.32	−0.500	···	···	···	···	···	···	···	···	···	16.3
5783.89	Cr I	3.32	−0.295	···	···	···	···	···	···	···	···	20.1	19.7
5787.96	Cr I	3.32	−0.083	···	···	···	···	···	···	···	···	13.4	···
6979.80	Cr I	3.46	−0.411	···	···	···	···	···	···	···	···	12.0	8.5
4030.75	Mn I	0.00	−0.470	112.3	95.0	···	···	···	···	···	···	···	···
4033.06	Mn I	0.00	−0.620	91.9	85.0	···	···	202.2	···	···	···	···	260.2
4451.59[a]	Mn I	2.89	0.280	···	···	···	45.5	42.4	···	75.0	···	···	59.6
4754.04	Mn I	2.28	−0.090	···	···	39.1	36.5	63.2	63.7	94.1	87.9	114.0	86.0
4783.42	Mn I	2.30	0.042	···	···	35.1	64.1	59.3	74.6	108.0	100.7	128.4	102.4
4823.51	Mn I	2.32	0.140	···	···	34.8	59.0	65.6	76.8	104.1	108.2	119.6	98.6
5537.74	Mn I	2.19	−2.020	···	···	···	···	···	···	···	···	18.7	10.9
6021.80	Mn I	3.08	0.034	···	···	···	7.7	25.0	21.0	32.8	36.1	53.0	48.7
4005.24	Fe I	1.56	−0.610	127.1	125.9	···	···	···	···	···	···	···	···
4063.59	Fe I	1.56	0.060	···	164.0	···	···	···	···	···	···	···	···
4071.74	Fe I	1.61	−0.020	162.4	166.9	···	···	···	···	···	···	···	···
4132.06	Fe I	1.61	−0.820	115.9	124.8	···	···	···	···	···	···	···	···
4143.87	Fe I	1.56	−0.620	129.4	119.2	···	···	···	···	···	···	···	···
4147.67	Fe I	1.49	−2.100	77.7	63.3	···	133.0	···	···	139.1	···	···	···
4181.75	Fe I	2.83	−0.370	54.4	50.5	···	···	···	···	···	···	···	···
4187.05	Fe I	2.45	−0.550	···	···	···	···	···	···	162.2	143.4	···	···
4187.81	Fe I	2.43	−0.550	···	53.3	···	129.4	···	···	···	···	···	···
4199.10	Fe I	3.05	0.160	···	76.9	···	124.8	119.8	···	···	···	···	···
4202.04	Fe I	1.49	−0.710	130.4	148.4	···	···	···	···	···	233.6	···	···
4216.19	Fe I	0.00	−3.360	120.0	···	···	···	···	···	···	···	···	···
4222.22	Fe I	2.45	−0.970	46.8	62.9	···	···	118.6	···	···	···	···	···
4233.61	Fe I	2.48	−0.600	63.9	65.8	···	···	122.5	···	···	···	···	···
4235.95	Fe I	2.43	−0.340	···	79.5	···	···	···	···	···	···	···	···
4250.13	Fe I	2.47	−0.404	79.4	88.8	···	131.4	151.2	···	152.9	···	···	···
4250.80	Fe I	1.56	−0.720	137.0	132.8	···	···	···	···	···	207.2	···	···
4260.49	Fe I	2.40	0.140	108.0	105.8	···	···	···	···	···	···	···	···
4271.16	Fe I	2.45	−0.350	···	88.6	···	145.0	···	···	···	···	···	···
4271.77	Fe I	1.49	−0.160	···	158.8	···	···	···	···	···	···	···	···
4282.41	Fe I	2.18	−0.780	64.5	88.9	···	139.5	134.8	···	···	···	···	···

Table 3—Continued

λ Å	Ion	χ (eV)	log(gf) (dex)	33533 (mÅ)	JI19 (mÅ)	36886 (mÅ)	41065 (mÅ)	COS233 (mÅ)	28104 (mÅ)	27940 (mÅ)	JI2 (mÅ)	N37 (mÅ)	COS171 (mÅ)
4307.91	Fe I	1.56	−0.070	···	172.8	···	···	···	···	···	···	···	···
4325.77	Fe I	1.61	0.010	···	150.0	···	···	···	···	···	···	···	···
4337.05	Fe I	1.56	−1.690	108.0	101.0	···	146.9	159.8	···	···	···	···	···
4375.94	Fe I	0.00	−3.030	149.8	···	···	···	···	···	···	···	···	···
4404.76	Fe I	1.56	−0.140	159.5	159.1	212.1	···	···	···	···	···	···	···
4415.13	Fe I	1.61	−0.610	137.4	124.4	169.8	···	···	···	···	···	···	···
4427.32	Fe I	0.05	−3.040	···	115.0	···	···	···	···	···	···	···	···
4430.62	Fe I	2.22	−1.660	30.4	38.9	84.8	81.0	103.9	···	···	···	···	···
4442.35	Fe I	2.20	−1.250	65.2	74.8	116.1	114.1	133.5	141.2	···	···	···	···
4447.73	Fe I	2.22	−1.340	55.3	59.1	101.7	101.1	134.0	132.4	144.9	131.4	···	167.6
4461.66	Fe I	0.09	−3.210	134.0	122.0	158.7	···	177.4	···	···	205.3	···	···
4489.75	Fe I	0.12	−3.970	96.0	83.0	128.9	···	142.9	160.2	···	160.7	···	171.4
4494.57	Fe I	2.20	−1.140	68.0	68.4	118.9	133.2	136.5	157.9	171.2	158.0	···	···
4531.16	Fe I	1.49	−2.150	74.2	82.6	116.8	126.4	···	154.4	167.5	146.4	···	···
4592.66	Fe I	1.56	−2.450	···	48.6	93.9	···	···	···	···	···	···	···
4602.95	Fe I	1.49	−2.220	70.6	74.5	110.4	137.0	133.5	148.6	156.4	142.5	163.4	153.4
4625.05	Fe I	3.24	−1.348	···	···	33.7	30.4	51.5	63.9	79.6	···	···	94.3
4788.77	Fe I	3.24	−1.806	···	···	···	16.5	17.8	35.4	45.4	49.9	57.5	75.1
4871.33	Fe I	2.86	−0.360	62.0	61.2	102.8	117.9	125.7	134.9	160.4	148.7	158.4	···
4872.14	Fe I	2.88	−0.570	46.2	44.5	88.6	110.8	122.3	121.0	159.3	138.1	143.6	160.0
4891.50	Fe I	2.85	−0.110	67.0	82.6	110.5	130.0	144.9	147.2	···	166.3	174.2	···
4919.00	Fe I	2.86	−0.340	56.8	65.7	···	117.0	127.6	133.5	159.5	145.9	156.7	168.3
4920.51	Fe I	2.83	0.150	81.0	82.0	142.8	···	175.6	172.2	···	···	···	···
4957.61	Fe I	2.81	0.230	99.9	108.2	145.6	···	···	···	···	200.4	···	···
5083.34	Fe I	0.96	−2.960	80.0	83.3	124.1	144.8	146.6	157.0	···	169.1	173.1	···
5166.28	Fe I	0.00	−4.200	101.4	86.0	139.9	159.0	159.9	175.9	···	180.1	···	···
5171.61	Fe I	1.48	−1.790	105.5	100.6	140.4	159.6	158.3	170.0	···	177.9	···	···
5192.35	Fe I	3.00	−0.420	40.0	···	···	110.3	118.9	···	154.6	151.9	147.4	···
5194.95	Fe I	1.56	−2.090	81.2	81.0	116.8	145.2	142.0	147.0	···	162.3	···	···
5198.72	Fe I	2.22	−2.140	20.0	30.0	60.1	85.6	91.8	96.7	116.7	114.7	125.9	134.5
5216.28	Fe I	1.61	−2.150	74.3	73.2	112.3	131.5	139.9	147.2	163.9	154.4	167.9	150.0
5217.40	Fe I	3.21	−1.070	17.4	10.5	43.5	45.5	71.3	73.4	96.7	97.8	101.4	109.6
5227.19	Fe I	1.56	−1.350	127.3	124.3	166.1	···	194.6	···	···	207.9	···	···
5232.95	Fe I	2.94	−0.100	72.0	72.9	115.6	132.2	139.7	149.7	174.6	162.9	···	···
5269.55	Fe I	0.86	−1.320	···	169.5	···	···	···	···	···	···	···	···
5393.18	Fe I	3.24	−0.720	25.7	20.0	61.2	73.5	90.0	98.6	118.5	117.2	133.2	138.9
5405.36	Fe I	4.39	−1.390	···	···	···	···	···	···	···	···	20.4	···
5405.79	Fe I	0.99	−1.840	145.0	139.9	···	···	···	···	···	230.9	···	···
5406.78	Fe I	4.37	−1.620	···	···	···	···	···	···	···	···	11.3	15.5
5409.14	Fe I	4.37	−1.200	···	···	···	···	···	···	11.4	···	···	33.0
5410.92	Fe I	4.47	0.400	9.1	8.2	28.2	40.3	56.0	57.6	69.8	74.0	84.8	95.6
5415.21	Fe I	4.39	0.640	21.6	17.8	45.9	65.2	73.0	77.3	98.6	92.2	106.9	124.3
5417.04	Fe I	4.41	−1.580	···	···	···	···	···	···	···	···	8.0	19.1
5424.08	Fe I	4.32	0.510	15.9	26.6	58.3	70.1	78.0	94.4	108.6	103.2	113.1	128.3
5434.53	Fe I	1.01	−2.130	133.1	131.8	172.7	···	···	···	···	207.4	···	···

Table 3—Continued

λ Å	Ion	χ (eV)	log(*gf*) (dex)	33533 (mÅ)	JI19 (mÅ)	36886 (mÅ)	41065 (mÅ)	COS233 (mÅ)	28104 (mÅ)	27940 (mÅ)	JI2 (mÅ)	N37 (mÅ)	COS171 (mÅ)
5441.33	Fe I	4.10	−1.630	···	···	···	···	···	···	···	···	···	12.0
5445.05	Fe I	4.39	−0.030	···	···	27.7	30.5	37.6	47.9	78.7	75.5	79.5	101.1
5466.39	Fe I	4.37	−0.620	···	···	9.8	7.3	14.6	25.8	27.5	37.6	51.5	57.8
5470.09	Fe I	4.44	−1.710	···	···	···	···	···	···	···	···	···	10.0
5473.90	Fe I	4.15	−0.690	···	···	···	7.6	20.2	27.2	38.9	39.0	52.9	68.1
5487.14	Fe I	4.41	−1.430	···	···	···	···	···	···	···	···	···	14.1
5487.77	Fe I	4.14	−0.620	···	···	10.9	14.9	23.5	32.1	36.5	48.4	59.7	80.5
5493.50	Fe I	4.10	−1.680	···	···	···	···	···	···	···	···	23.9	27.6
5494.46	Fe I	4.07	−1.990	···	···	···	···	···	···	···	···	14.2	17.3
5497.52	Fe I	1.01	−2.830	88.6	87.5	138.5	150.8	162.2	···	···	180.4	···	···
5501.46	Fe I	0.96	−3.050	84.0	79.4	132.2	130.0	154.0	172.5	···	172.4	···	172.1
5506.79	Fe I	0.99	−2.790	101.0	96.8	138.4	163.6	165.4	170.7	···	179.7	···	···
5522.45	Fe I	4.21	−1.450	···	···	···	···	···	···	···	7.0	20.5	38.5
5525.55	Fe I	4.23	−1.080	···	···	···	···	···	···	···	19.8	25.9	41.9
5536.58	Fe I	2.83	−3.710	···	···	···	···	···	···	···	···	···	9.7
5539.29	Fe I	3.64	−2.590	···	···	···	···	···	···	···	···	···	11.8
5554.88	Fe I	4.55	−0.350	···	···	···	15.1	16.5	20.6	33.1	26.5	49.5	71.1
5560.21	Fe I	4.43	−1.100	···	···	···	···	···	9.6	17.7	11.5	26.3	35.5
5567.39	Fe I	2.61	−2.670	···	···	···	20.4	30.5	36.6	47.6	51.0	69.8	85.8
5568.87	Fe I	3.63	−2.850	···	···	···	···	···	···	···	···	···	7.9
5569.62	Fe I	3.42	−0.486	14.2	22.4	61.8	74.5	91.3	93.5	119.4	115.5	124.0	134.9
5572.84	Fe I	3.40	−0.275	31.0	29.0	72.5	91.7	103.7	115.6	130.6	127.6	133.9	152.4
5576.09	Fe I	3.43	−0.920	12.1	···	40.0	52.4	68.1	76.0	91.9	94.4	104.3	115.6
5586.76	Fe I	3.37	−0.140	37.4	44.6	84.0	100.0	115.5	121.0	136.9	128.2	144.6	165.3
5618.63	Fe I	4.21	−1.630	···	···	···	···	···	···	···	10.3	22.1	41.0
5619.59	Fe I	4.39	−1.530	···	···	···	···	···	···	9.5	···	···	17.7
5620.49	Fe I	4.15	−1.810	···	···	···	···	···	···	···	7.3	···	···
5624.04	Fe I	4.39	−1.220	···	···	···	···	···	···	···	···	15.0	30.3
5624.54	Fe I	3.42	−0.755	21.7	···	52.3	60.8	75.0	84.5	104.4	102.1	115.4	130.4
5641.44	Fe I	4.26	−1.080	···	···	···	···	9.7	10.8	15.0	24.4	37.4	46.0
5652.32	Fe I	4.26	−1.850	···	···	···	···	···	···	···	···	···	7.2
5653.89	Fe I	4.39	−1.540	···	···	···	···	···	···	···	10.1	12.5	13.4
5662.52	Fe I	4.18	−0.570	···	···	13.2	13.9	34.8	40.0	49.0	51.9	74.4	85.6
5667.52	Fe I	4.48	−1.500	···	···	···	···	···	···	15.8	···	···	29.0
5679.02	Fe I	4.65	−0.820	···	···	···	···	···	11.5	9.3	11.7	21.0	36.1
5698.02	Fe I	3.64	−2.580	···	···	···	···	···	···	···	···	11.3	···
5701.54	Fe I	2.56	−2.140	···	5.2	36.4	41.0	68.2	68.1	86.9	89.5	99.2	115.2
5705.47	Fe I	4.30	−1.360	···	···	···	···	···	···	···	···	···	21.4
5705.98	Fe I	4.61	−0.490	···	···	···	10.2	···	···	33.4	···	···	54.6
5731.76	Fe I	4.26	−1.200	···	···	···	···	9.5	6.4	18.7	15.8	30.3	40.3
5741.85	Fe I	4.26	−1.850	···	···	···	···	···	···	···	···	···	19.0
5742.96	Fe I	4.18	−2.410	···	···	···	···	···	···	···	···	···	5.3
5752.04	Fe I	4.55	−0.940	···	···	···	···	···	8.6	8.2	···	21.8	37.4
5753.12	Fe I	4.26	−0.690	···	···	···	11.1	18.2	26.1	33.3	34.2	50.1	69.5
5760.35	Fe I	3.64	−2.390	···	···	···	···	···	···	···	···	14.7	17.3

Table 3—Continued

λ Å	Ion	χ (eV)	$\log(gf)$ (dex)	33533 (mÅ)	JI19 (mÅ)	36886 (mÅ)	41065 (mÅ)	COS233 (mÅ)	28104 (mÅ)	27940 (mÅ)	JI2 (mÅ)	N37 (mÅ)	COS171 (mÅ)
5762.42	Fe I	3.64	−2.180	···	···	···	···	···	8.3	···	···	13.7	37.6
5762.99	Fe I	4.21	−0.410	···	···	16.0	17.0	···	40.1	55.8	60.4	77.4	86.1
5775.06	Fe I	4.22	−1.300	···	···	···	···	···	11.8	14.2	25.0	27.5	56.2
5778.46	Fe I	2.59	−3.430	···	···	···	···	···	···	···	···	20.7	32.4
5793.91	Fe I	4.22	−1.600	···	···	···	···	···	···	16.4	11.5	16.0	24.2
5806.72	Fe I	4.61	−0.950	···	···	···	···	···	···	16.0	7.2	16.0	26.1
5827.88	Fe I	3.28	−3.310	···	···	···	···	···	···	···	···	···	9.5
5838.37	Fe I	3.94	−2.240	···	···	···	···	···	···	···	···	···	12.5
5852.22	Fe I	4.55	−1.230	···	···	···	···	···	···	···	···	13.0	18.0
5855.09	Fe I	4.61	−1.480	···	···	···	···	···	···	···	···	···	10.1
5856.08	Fe I	4.29	−1.330	···	···	···	···	···	···	···	···	14.0	18.8
5859.60	Fe I	4.55	−0.550	···	···	···	6.1	9.6	16.7	26.1	23.0	39.8	51.0
5862.35	Fe I	4.55	−0.330	···	···	···	13.0	20.6	23.6	35.3	33.2	50.9	66.7
5873.21	Fe I	4.26	−2.040	···	···	···	···	···	···	···	···	···	8.8
5883.81	Fe I	3.96	−1.260	···	···	···	···	10.5	24.0	29.5	29.2	41.9	61.0
5927.79	Fe I	4.65	−0.990	···	···	···	···	···	···	···	···	11.9	22.3
5929.67	Fe I	4.55	−1.310	···	···	···	···	···	···	16.0	···	21.0	24.1
5930.17	Fe I	4.65	−0.140	···	···	···	9.0	28.0	20.1	32.3	36.1	52.8	65.9
5934.65	Fe I	3.93	−1.070	···	···	7.1	10.3	22.5	24.6	42.5	38.9	58.0	68.3
5952.72	Fe I	3.98	−1.340	···	···	···	···	···	11.5	24.6	20.5	35.5	43.5
5956.69	Fe I	0.86	−4.500	···	···	35.1	48.8	70.3	76.1	95.6	93.7	118.1	121.8
5976.79	Fe I	3.94	−1.330	···	···	···	15.5	···	19.8	34.4	31.0	43.7	66.8
5983.69	Fe I	4.55	−0.660	···	···	···	···	9.5	···	22.9	22.4	43.5	54.3
5984.83	Fe I	4.73	−0.260	···	···	12.2	···	14.3	10.1	35.8	27.0	46.5	56.7
6024.05	Fe I	4.55	0.030	···	···	20.6	27.2	39.7	44.4	60.8	56.7	71.8	89.1
6027.05	Fe I	4.07	−1.090	···	···	···	···	14.4	15.9	31.3	26.4	42.6	59.6
6055.99	Fe I	4.73	−0.370	···	···	···	···	13.1	13.9	19.5	20.2	31.6	49.9
6065.48	Fe I	2.61	−1.410	25.0	27.2	73.5	91.8	105.1	113.8	137.9	131.0	142.6	152.6
6078.50	Fe I	4.79	−0.330	···	···	···	10.3	11.7	11.1	16.8	21.0	36.4	51.3
6079.00	Fe I	4.65	−1.020	···	···	···	···	···	···	11.9	8.9	12.0	22.4
6089.57	Fe I	5.02	−0.900	···	···	···	···	···	···	···	11.0	18.0	28.0
6093.67	Fe I	4.61	−1.400	···	···	···	···	···	···	···	···	···	11.1
6096.66	Fe I	3.98	−1.830	···	···	···	···	···	···	···	···	19.8	27.9
6136.62	Fe I	2.45	−1.410	48.4	53.4	95.9	118.8	128.5	134.1	156.3	155.9	159.0	173.3
6136.99	Fe I	2.20	−2.930	···	···	22.6	32.6	61.8	59.7	91.2	78.5	98.2	108.3
6137.69	Fe I	2.59	−1.350	41.3	38.8	88.3	106.9	117.6	124.4	154.3	141.1	161.6	164.4
6151.62	Fe I	2.18	−3.370	···	···	12.8	17.1	33.3	35.2	53.7	53.9	76.0	89.0
6157.73	Fe I	4.07	−1.160	···	···	···	···	10.9	10.9	25.7	32.4	44.9	53.5
6165.36	Fe I	4.14	−1.470	···	···	···	···	···	6.2	···	···	20.3	27.7
6173.34	Fe I	2.22	−2.880	···	···	25.5	37.5	52.8	65.0	81.0	79.4	92.7	104.7
6180.20	Fe I	2.73	−2.650	···	···	···	15.5	21.5	28.0	41.5	40.2	62.0	73.2
6187.99	Fe I	3.94	−1.620	···	···	···	···	···	11.4	15.6	22.4	23.7	40.0
6191.56	Fe I	2.43	−1.420	42.0	44.0	95.7	114.7	123.5	132.0	159.1	148.3	162.4	168.8
6200.31	Fe I	2.61	−2.370	···	···	30.4	38.7	50.3	59.2	67.9	75.7	95.0	103.9
6240.65	Fe I	2.22	−3.170	···	···	10.7	16.9	28.3	36.5	59.6	44.5	68.3	79.7

Table 3—Continued

λ Å	Ion	χ (eV)	log(gf) (dex)	33533 (mÅ)	JI19 (mÅ)	36886 (mÅ)	41065 (mÅ)	COS233 (mÅ)	28104 (mÅ)	27940 (mÅ)	JI2 (mÅ)	N37 (mÅ)	COS171 (mÅ)
6246.32	Fe I	3.60	−0.880	14.9	···	46.6	40.5	70.2	69.7	93.8	80.8	102.4	113.4
6252.55	Fe I	2.40	−1.770	32.8	30.5	83.7	104.3	116.3	121.9	143.2	132.2	145.5	148.7
6254.26	Fe I	2.28	−2.430	12.7	10.3	48.5	64.0	81.6	94.6	116.6	106.0	126.1	127.6
6265.13	Fe I	2.18	−2.540	16.6	21.0	51.6	68.1	84.8	92.5	113.0	106.2	117.9	128.4
6271.28	Fe I	3.33	−2.700	···	···	···	···	7.6	···	8.0	···	11.8	19.8
6290.97	Fe I	4.73	−0.730	···	···	···	···	6.8	11.7	···	14.6	17.9	32.7
6297.79	Fe I	2.22	−2.640	···	···	55.5	54.5	···	73.6	···	88.4	121.8	110.1
6301.51	Fe I	3.65	−0.718	11.2	···	28.8	···	···	65.0	81.7	87.6	95.3	120.2
6302.50	Fe I	3.69	−1.110	···	···	14.1	···	32.1	36.0	53.1	53.7	69.2	83.8
6311.50	Fe I	2.83	−3.140	···	···	···	···	···	···	···	···	47.5	···
6315.31	Fe I	4.14	−1.230	···	···	···	···	···	···	···	···	···	43.5
6315.81	Fe I	4.07	−1.610	···	···	···	···	···	···	21.1	···	···	···
6355.03	Fe I	2.84	−2.290	···	···	···	27.9	39.1	65.3	73.2	64.3	87.4	97.0
6380.75	Fe I	4.19	−1.380	···	···	···	···	8.3	6.6	16.4	14.1	25.2	32.4
6392.54	Fe I	2.28	−3.990	···	···	···	6.9	···	12.5	20.6	19.9	26.0	38.0
6393.60	Fe I	2.43	−1.580	40.7	40.0	94.8	108.8	122.6	128.6	151.2	145.3	155.6	165.3
6408.03	Fe I	3.69	−1.020	···	···	21.1	22.8	37.5	46.7	64.0	63.2	82.5	91.8
6411.65	Fe I	3.65	−0.720	13.1	···	36.6	48.9	66.8	75.3	92.9	90.8	103.9	122.8
6421.35	Fe I	2.28	−2.010	31.0	38.2	80.5	···	···	113.5	129.3	129.4	148.2	159.6
6430.84	Fe I	2.18	−1.950	43.3	33.3	88.7	109.1	···	129.5	157.7	···	154.4	···
6469.21	Fe I	4.83	−0.730	···	···	···	···	···	···	14.3	···	···	40.8
6475.63	Fe I	2.56	−2.940	···	···	12.2	18.0	31.6	34.9	47.2	43.7	66.9	83.7
6481.87	Fe I	2.28	−3.010	···	···	20.4	31.2	46.2	57.4	71.5	71.1	89.6	103.7
6494.98	Fe I	2.40	−1.240	60.2	60.4	114.1	129.1	138.1	150.1	168.4	162.3	172.6	183.9
6495.74	Fe I	4.83	−0.840	···	···	···	···	···	···	···	···	···	15.5
6498.94	Fe I	0.96	−4.690	6.3	···	23.3	41.3	57.3	61.9	88.5	76.8	107.0	105.5
6533.93	Fe I	4.56	−1.360	···	···	···	···	···	···	···	···	7.5	21.7
6581.21	Fe I	1.48	−4.680	···	···	···	···	7.0	23.9	36.9	23.5	41.4	53.6
6592.91	Fe I	2.73	−1.470	24.0	25.7	69.5	86.2	101.8	106.9	130.4	121.8	133.3	139.8
6593.87	Fe I	2.43	−2.370	9.4	···	42.1	57.2	69.9	83.6	103.5	95.9	108.6	119.0
6597.56	Fe I	4.79	−0.970	···	···	···	···	···	···	···	9.0	12.4	18.7
6608.02	Fe I	2.28	−3.930	···	···	···	···	···	10.7	11.3	15.0	24.5	37.7
6609.11	Fe I	2.56	−2.660	···	···	15.0	24.3	39.7	42.7	62.1	63.8	88.2	97.6
6625.02	Fe I	1.01	−5.370	···	···	···	10.5	21.0	20.5	24.4	25.3	50.3	62.1
6627.54	Fe I	4.55	−1.580	···	···	···	···	···	···	···	···	7.9	11.4
6633.75	Fe I	4.79	−0.800	···	···	···	···	13.8	14.0	···	22.0	30.4	···
6646.93	Fe I	2.61	−3.960	···	···	···	···	···	···	···	···	7.2	···
6648.12	Fe I	1.01	−5.920	···	···	···	···	···	···	13.9	···	···	25.5
6703.57	Fe I	2.76	−3.060	···	···	···	···	13.8	21.0	18.2	31.1	45.5	55.8
6716.22	Fe I	4.58	−1.850	···	···	···	···	···	···	···	···	···	7.4
6725.35	Fe I	4.19	−2.250	···	···	···	···	···	···	···	···	8.3	13.6
6726.67	Fe I	4.61	−1.070	···	···	···	···	···	···	···	···	17.1	27.1
6733.15	Fe I	4.64	−1.480	···	···	···	···	···	···	···	···	6.6	12.1
6739.52	Fe I	1.56	−4.790	···	···	···	···	8.5	6.3	···	···	24.6	33.1
6746.95	Fe I	2.61	−4.300	···	···	···	···	···	···	···	5.4	6.6	13.2

Table 3—Continued

λ Å	Ion	χ (eV)	$\log(gf)$ (dex)	33533 (mÅ)	JI19 (mÅ)	36886 (mÅ)	41065 (mÅ)	COS233 (mÅ)	28104 (mÅ)	27940 (mÅ)	JI2 (mÅ)	N37 (mÅ)	COS171 (mÅ)
6750.15	Fe I	2.42	−2.580	5.9	···	34.3	47.9	56.3	65.5	86.8	86.6	102.0	107.1
6752.71	Fe I	4.64	−1.200	···	···	···	···	···	···	···	10.8	9.6	17.4
6783.71	Fe I	2.59	−3.920	···	···	···	···	···	···	···	···	15.9	15.2
6786.86	Fe I	4.19	−1.970	···	···	···	···	···	···	···	···	7.2	17.8
6839.83	Fe I	2.56	−3.350	···	···	···	12.4	8.1	11.2	19.0	17.0	39.1	49.2
6842.68	Fe I	4.64	−1.220	···	···	···	···	···	···	11.3	7.3	···	22.1
6843.65	Fe I	4.55	−0.830	···	···	···	···	···	···	13.3	10.5	28.6	42.2
6851.63	Fe I	1.61	−5.280	···	···	···	···	···	···	···	···	12.8	16.1
6855.18	Fe I	4.56	−0.740	···	···	···	···	15.9	14.3	25.3	20.0	38.0	54.1
6855.71	Fe I	4.61	−1.780	···	···	···	···	···	···	···	···	10.0	8.7
6858.15	Fe I	4.61	−0.930	···	···	···	···	···	···	11.9	···	20.2	26.6
6861.95	Fe I	2.42	−3.850	···	···	···	···	···	7.9	16.3	15.9	20.6	30.2
6862.49	Fe I	4.56	−1.470	···	···	···	···	···	···	···	···	···	13.7
6971.93	Fe I	3.02	−3.340	···	···	···	···	···	···	···	···	7.5	14.1
6978.85	Fe I	2.48	−2.450	7.2	14.0	···	48.6	69.6	···	94.9	95.8	111.1	121.2
6988.52	Fe I	2.40	−3.560	···	···	···	···	···	20.5	27.0	24.9	41.9	58.9
6999.88	Fe I	4.10	−1.460	···	···	···	···	···	15.3	25.9	25.1	29.6	50.1
7007.96	Fe I	4.18	−1.960	···	···	···	···	···	···	···	···	···	19.5
7014.98	Fe I	2.45	−4.200	···	···	···	···	···	···	···	···	···	14.9
7022.95	Fe I	4.19	−1.150	···	···	···	···	···	18.1	20.8	19.4	43.5	54.1
7038.22	Fe I	4.22	−1.200	···	···	···	···	···	11.3	17.5	16.9	26.1	40.4
7112.17	Fe I	2.99	−3.100	···	···	···	5.8	···	···	14.2	···	22.6	41.0
7114.55	Fe I	2.69	−4.000	···	···	···	···	···	···	···	···	···	9.7
7130.92	Fe I	4.22	−0.750	···	···	9.2	13.5	19.8	26.3	38.8	41.7	56.4	71.9
7132.98	Fe I	4.07	−1.750	···	···	···	···	···	···	12.1	0.0	16.5	34.6
7142.52	Fe I	4.95	−1.030	···	···	···	···	···	···	···	···	···	11.2
7151.47	Fe I	2.48	−3.660	···	···	···	···	···	12.6	16.1	19.1	28.8	38.3
7179.99	Fe I	1.48	−4.750	···	···	···	···	···	29.8	···	···	···	···
7181.20	Fe I	4.22	−1.250	···	···	···	···	···	12.8	···	···	···	···
7189.15	Fe I	3.07	−2.830	···	···	···	···	···	12.0	···	···	···	39.5
7284.84	Fe I	4.14	−1.700	···	···	···	···	···	···	···	···	15.9	···
7285.27	Fe I	4.61	−1.660	···	···	···	···	···	···	···	···	···	7.7
7288.74	Fe I	4.22	−1.280	···	···	···	···	···	···	···	23.1	42.8	···
7306.56	Fe I	4.18	−1.690	···	···	···	···	···	···	···	10.0	15.6	27.5
7401.69	Fe I	4.19	−1.350	···	···	···	···	5.7	···	···	···	26.9	26.8
7411.16	Fe I	4.28	−0.280	···	···	21.3	19.3	35.0	37.2	55.0	54.8	71.9	90.8
7418.67	Fe I	4.14	−1.380	···	···	···	···	···	···	8.4	13.7	25.5	32.6
7440.92	Fe I	4.91	−0.720	···	···	···	···	···	···	···	11.4	17.9	27.9
7443.02	Fe I	4.19	−1.780	···	···	···	···	···	···	···	···	17.8	18.7
7445.75	Fe I	4.26	0.030	···	11.3	···	37.3	51.6	···	75.0	61.0	90.7	106.4
7461.52	Fe I	2.56	−3.530	···	···	···	···	···	11.5	18.8	20.9	35.6	48.9
7491.65	Fe I	4.30	−1.070	···	···	···	···	···	21.1	29.3	29.6	38.2	53.0
7495.06	Fe I	4.22	0.230	···	···	37.4	···	64.1	···	96.1	90.0	108.5	126.8
7568.91	Fe I	4.28	−0.940	···	···	···	14.6	17.0	14.9	34.2	40.1	46.5	67.2
7583.79	Fe I	3.02	−1.890	···	6.5	24.9	34.3	51.7	56.9	84.6	73.7	90.5	111.6

Table 3—Continued

λ Å	Ion	χ (eV)	log(gf) (dex)	33533 (mÅ)	JI19 (mÅ)	36886 (mÅ)	41065 (mÅ)	COS233 (mÅ)	28104 (mÅ)	27940 (mÅ)	JI2 (mÅ)	N37 (mÅ)	COS171 (mÅ)
7586.04	Fe I	4.31	−0.130	···	7.7	21.4	25.8	45.0	47.4	65.5	65.0	84.6	97.5
7742.72	Fe I	4.99	−0.420	···	···	···	···	11.2	···	15.6	15.6	18.3	22.5
7748.27	Fe I	2.95	−1.750	7.0	···	39.7	52.3	77.3	80.5	102.0	99.0	117.9	123.2
7751.12	Fe I	4.99	−0.850	···	···	···	···	···	···	8.4	···	17.7	24.5
7780.57	Fe I	4.47	−0.040	···	···	20.1	24.3	43.4	45.4	63.0	63.1	83.0	97.5
7807.92	Fe I	4.99	−0.620	···	···	···	···	···	8.2	···	···	···	36.2
4178.86	Fe II	2.57	−2.530	···	34.6	68.0	81.2	···	···	···	···	···	99.2
4233.17	Fe II	2.57	−2.000	77.0	78.2	105.0	···	86.0	···	···	···	···	129.1
4416.82	Fe II	2.77	−2.430	46.0	25.0	52.7	65.3	63.2	76.0	89.2	91.0	101.4	97.0
4491.40	Fe II	2.84	−2.600	25.5	31.0	37.8	···	68.1	65.0	65.6	···	74.7	92.0
4508.30	Fe II	2.84	−2.280	34.2	40.0	60.4	69.4	78.8	91.2	103.1	117.2	94.4	124.0
4555.89	Fe II	2.82	−2.170	29.1	44.9	73.3	69.2	82.4	91.9	···	···	···	···
4576.34	Fe II	2.83	−2.900	···	···	28.6	37.9	55.6	46.1	52.0	75.3	77.2	89.0
4583.84	Fe II	2.81	−2.020	74.0	64.0	91.8	124.5	110.1	···	···	···	···	···
4923.93	Fe II	2.88	−1.320	90.0	97.5	122.1	133.6	140.7	137.4	···	148.0	151.0	170.0
5018.45	Fe II	2.89	−1.220	103.7	109.0	134.9	151.4	142.1	···	169.7	165.7	···	···
5197.58	Fe II	3.23	−2.230	22.5	34.4	53.4	53.0	71.3	66.9	91.4	88.0	88.0	98.8
5234.63	Fe II	3.22	−2.220	24.3	27.9	53.7	62.4	71.5	71.4	83.8	82.0	87.6	99.8
5414.08	Fe II	3.22	−3.620	···	···	···	···	11.3	12.4	18.2	19.0	20.5	35.0
5425.26	Fe II	3.00	−3.240	···	···	···	19.6	17.0	24.9	28.5	25.0	38.9	40.0
5534.85	Fe II	3.25	−2.640	10.6	12.0	21.6	24.8	42.3	43.4	54.0	47.3	55.4	72.0
5991.38	Fe II	3.15	−3.570	···	···	···	11.3	17.6	···	23.5	16.7	21.3	44.6
6084.11	Fe II	3.20	−3.800	···	···	···	···	···	···	···	···	19.2	26.3
6149.26	Fe II	3.89	−2.690	···	···	10.3	···	9.8	11.6	12.2	···	18.6	31.8
6247.56	Fe II	3.89	−2.360	···	···	···	24.8	20.4	42.6	57.0	30.5	35.5	56.3
6369.46	Fe II	2.89	−4.200	···	···	···	9.3	11.2	7.6	13.1	···	16.9	26.9
6416.92	Fe II	3.89	−2.690	···	···	···	···	···	···	19.8	18.0	16.5	31.5
6516.08	Fe II	2.89	−3.450	7.8	···	21.4	21.8	31.7	37.1	51.9	44.5	49.9	63.0
7449.34	Fe II	3.89	−3.310	···	···	···	···	···	···	···	10.0	···	19.2
4121.31	Co I	0.92	−0.315	···	70.0	158.6	141.7	148.9	163.6	···	···	···	···
5530.79	Co I	1.71	−2.060	···	···	···	···	···	11.4	15.0	···	18.0	21.8
5647.23	Co I	2.28	−1.560	···	···	···	···	···	···	···	···	11.7	···
6189.00	Co I	1.71	−2.450	···	···	···	12.0	···	8.9	11.5	···	12.9	···
6632.45	Co I	2.28	−2.000	···	···	···	···	···	···	···	···	10.0	···
7417.41	Co I	2.04	−2.070	···	···	···	···	···	···	···	···	11.5	···
5578.72	Ni I	1.68	−2.640	···	···	20.9	20.9	30.6	48.3	46.7	50.6	68.3	51.7
5587.86	Ni I	1.93	−2.140	···	···	15.5	21.8	34.8	47.6	52.4	48.8	69.5	53.8
5592.26	Ni I	1.95	−2.590	···	···	13.0	16.4	···	39.2	47.8	···	···	60.2
5748.35	Ni I	1.68	−3.260	···	···	8.7	11.1	16.1	20.4	···	22.2	31.5	17.2
5760.83	Ni I	4.10	−0.805	···	···	···	···	···	···	···	···	8.5	···
5846.99	Ni I	1.68	−3.210	···	···	···	···	···	12.4	13.9	17.5	24.1	13.1
5892.87	Ni I	1.99	−2.340	···	···	···	25.4	50.5	56.5	51.5	55.0	76.8	75.0
6086.28	Ni I	4.26	−0.515	···	···	···	···	···	···	···	···	7.8	···
6128.97	Ni I	1.68	−3.330	···	···	···	4.7	7.7	20.3	22.8	22.0	30.1	17.2
6175.37	Ni I	4.09	−0.535	···	···	···	···	8.5	···	12.1	···	13.5	16.2

Table 3—Continued

λ Å	Ion	χ (eV)	$\log(gf)$ (dex)	33533 (mÅ)	JI19 (mÅ)	36886 (mÅ)	41065 (mÅ)	COS233 (mÅ)	28104 (mÅ)	27940 (mÅ)	JI2 (mÅ)	N37 (mÅ)	COS171 (mÅ)
6176.81	Ni I	4.09	−0.529	···	···	···	···	10.4	16.5	14.1	···	14.0	17.5
6177.24	Ni I	1.83	−3.510	···	···	···	···	···	10.8	9.2	9.1	13.0	···
6314.66	Ni I	1.93	−1.770	···	···	···	···	···	···	···	110.2	···	···
6482.80	Ni I	1.93	−2.630	···	···	11.3	8.0	···	26.2	24.4	26.6	37.1	31.5
6586.31	Ni I	1.95	−2.810	···	···	15.4	12.2	15.7	26.5	34.6	35.0	43.0	34.6
6643.63	Ni I	1.68	−2.300	8.4	14.6	46.6	58.1	76.9	96.9	106.3	104.0	120.7	102.3
6767.77	Ni I	1.83	−2.170	9.0	10.0	42.0	45.8	65.7	83.8	91.9	83.8	105.4	88.3
6772.31	Ni I	3.66	−0.987	···	···	···	···	10.8	12.1	12.4	16.7	18.8	17.0
6842.04	Ni I	3.66	−1.470	···	···	···	···	···	···	···	···	8.4	3.7
7110.88	Ni I	1.93	−2.970	···	···	···	10.1	9.9	23.9	29.9	18.4	37.0	23.6
7122.20	Ni I	3.54	0.048	···	···	35.2	40.1	38.7	···	65.9	59.2	75.0	65.7
7197.01	Ni I	1.93	−2.680	···	···	···	24.1	···	···	···	···	···	···
7261.92	Ni I	1.95	−2.700	···	···	9.2	17.7	31.0	37.6	45.3	49.7	···	57.3
7409.35	Ni I	3.80	−0.100	···	···	9.4	15.3	···	34.9	39.1	···	···	48.0
7414.50	Ni I	1.99	−2.570	···	···	13.3	21.7	38.6	53.1	59.0	53.0	75.7	64.2
7422.27	Ni I	3.63	−0.129	···	13.7	22.0	20.0	37.7	41.8	45.6	51.7	63.4	56.1
7574.05	Ni I	3.83	−0.580	···	···	···	···	14.8	14.1	22.0	18.0	34.0	29.9
7727.62	Ni I	3.68	−0.162	···	···	22.6	21.3	27.3	48.7	48.1	45.5	58.1	50.4
7748.89	Ni I	3.70	−0.130	···	···	12.4	26.6	35.0	40.0	32.0	42.8	55.4	50.0
7788.93	Ni I	1.95	−2.420	···	···	35.6	···	63.0	81.5	92.2	86.0	102.5	92.8
7797.59	Ni I	3.90	−0.180	···	···	···	···	13.5	26.9	32.4	24.2	45.1	31.3
5105.54	Cu I	1.39	−1.505	···	···	···	···	28.0	30.0	39.8	47.0	62.5	34.0
5782.12	Cu I	1.64	−1.780	···	···	···	···	13.3	11.5	20.8	11.0	30.1	11.1
4722.16	Zn I	4.03	−0.390	···	15.0	23.8	17.2	26.9	25.2	30.0	29.9	35.9	16.0
4810.54	Zn I	4.08	−0.170	14.0	21.0	23.1	20.3	27.9	25.1	38.0	44.0	40.8	24.4
4077.71	Sr II	0.00	0.170	207.3	168.3	205.1	239.5	···	245.0	···	···	···	···
4215.52	Sr II	0.00	−0.140	188.8	162.6	199.6	218.8	186.0	236.0	237.7	···	···	243.0
4554.04	Ba II	0.00	0.170	74.1	89.2	181.9	193.4	215.0	153.2	243.7	251.7	···	190.4
4934.16	Ba II	0.00	−0.150	71.7	68.1	210.0	200.0	214.0	···	264.0	265.0	275.0	···
5853.70	Ba II	0.60	−1.010	10.0	···	60.8	63.1	86.0	40.6	102.3	134.0	128.0	93.5
6141.70	Ba II	0.70	−0.070	34.5	35.2	107.7	120.8	130.0	95.2	170.5	171.2	173.8	129.4
6496.90	Ba II	0.60	−0.380	22.7	12.6	109.0	120.9	127.2	90.7	168.1	174.7	170.6	125.7
3950.36	Y II	0.10	−0.490	55.2	···	···	···	···	···	···	···	···	···
4398.01	Y II	0.13	−1.000	43.5	24.7	34.6	53.0	70.4	45.0	75.0	94.9	94.0	47.5
4883.69	Y II	1.08	0.070	32.3	31.0	23.3	31.0	39.4	39.3	74.0	73.1	82.8	49.8
5087.43	Y II	1.08	−0.170	24.3	···	13.2	21.0	28.2	23.7	55.0	60.0	66.3	27.4
5123.22	Y II	0.99	−0.830	13.0	···	···	···	···	···	20.8	···	35.6	···
5200.42	Y II	0.99	−0.570	···	···	13.6	···	···	13.3	35.4	52.4	58.5	25.3
6134.55	Zr I	0.00	−1.280	···	···	···	···	···	···	···	···	9.0	···
4161.21	Zr II	0.71	−0.720	···	···	···	···	···	40.1	···	···	···	···
4208.99	Zr II	0.71	−0.460	43.3	41.0	25.7	46.5	42.9	54.7	62.0	88.4	83.0	40.5
5112.28	Zr II	1.66	−0.590	···	···	···	···	···	···	···	24.0	28.0	···
4086.71	La II	0.00	−0.070	···	···	35.0	53.2	44.9	···	73.9	···	···	···
4333.76	La II	0.17	−0.060	···	···	42.4	21.5	43.3	13.3	85.0	···	···	···
5114.56	La II	0.23	−1.030	···	···	···	···	···	···	···	54.0	66.0	···

Table 3—Continued

λ Å	Ion	χ (eV)	log(gf) (dex)	33533 (mÅ)	JI19 (mÅ)	36886 (mÅ)	41065 (mÅ)	COS233 (mÅ)	28104 (mÅ)	27940 (mÅ)	JI2 (mÅ)	N37 (mÅ)	COS171 (mÅ)
6320.38	La II	0.17	−1.562	···	···	···	···	···	···	···	···	31.0	···
6390.48	La II	0.32	−1.410	···	···	···	···	···	···	13.5	28.6	29.3	6.3
6774.26	La II	0.13	−1.720	···	···	···	···	···	···	···	21.5	···	···
4222.60	Ce II	0.12	−0.180	···	···	···	···	···	···	···	···	65.9	···
4418.79	Ce II	0.86	0.310	···	···	···	···	···	···	···	···	32.5	···
4486.91	Ce II	0.30	−0.360	···	···	···	···	27.0	···	16.7	48.4	57.8	···
4562.37	Ce II	0.48	0.330	···	···	14.6	24.8	34.0	···	39.0	68.5	64.8	30.6
4628.16	Ce II	0.52	0.260	···	···	···	···	16.0	···	41.3	59.3	59.9	23.5
5274.23	Ce II	1.04	0.150	···	···	···	···	···	···	···	···	30.0	···
5220.12	Pr II	0.80	0.170	···	···	···	···	7.4	···	13.2	15.6	29.5	···
5259.74	Pr II	0.63	0.082	···	···	···	···	···	···	···	26.0	33.0	···
4061.09	Nd II	0.47	0.550	···	···	31.9	···	56.0	···	···	···	88.0	···
4109.46	Nd II	0.32	0.350	···	···	49.8	81.3	60.0	···	···	···	···	···
4232.38	Nd II	0.06	−0.470	···	···	21.8	···	28.8	···	···	···	···	···
4446.39	Nd II	0.20	−0.350	···	···	···	···	31.1	···	46.5	69.7	84.0	23.1
4462.99	Nd II	0.56	0.040	···	···	···	···	26.1	···	49.0	···	87.0	···
4947.02	Nd II	0.56	−1.130	···	···	···	···	···	···	···	···	17.2	···
4959.12	Nd II	0.06	−0.800	···	···	···	···	···	···	···	65.0	74.0	···
5076.58	Nd II	0.74	−0.386	···	···	···	···	···	···	···	···	37.0	···
5092.79	Nd II	0.38	−0.610	···	···	···	13.5	14.0	···	28.8	43.8	44.0	11.1
5130.59	Nd II	1.30	0.450	···	···	···	···	···	···	24.8	35.6	43.9	···
5212.35	Nd II	0.20	−0.960	···	···	···	···	20.0	···	27.6	37.8	50.4	···
5249.58	Nd II	0.98	0.200	···	···	5.5	···	18.4	···	34.5	46.3	59.5	18.4
4318.94	Sm II	0.28	−0.270	···	···	···	···	20.7	···	51.1	73.8	···	···
4537.95	Sm II	0.48	−0.230	···	···	···	···	···	···	···	···	50.0	···
4815.81	Sm II	0.19	−0.770	···	···	···	···	···	···	···	51.0	61.0	···
4948.63	Sm II	0.54	−0.840	···	···	···	···	···	···	···	···	26.0	···
4129.70	Eu II	0.00	0.220	24.0	≤29.7	95.0	110.0	···	30.0	194.0	···	···	···
6437.64	Eu II	1.32	−0.320	···	···	···	···	···	···	···	24.0	32.0	···
6645.11	Eu II	1.38	0.120	···	···	6.4	6.5	11.3	···	19.0	38.5	44.0	11.7
4085.57	Gd II	0.56	−0.230	···	···	···	···	···	···	···	···	42.0	···
4103.31[b]	Dy II	0.10	−0.370	···	···	48.4	···	91.1	···	106.9	111.8	131.0	···
4468.14	Dy II	0.10	−1.500	···	···	···	···	···	···	···	20.0	35.2	···
5169.69	Dy II	0.10	−1.660	···	···	···	···	···	···	6.5	13.0	21.5	···

[a] Dubious line, probably should not have been used.

[b] This line gives an abundance ∼1.0 dex higher than the other two Dy II lines, and is ignored in computing the Dy abundance.

Table 4. Fit Fe I Slopes With EP, Equivalent Width, and Wavelength

Star ID	Δ[X/Fe]/Δ(EP)[a] (dex/eV)	Δ[X/Fe]/Δ[W_λ/λ] (dex)	Δ[X/Fe]/Δλ (10^{-4}dex/Å)
COS171	0.00	−0.03	−0.07
COS233	−0.05	0.01	−0.09
JI2	−0.04	0.00	−0.18
JI19	−0.07	0.03	−0.05
N37	−0.04	0.00	−0.59
27940	−0.02	−0.02	−0.43
28104	−0.05	−0.02	−0.25
36886	−0.05	−0.03	−0.29
33533	−0.11[b]	0.01	0.04
41065	−0.06	−0.02	−0.23

[a] Typical range of EP is 4 eV. This slope decreases by ∼0.1 dex/eV for an increase in T_{eff} of 250 K.

[b] Correlation coefficient is very low.

Table 5a. Abundances for the First Five UMi Stars

Species	UMi 33533 [Fe/H] −3.10				UMi JI19 [Fe/H] −3.08				UMi 36886 [Fe/H] −2.43				UMI 41065 [Fe/H] −2.42				UMi COS233 [Fe/H] −2.15			
	[X/Fe] (dex)	logϵ(X) (dex)	No. Lines	σ[a] (dex)	[X/Fe] (dex)	logϵ(X) (dex)	No. Lines	σ[a] (dex)	[X/Fe] (dex)	logϵ(X) (dex)	No. Lines	σ[a] (dex)	[X/Fe] (dex)	logϵ(X) (dex)	No. Lines	σ[a] (dex)	[X/Fe] (dex)	logϵ(X) (dex)	No. Lines	σ[a] (dex)
C(CH)[b]	−0.03	5.46	1	···	−0.15	5.36	1	···	−0.88	5.28	1	···	−0.66	5.51	1	···	−0.76	5.68	1	···
O I	···	···	···	···	···	···	···	···	0.58	6.99	1	···	0.39	6.80	1	···	0.56	7.24	1	···
Na I	−0.42	2.80	2	0.06	−0.23	3.01	2	0.06	−0.17	3.73	2	0.06	−0.29	3.61	3	0.15	−0.37	3.80	3	0.17
Mg I	0.28	4.72	4	0.13	0.43	4.89	4	0.12	0.42	5.53	5	0.05	0.42	5.54	5	0.21	0.34	5.73	5	0.19
Al I[c]	0.53	3.90	1	···	0.47	3.85	1	···	−0.53	3.51	1	···	···	···	···	···	−0.18	4.15	1	···
Si I	0.36	4.81	1	···	0.98	5.45	2	0.10	0.34	5.47	5	0.17	0.44	5.57	4	0.24	0.29	5.69	4	0.16
K I	0.04	2.06	1	···	0.45	2.49	1	···	0.40	3.09	1	···	0.22	2.92	1	···	0.35	3.32	1	···
Ca I	0.05	3.31	8	0.19	0.33	3.61	12	0.19	0.14	4.07	18	0.15	0.11	4.05	16	0.16	0.05	4.26	19	0.15
Sc II	−0.30	−0.30	3	0.17	0.03	0.05	6	0.08	0.05	0.72	10	0.14	0.02	0.70	8	0.21	0.14	1.09	8	0.16
Ti I	−0.03	1.85	9	0.10	0.35	2.25	8	0.09	0.00	2.57	17	0.13	0.03	2.60	17	0.15	−0.03	2.81	22	0.13
Ti II	0.02	1.91	12	0.19	0.37	2.28	19	0.19	0.23	2.79	18	0.13	0.24	2.81	14	0.21	0.20	3.04	13	0.23
V I	···	···	···	···	···	···	···	···	0.04	1.61	2	0.11	−0.04	1.54	3	0.15	−0.05	1.81	4	0.19
Cr I	−0.54	2.03	6	0.25	−0.44	2.15	6	0.24	−0.30	2.94	8	0.09	−0.29	2.96	8	0.18	−0.32	3.21	7	0.08
Mn I	−0.71[d]	1.58[d]	2	0.11	−0.85[d]	1.46[d]	2	0.04	−0.41	2.55	3	0.13	−0.27	2.70	5	0.34	−0.47	2.77	6	0.14
Fe I[e]	−3.10	4.35	76	0.22	−3.08	4.37	79	0.19	−2.43	5.02	85	0.16	−2.41	5.03	100	0.20	−2.15	5.30	115	0.17
Fe II	0.08	4.43	12	0.22	0.09	4.46	12	0.13	−0.06	4.97	15	0.14	0.03	5.06	16	0.26	−0.03	5.27	19	0.20
Co I	···	···	···	···	−0.04	1.79	1	···	0.53	3.02	1	···	0.39	2.89	2	0.31	−0.08	2.69	1	···
Ni I	−0.08	3.07	2	0.06	0.14	3.31	3	0.15	−0.03	3.79	16	0.21	−0.12	3.71	19	0.18	−0.08	4.02	21	0.21
Cu I	···	···	···	···	···	···	···	···	···	···	···	···	···	···	···	···	−0.68	1.39	2	0.10
Zn I	0.39	1.88	1	···	0.58	2.09	2	0.01	0.07	2.24	2	0.13	−0.14	2.04	2	0.07	−0.17	2.28	2	0.11
Sr II	0.17	−0.03	2	0.08	−0.25	−0.43	2	0.07	−0.27	0.21	2	0.11	−0.19	0.29	2	0.04	−0.53	0.22	1	···
Y II	0.16	−0.70	5	0.18	−0.08	−0.92	2	0.12	−0.71	−0.90	4	0.14	−0.65	−0.83	3	0.19	−0.58	−0.49	3	0.31
Zr II	0.57	0.07	1	···	0.52	0.04	1	···	−0.40	−0.23	1	···	−0.10	0.08	1	···	−0.36	0.09	1	···
Ba II	−0.99	−1.96	5	0.21	−1.16	−2.11	4	0.07	−0.35	−0.65	5	0.18	−0.51	−0.80	5	0.09	−0.18	−0.20	5	0.13
La II	···	···	···	···	···	···	···	···	−0.11	−1.39	2	0.15	−0.26	−1.54	2	0.42	−0.27	−1.27	2	0.08
Ce II	···	···	···	···	···	···	···	···	−0.31	−1.19	1	···	−0.09	−0.96	1	···	−0.11	−0.70	3	0.33
Pr II	···	···	···	···	···	···	···	···	···	···	···	···	···	···	···	···	0.25	−1.19	1	···
Nd II	···	···	···	···	···	···	···	···	−0.05	−0.97	4	0.19	0.32	−0.60	2	0.53	0.03	−0.62	8	0.11
	···	···	···	···	···	···	···	···	···	···	···	···	···	···	···	···	0.08	−1.07	1	···
Eu II	−0.24	−2.83	1	···	≤0.40	≤-2.17	1	···	0.44	−1.48	2	0.09	−0.02	−1.93	2	0.14	0.52	−1.12	1	···

[a] σ is the dispersion of the abundance ratio for each absorption line about the mean for the species.

[b] The 4320 Å region of the G band of CH was used.

[c] A non-LTE correction of +0.6 dex was used for stars where only the 3961 Å resonance line was measured.

[d] An offset of +0.2 dex was applied if only the 4030 Å triplet lines could be detected.

[e] [Fe/H](Fe I) is given instead of [X/Fe].

Table 5b. Abundances for the Last Five UMi Stars

Species	UMi 28104 [Fe/H] −2.08				UMi 27940 [Fe/H] −1.91				UMi JI2 [Fe/H] −1.76				UMi N37 [Fe/H] −1.55				UMi COS171 [Fe/H] −1.35			
	[X/Fe] (dex)	$\log\epsilon(X)$ (dex)	No. Lines	σ^{a} (dex)	[X/Fe] (dex)	$\log\epsilon(X)$ (dex)	No. Lines	σ^{a} (dex)	[X/Fe] (dex)	$\log\epsilon(X)$ (dex)	No. Lines	σ^{a} (dex)	[X/Fe] (dex)	$\log\epsilon(X)$ (dex)	No. Lines	σ^{a} (dex)	[X/Fe] (dex)	$\log\epsilon(X)$ (dex)	No. Lines	σ^{a} (dex)
C(CH)[b]	−0.54	5.97	1	···	−0.82	5.86	1	···	−0.77	6.06	1	···	−0.68	6.36	1	···	−1.06	6.18	1	···
O I	0.44	7.20	1	···	0.34	7.26	1	···	0.20	7.26	1	···	0.15	7.43	2	0.09	0.02	7.51	2	0.24
Na I	−0.40	3.84	3	0.12	−0.44	3.97	4	0.06	−0.64	3.92	4	0.03	−0.72	4.05	4	0.10	−1.27	3.70	3	0.08
Mg I	0.40	5.87	5	0.19	0.30	5.93	6	0.15	0.23	6.00	4	0.12	0.13	6.12	4	0.18	−0.35	5.85	3	0.22
Al I[c]	0.13	4.52	1	···	···	···	···	···	···	···	···	···	0.01	4.93	2	0.21	···	···	···	···
Si I	0.21	5.68	6	0.16	0.12	5.77	10	0.12	0.14	5.93	9	0.18	0.04	6.04	9	0.10	−0.19	6.01	9	0.15
K I	0.24	3.29	1	···	0.26	3.47	1	···	0.16	3.52	1	···	0.20	3.78	1	···	−0.12	3.65	1	···
Ca I	0.02	4.30	20	0.14	0.01	4.46	17	0.21	−0.08	4.52	18	0.18	−0.10	4.71	17	0.16	−0.36	4.66	18	0.18
Sc II	−0.04	0.98	8	0.07	−0.07	1.12	8	0.20	−0.24	1.09	7	0.08	−0.25	1.30	7	0.10	−0.74	1.01	7	0.10
Ti I	−0.08	2.83	26	0.16	−0.05	3.03	28	0.16	−0.02	3.20	23	0.13	−0.05	3.40	31	0.15	−0.59	3.06	22	0.14
Ti II	0.16	3.08	14	0.19	0.10	3.18	7	0.23	0.08	3.31	11	0.22	0.05	3.49	8	0.25	−0.41	3.24	14	0.19
V I	−0.21	1.71	5	0.18	−0.25	1.84	7	0.22	−0.26	1.98	4	0.08	−0.27	2.18	8	0.09	−0.85	1.80	7	0.13
Cr I	−0.37	3.22	8	0.08	−0.22	3.54	6	0.10	−0.22	3.69	7	0.15	−0.12	4.01	9	0.18	−0.34	3.98	9	0.17
Mn I	−0.48	2.83	4	0.03	−0.32	3.16	5	0.21	−0.34	3.29	4	0.12	−0.26	3.58	5	0.15	−0.83	3.21	7	0.14
Fe I[d]	−2.08	5.37	126	0.15	−1.91	5.54	134	0.18	−1.76	5.69	148	0.16	−1.55	5.90	164	0.16	−1.35	6.10	190	0.14
Fe II	−0.05	5.32	15	0.14	0.06	5.60	16	0.21	−0.06	5.63	15	0.33	−0.11	5.79	17	0.19	0.00	6.10	20	0.17
Co I	0.10	2.94	3	0.15	−0.01	3.00	2	0.14	···	···	···	···	−0.14	3.24	5	0.13	−0.36	3.21	1	···
Ni I	−0.02	4.15	24	0.16	−0.25	4.09	25	0.21	−0.23	4.26	23	0.21	−0.27	4.43	26	0.19	−0.62	4.29	26	0.21
Cu I	−0.81	1.32	2	0.02	−0.91	1.39	2	0.11	−0.95	1.50	2	0.19	−0.90	1.76	2	0.02	−1.56	1.31	2	0.03
Zn I	−0.30	2.22	2	0.13	−0.26	2.43	2	0.02	−0.34	2.49	2	0.10	−0.47	2.58	2	0.06	−1.10	2.16	2	0.04
Sr II	−0.25	0.57	2	0.11	−0.33	0.67	1	···	···	···	···	···	···	···	···	···	−0.62	0.93	1	···
Y II	−0.91	−0.75	4	0.09	−0.55	−0.22	5	0.11	−0.39	0.09	4	0.20	−0.39	0.30	5	0.12	−1.31	−0.41	4	0.10
Zr II	−0.23	0.29	2	0.03	−0.25	0.44	1	···	0.14	0.98	2	0.07	0.01	1.06	2	0.06	−1.10	0.15	1	···
Ba II	−1.04	−0.99	4	0.06	−0.05	0.17	5	0.15	0.27	0.64	5	0.25	0.19	0.77	4	0.09	−0.75	0.03	4	0.12
La II	−1.03	−1.97	1	···	0.02	−0.75	3	0.04	0.37	−0.25	3	0.10	0.39	−0.01	3	0.15	−0.68	−0.88	1	···
Ce II	···	···	···	···	−0.29	−0.65	3	0.10	0.15	−0.06	3	0.10	0.06	0.07	6	0.12	−0.70	−0.50	3	0.36
Pr II	···	···	···	···	0.19	−1.01	1	···	0.28	−0.77	2	0.10	0.41	−0.43	2	0.05	···	···	···	···
Nd II	···	···	···	···	0.03	−0.37	6	0.06	0.25	−0.01	6	0.06	0.36	0.31	10	0.15	−0.82	−0.66	3	0.11
	···	···	···	···	0.38	−0.52	1	···	0.66	−0.10	2	0.12	0.48	−0.06	3	0.15	···	···	···	···
Eu II	−0.74	−2.31	1	···	0.61	−0.79	2	0.27	0.83	−0.42	2	0.07	0.87	−0.16	2	0.12	−0.18	−1.02	1	···
	···	···	···	···	···	···	···	···	···	···	···	···	0.46	0.03	1	···	···	···	···	···
Dy II	···	···	···	···	0.35	−0.46	1	···	0.97	0.31	2	0.03	0.76	0.31	2	0.03	···	···	···	···

[a] σ is the dispersion of the abundance ratio for each absorption line about the mean for the species.

[b] The 4320 Å region of the G band of CH was used.

[c] A non-LTE correction of +0.6 dex was used for stars where only the 3961 Å resonance line was measured.

[d] [Fe/H](Fe I) is given instead of [X/Fe].

Table 6. Parameters for the Toy Model of Abundance Ratios[a] Applied to the Ursa Minor Giants

Species [X/Fe]	A(X) (dex)	B(X) (dex)	[Fe/H](A) (dex)	[Fe/H](B) (dex)	[Fe/H](low,X) (dex)	[Fe/H](high,X) (dex)
[Na/Fe]	−0.33	−0.70	−3.09	−1.58	−2.18	−1.75
[Mg/Fe][c]	0.36	0.22	−3.09	−1.58	−1.94	−1.82
thick disk[b]	0.35	0.00	−1.00	0.00	−0.53	−0.07
thin disk[b]	0.11	0.02	−0.70	0.05	−0.50	−0.10
[Si/Fe]	0.67	0.05	−3.09	−1.58	−2.91	−1.64
[Ca/Fe]	0.19	0.04	−3.09	−1.58	−2.67	−2.12
[Sc/Fe]	−0.13	−0.17	−3.09	−1.58	−1.88	−1.82
[Ti12/Fe][c]	0.13	0.04	−3.09	−1.58	−3.03	−1.64
[Cr/Fe]	−0.49	−0.06	−3.09	−1.58	−2.79	−1.64
[Mn/Fe][d]	−0.78	−0.12	−3.09	−1.58	−3.03	−1.64
[Ni/Fe]	0.03	−0.20	−3.09	−1.58	−3.03	−2.24
[Zn/Fe]	0.48	−0.23	−3.09	−1.58	−3.03	−1.64
[Ba/Fe]	−1.08	0.25	−3.09	−1.58	−2.73	−1.64
$[\alpha/\mathrm{Fe}]$[e]	… [f]	… [f]	… [f]	… [f]	−2.78 ± 0.3	−1.53 (−0.3)
[Fe − peak/Fe][e]	… [f]	… [f]	… [f]	… [f]	−3.0 ± 0.25	−1.53 (−0.2)
[Combo/Fe][g]	… [f]	… [f]	… [f]	… [f]	−2.85 ± 0.2	−1.52 (−0.2)

[a] The model and its parameters are described in §5.1. The low outlier COS171 is not used for any of the fits.

[b] Fits to the Milky Way thin and thick disk sample of Reddy et al (2003) and Reddy, Lambert & Allende Prieto (2006) for [Mg/Fe] vs [Fe/H].

[c] [Ti12/Fe] = [Ti from TiI/Fe from FeI] + [Ti from TiII/Fe from FeII])/2.

[d] An offset of +0.2 dex was applied to [Mn/Fe] for the two lowest [Fe/H] stars as only the 4030 Å lines were detected.

[e] α elements = Mg, Si, Ca and Ti12. Fe-peak elements = Cr, Mn, and Ni. 2-σ uncertainties are tabulated.

[f] The values of A(X), B(X), [Fe/H](A) and [Fe/H](B) were assumed from each individual fit.

[g] “Combo” combines Si, Cr, Mn, Ni, and Ba, the elements with the strongest dependence of

[X/Fe] on [Fe/H] in our UMi sample. 2-σ uncertainties are tabulated.

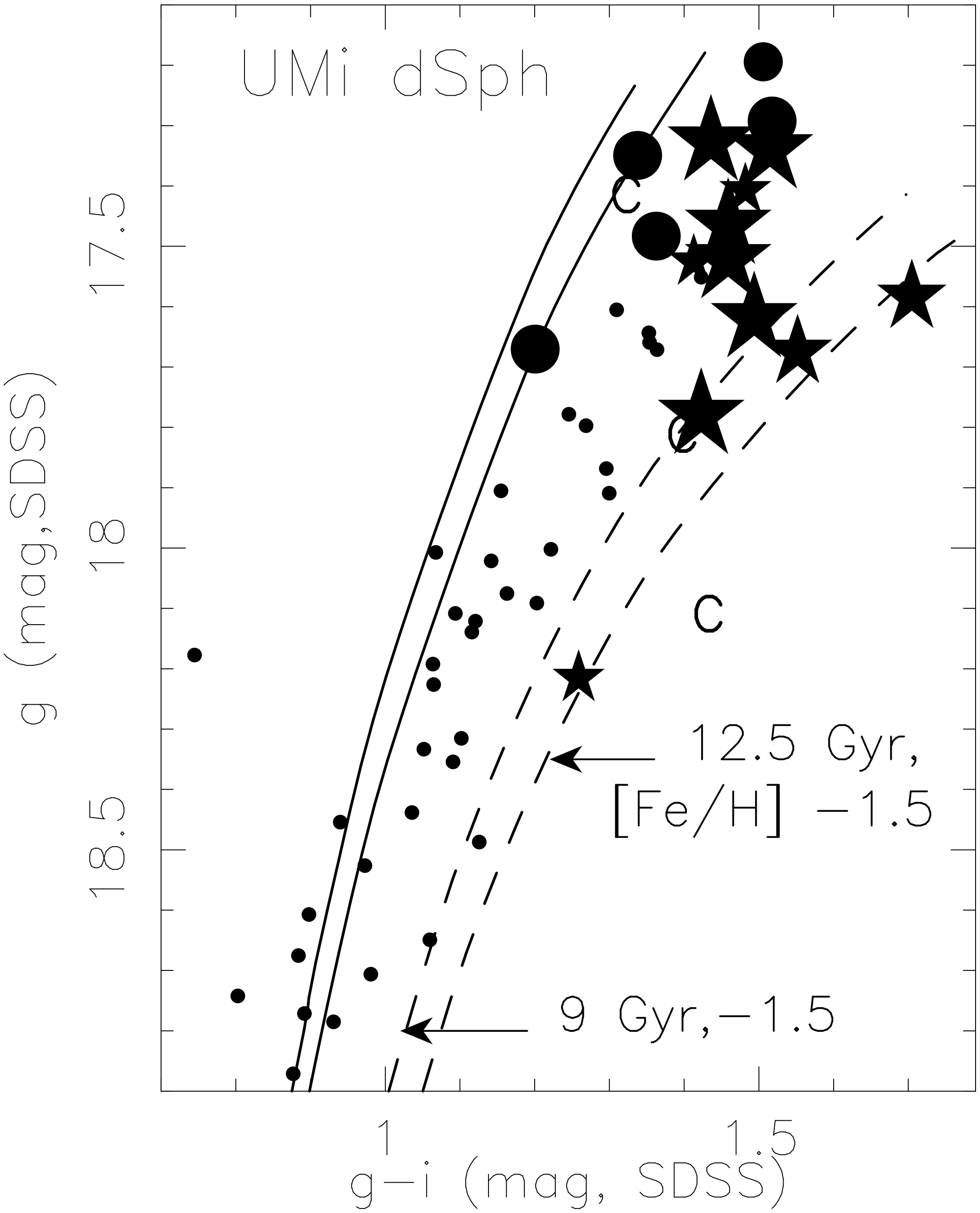

Fig. 1.— Our UMi HIRES sample is shown in a plot of $g' - i$ versus g' (large symbols), where filled circles indicate giants with [Fe/H] < -2.5 dex, and star symbols have higher Fe-metallicity. The sample of UMi stars studied by Shetrone, Côté & Sargent (2001) and by Sadakane et al. (2004) are indicated by the small and intermediate sized symbols. The dots indicate UMi members from Winnick (2003) with photometry from the SDSS. Carbon stars that are confirmed members of UMi from Shetrone, Bolte & Stetson (1998) are indicated by the letter C. All observerational data are corrected for interstellar reddening. Isochrones from the Dartmouth Stellar Evolution Database (Dotter *et al.* 2008) for [Fe/H] -2.5 dex with $[\alpha/\mathrm{Fe}] = +0.2$ dex (solid lines) and for [Fe/H] -1.5 dex with $[\alpha/\mathrm{Fe}]$ Solar (dashed lines) for ages 9 and 12.5 Gyr are shown.

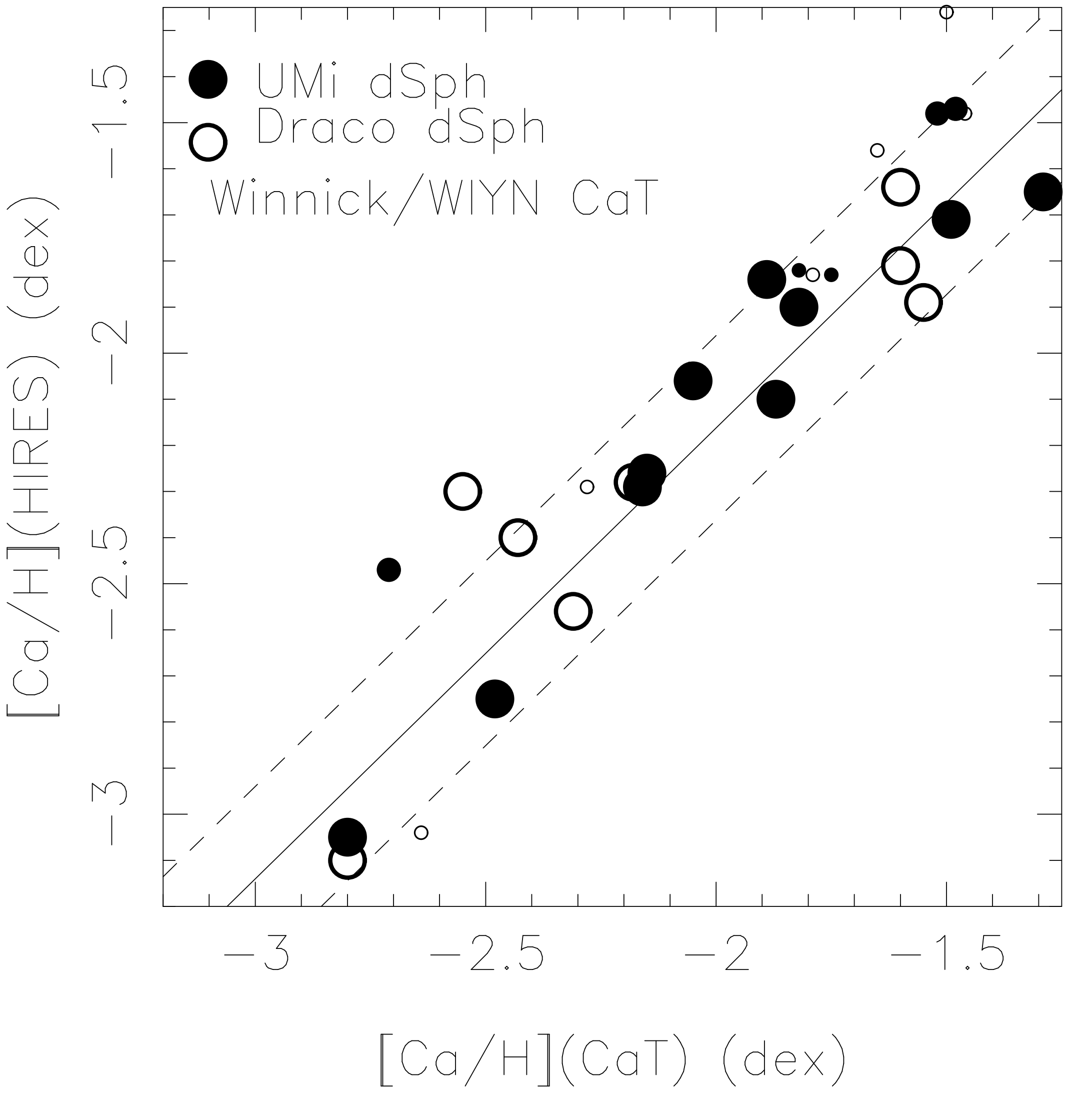

Fig. 2.— The [Ca/H] values derived from indices of the strength of the infrared Ca triplet by Winnick (2003) are compared to the results of our high-resolution detailed abundance analyses for our sample of 10 RGB stars in each of the UMi and the Draco dSph galaxy. The solid line represents the best fit to the UMi data, while the dashed lines show offsets between the two determinations of ±0.2 dex. Smaller symbols denote 3 UMi stars from Sadakane et al. (2004), while the smallest symbols are from Shetrone, Côté & Sargent (2001).

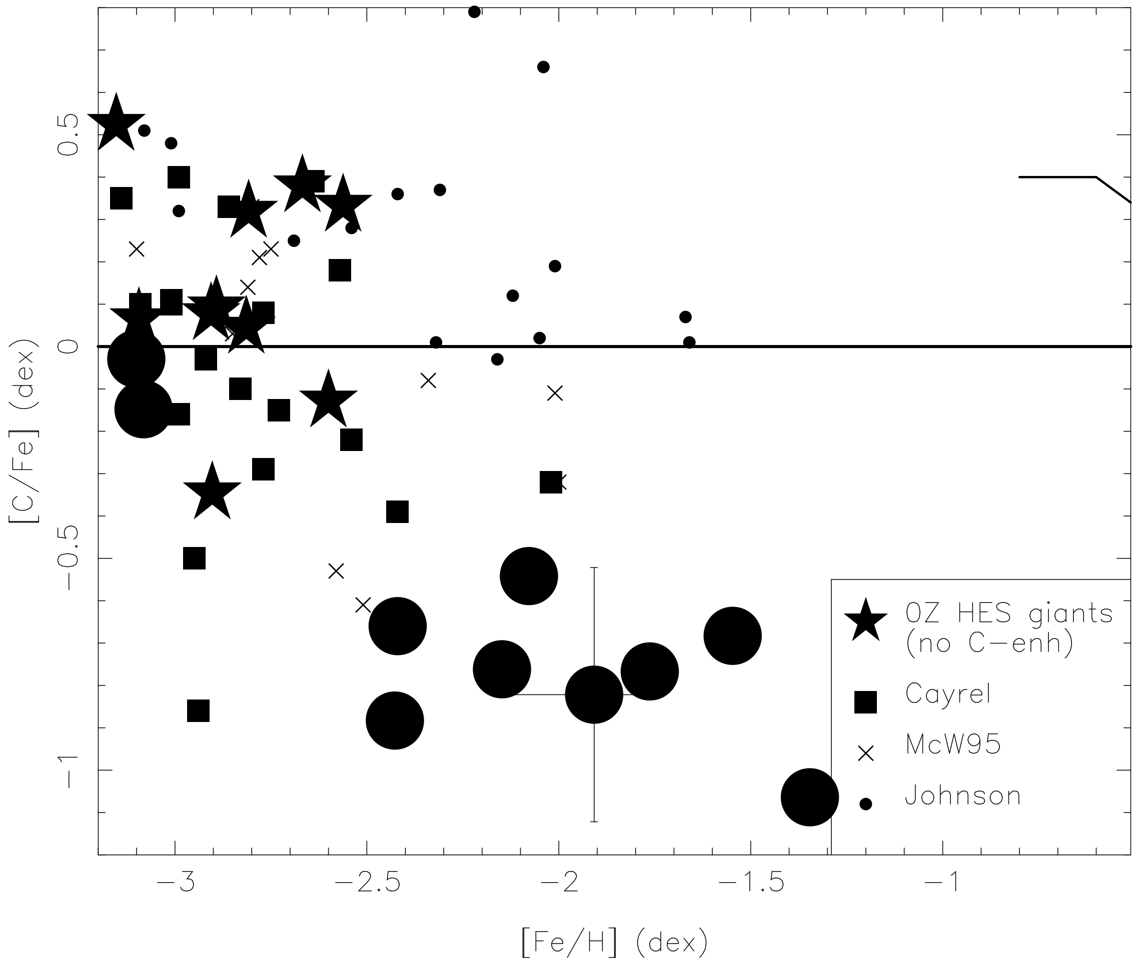

Fig. 3.— [C/Fe] from the G band of CH vs [Fe/H] for UMi giants from our sample (large filled circles). The symbol key for the other sources is given on each figure. Typical uncertainties are shown for one star. The line represents the behavior of halo dwarfs from Reddy, Lambert & Allende Prieto (2006).

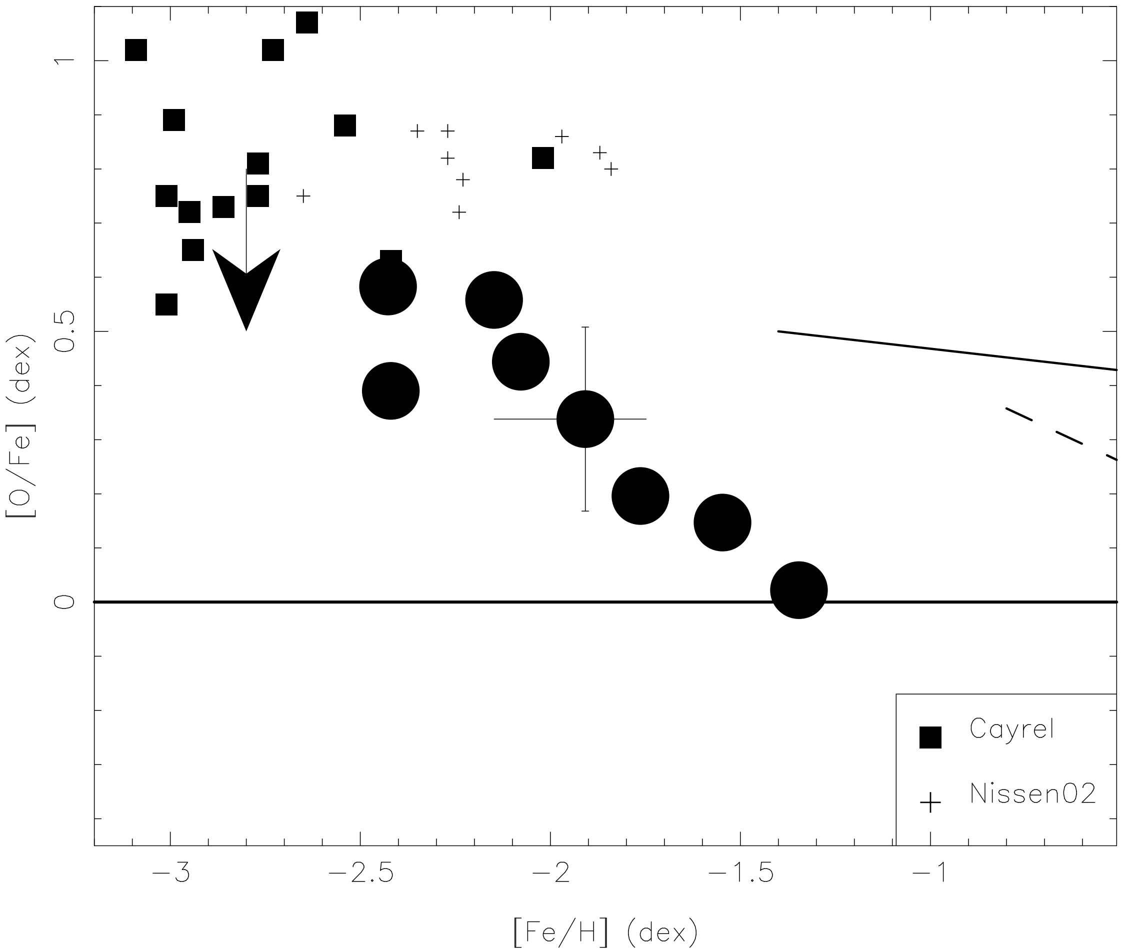

Fig. 4.— [O/Fe] vs [Fe/H]. UMi stars from our sample are shown as large filled circles. Typical uncertainties are shown for one star. The small crosses are from Nissen et al (2002) whose sample includes main sequence and subgiant stars. Linear fits to the thick disk and halo stars (solid line) and thin disk (dashed line) relations of Ramirez, Allende Prieto & Lambert (2007) are shown. The arrow indicates the probable magnitude of 1D to 3D model corrections required for the Cayrel et al (2004) and the UMi [O/Fe] values.

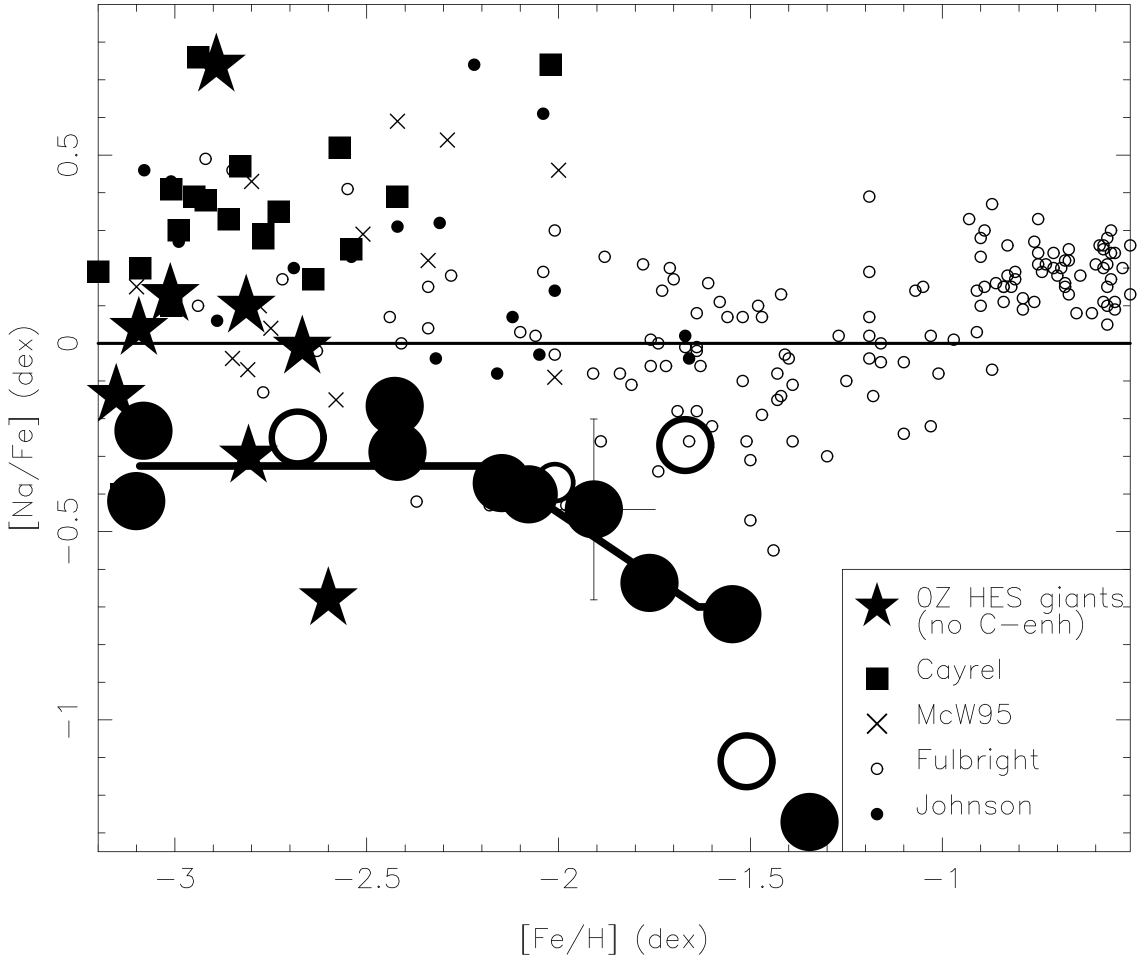

Fig. 5.— [Na/Fe] vs [Fe/H] for UMi stars. Stars from our HIRES sample (large filled circles) are combined with those from Sadakane et al. (2004) (large open circles). Smaller open circles denote the somewhat less accurate abundances from Shetrone, Côté & Sargent (2001). These symbols are used for the rest of the figures in this paper. Typical uncertainties are shown for one star. The symbol key for other sources is shown on the figure. The thick line indicates the fit of the toy model described in §5.1 (see also Table 6) to the UMi data with COS171 excluded.

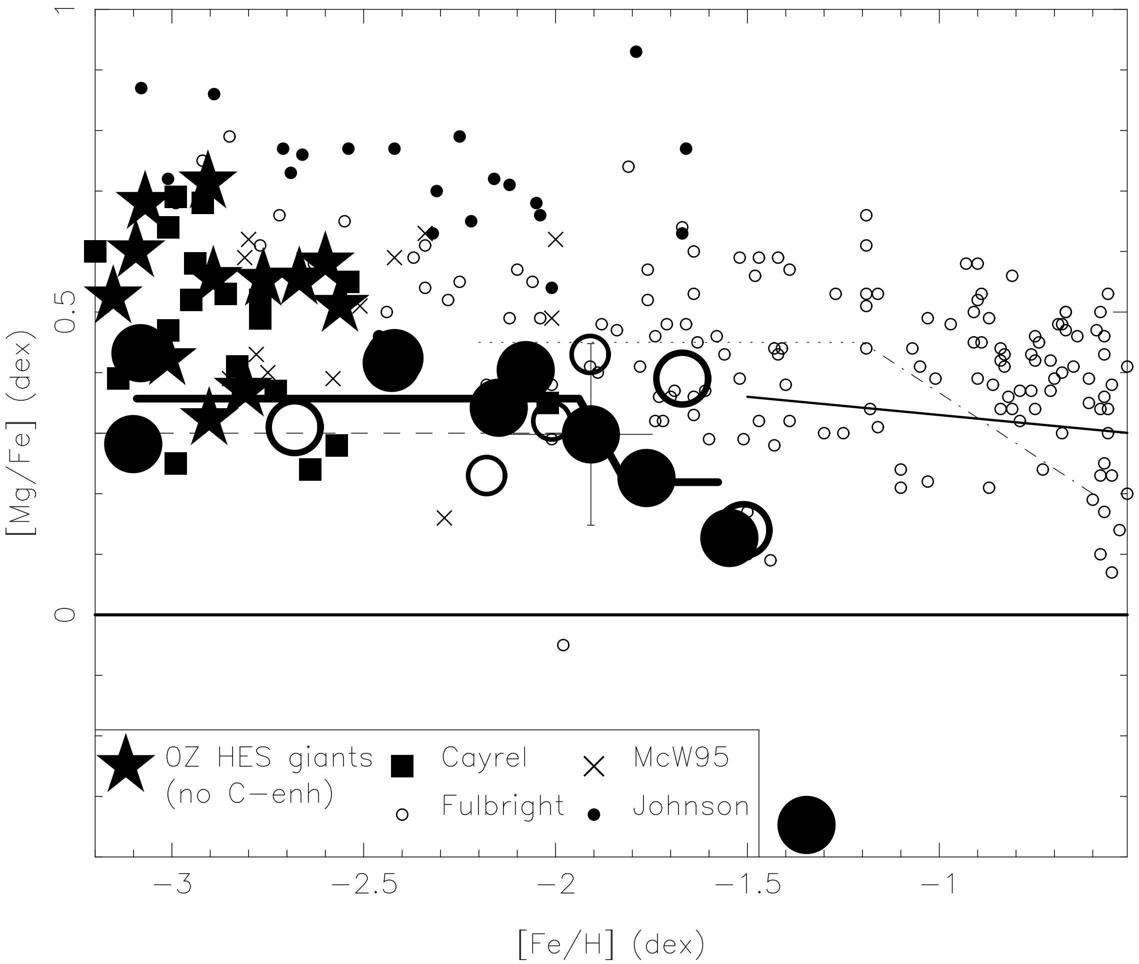

Fig. 6.— [Mg/Fe] vs [Fe/H] for the UMi giants. See Fig. 5 for details regarding the symbols for the UMi stars and uncertainties. The symbol key for sources of data for Galactic halo field stars is shown on the figure. Note that 0.15 dex has been added to the [Mg/Fe] values from Cayrel et al (2004); see the text for details. The thick line indicates the fit of the toy model described in §5.1 (see also Table 6) to the UMi data with COS171 excluded. The solid line is the mean relation for thick disk stars from Reddy, Lambert & Allende Prieto (2006). The dotted line is the mean relation for inner halo stars from Roederer (2008), while his outer halo mean is shown as the dashed line.

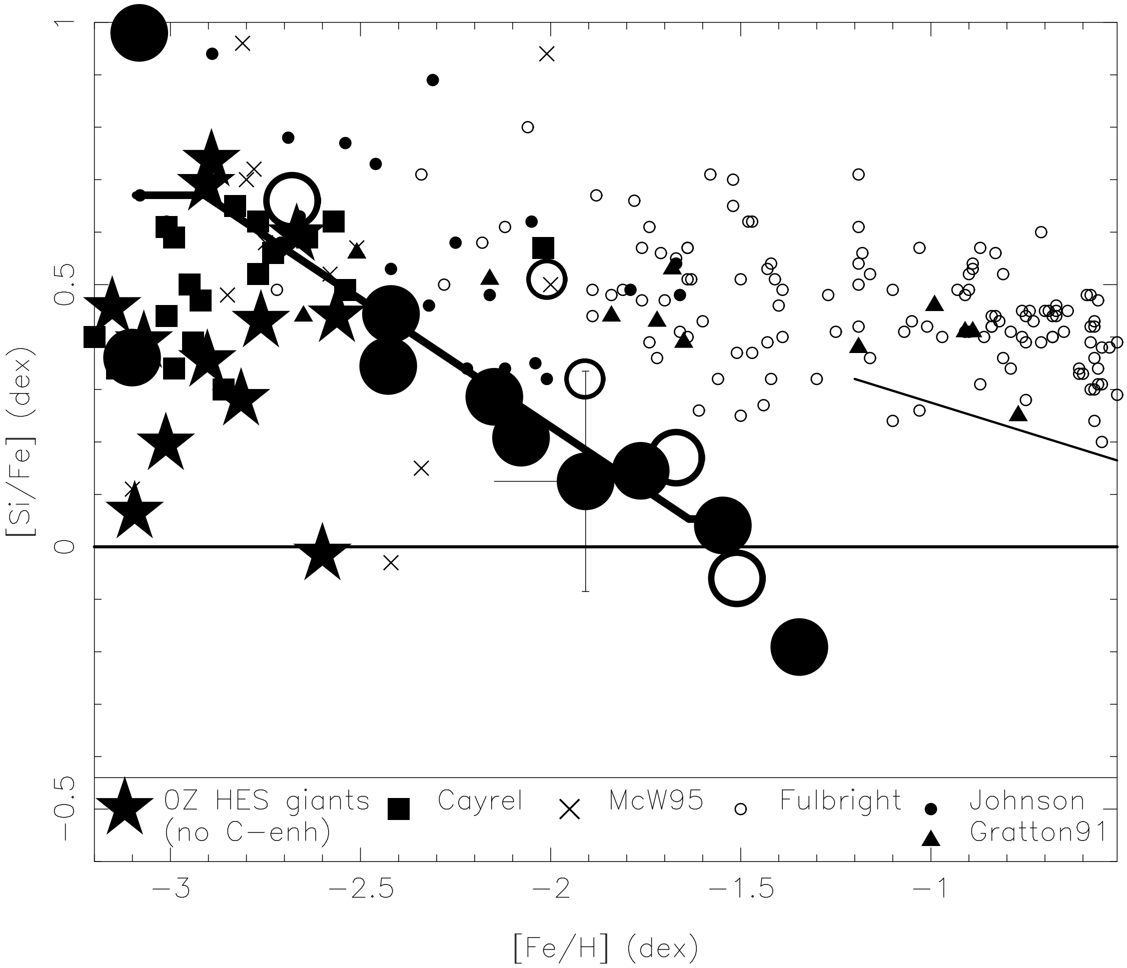

Fig. 7.— [Si/Fe] vs [Fe/H] for UMi stars. See Fig. 5 for details regarding the symbols for the UMi stars and uncertainties. The symbol key for sources of data for Galactic halo field stars is shown on the figure. The thick line indicates the fit of the toy model described in §5.1 (see also Table 6) to the UMi data. The solid line is the mean relation for thick disk stars from Reddy, Lambert & Allende Prieto (2006).

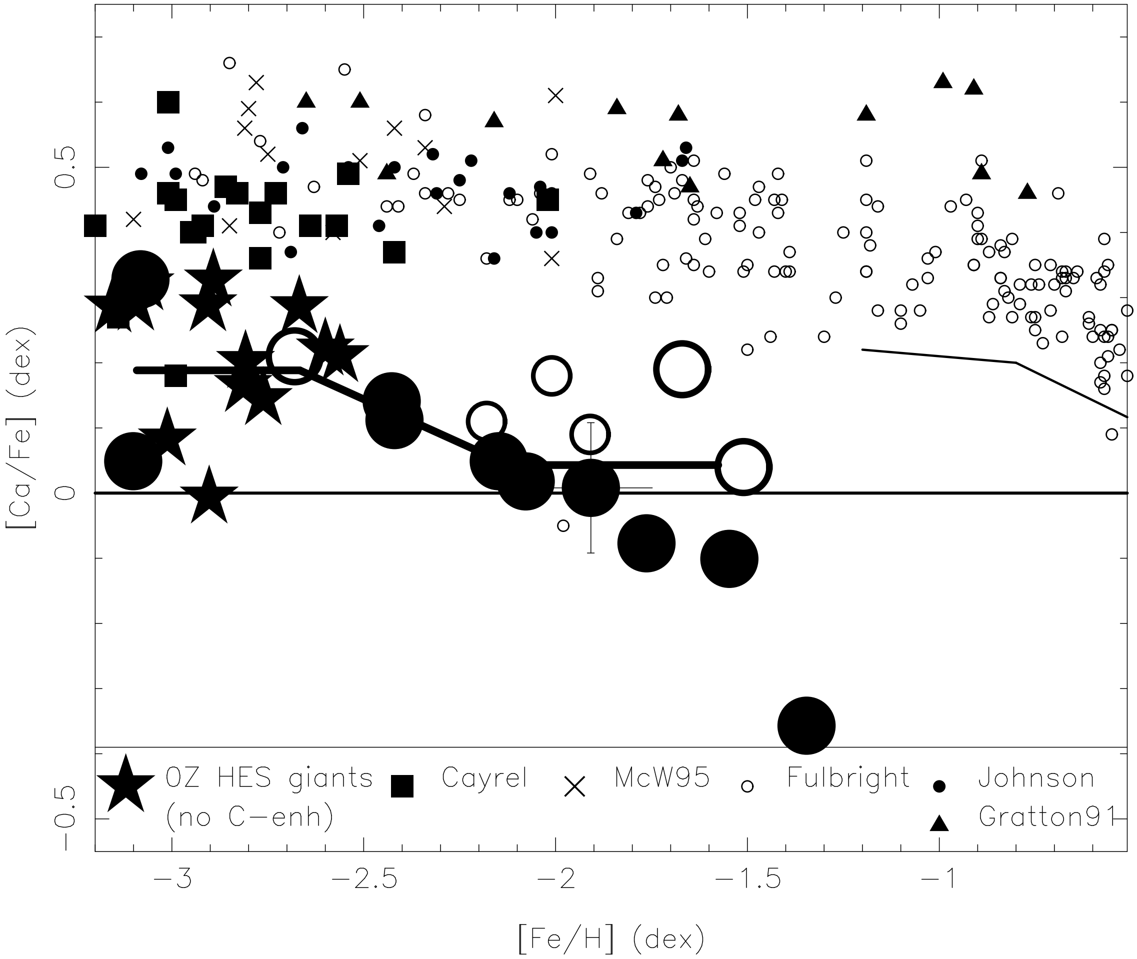

Fig. 8.— [Ca/Fe] vs [Fe/H] for UMi stars. See Fig. 5 for details regarding the symbols for the UMi stars and uncertainties. The symbol key for sources of data for Galactic halo field stars is shown on the figure. The thick line indicates the fit of the toy model described in §5.1 (see also Table 6) to the UMi data data with COS171 excluded. The solid line is the mean relation for thick disk stars from Reddy, Lambert & Allende Prieto (2006).

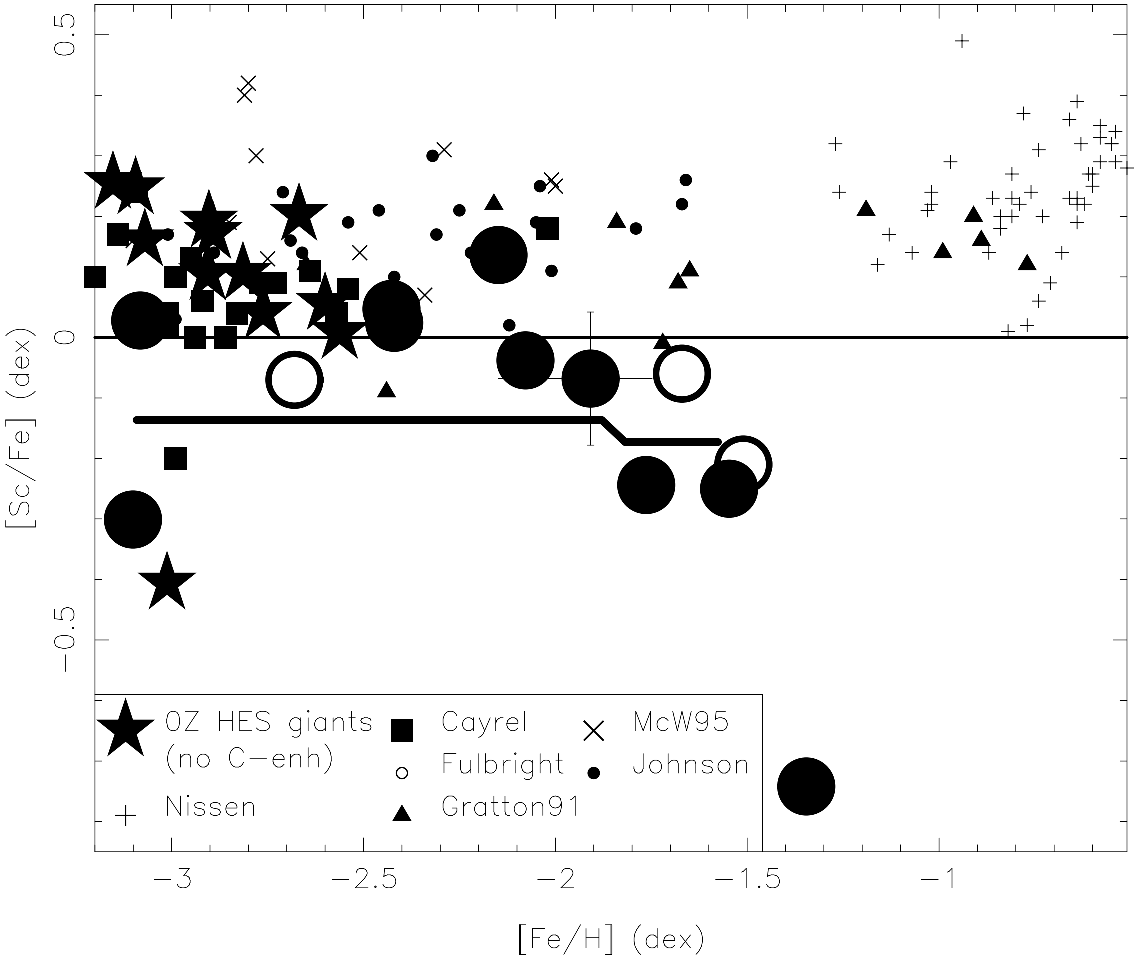

Fig. 9.— [Sc/Fe] vs [Fe/H] for UMi giants. See Fig. 5 for details regarding the symbols for the UMi stars and uncertainties. The thick line indicates the fit of the toy model described in §5.1 (see also Table 6) to the UMi data data with COS171 excluded. The symbol key for sources of data for Galactic halo field stars is shown on the figure.

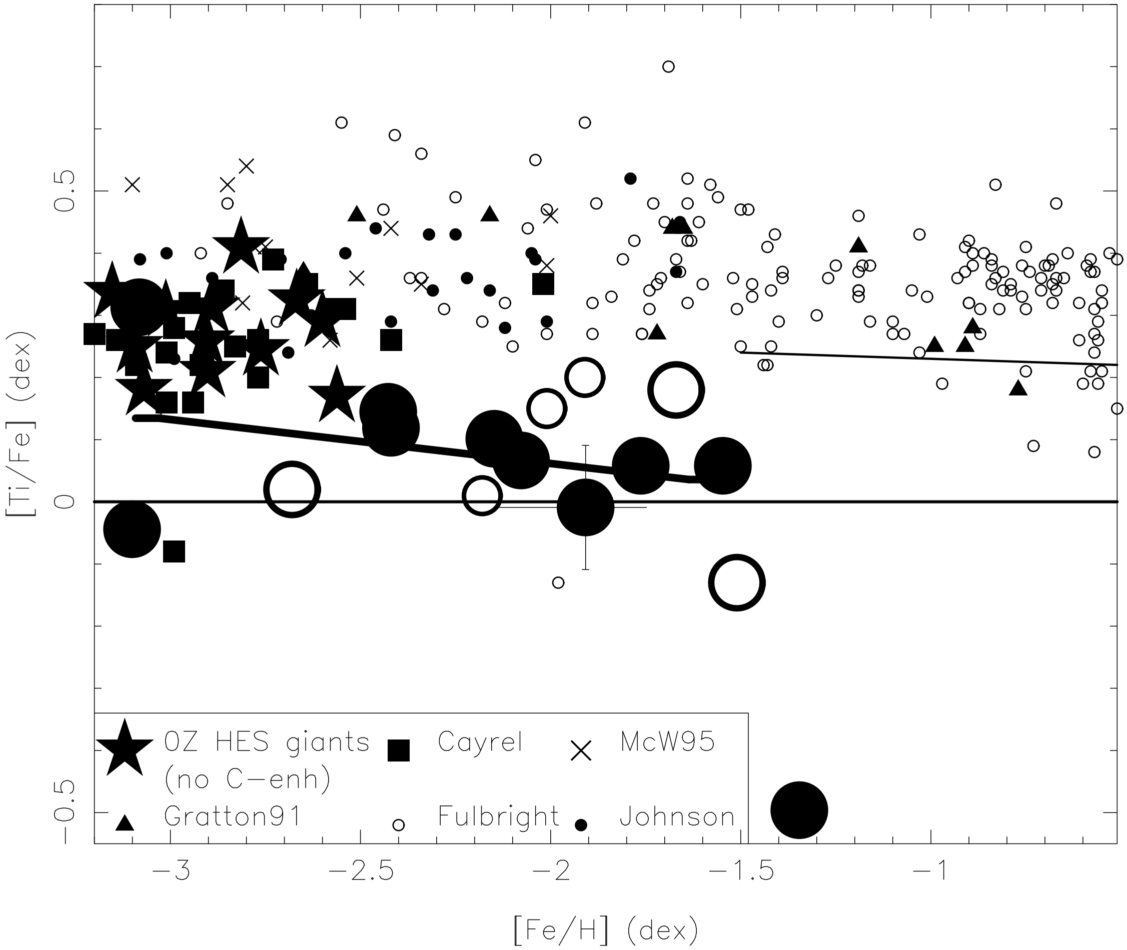

Fig. 10.— [Ti/Fe] vs [Fe/H] for UMi stars. [Ti12/Fe12], which relates ionized Ti to ionized Fe, and neutral Ti to Fe I, is shown for our UMi stars. See Fig. 5 for details regarding the symbols for the UMi stars and uncertainties. The symbol key for sources of data for Galactic halo field stars is shown on the figure. The thick line indicates the fit of the toy model described in §5.1 (see also Table 6) to the UMi data with COS171 excluded. The solid line denotes the mean relation for the thick disk stars from Reddy, Lambert & Allende Prieto (2006).

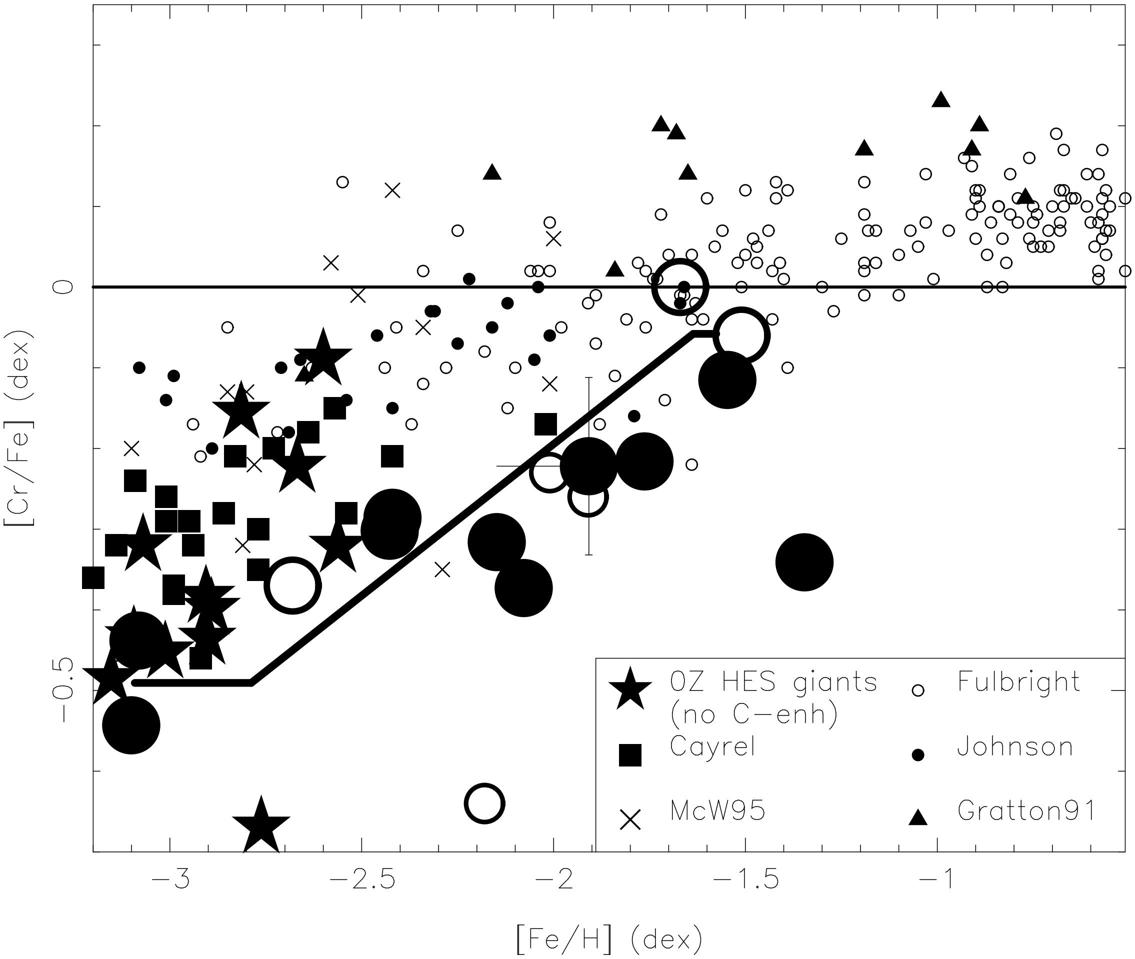

Fig. 11.— [Cr/Fe] vs [Fe/H] for UMi stars. See Fig. 5 for details regarding the symbols for the UMi stars and uncertainties. The symbol key for sources of data for Galactic halo field stars is shown on the figure. The thick line indicates the fit of the toy model described in §5.1 (see also Table 6) to the UMi data with COS171 excluded.

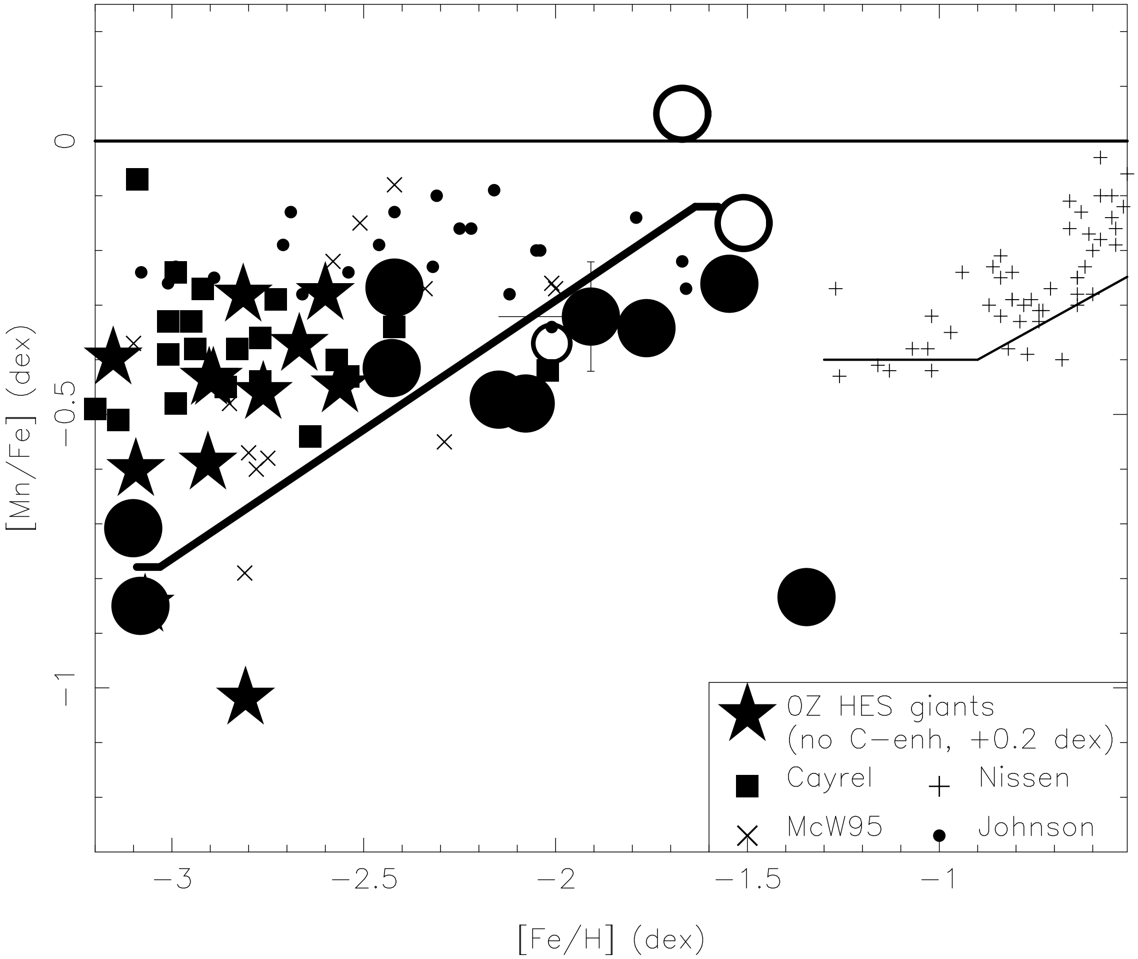

Fig. 12.— [Mn/Fe] vs. [Fe/H] for UMi giants. See Fig. 5 for details regarding the symbols for the UMi stars and uncertainties. The symbol key for sources of data for Galactic halo field stars is shown on the figure. The thick line indicates the fit of the toy model described in §5.1 (see also Table 6) to the UMi data with COS171 excluded. The solid line denotes the mean relation for the thick disk stars from Reddy, Lambert & Allende Prieto (2006).

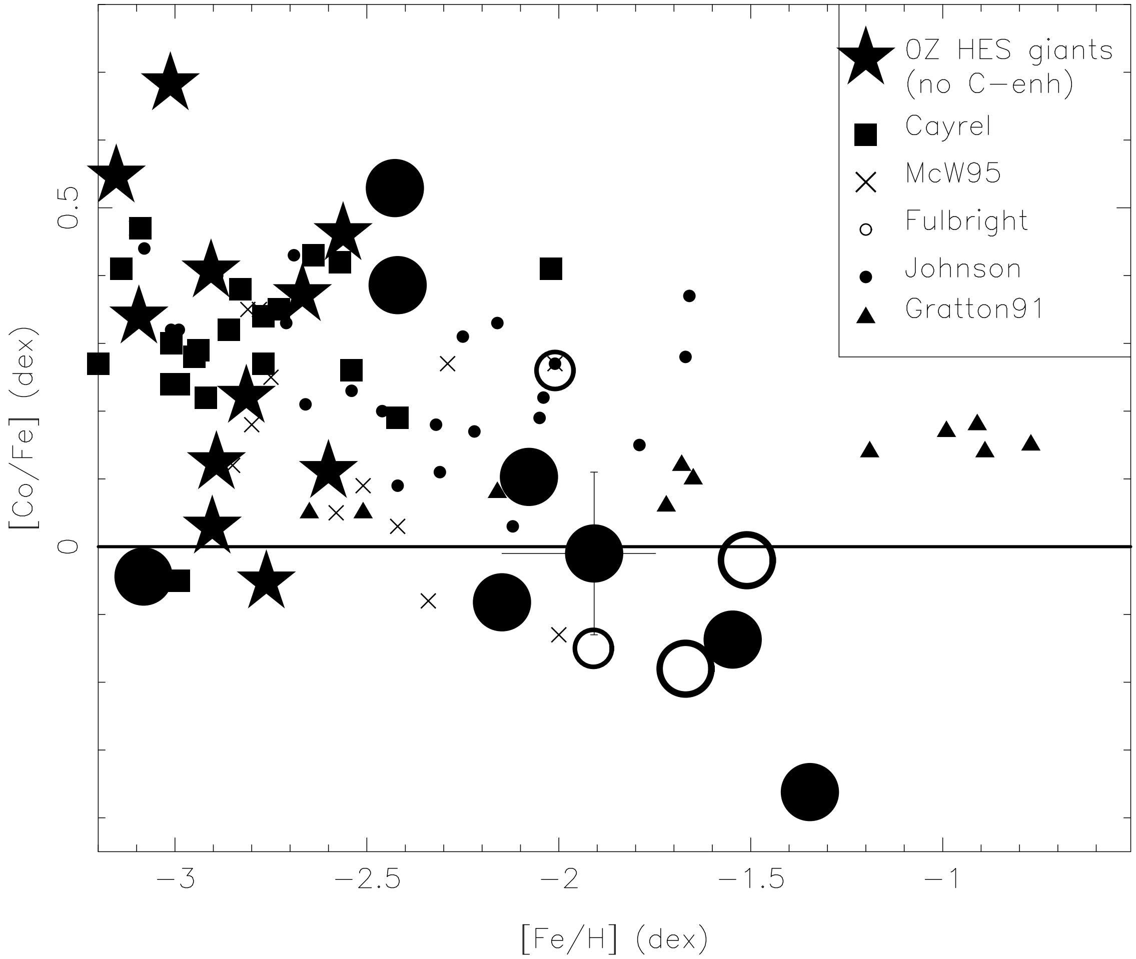

Fig. 13.— [Co/Fe] vs [Fe/H] for UMi stars. See Fig. 5 for details regarding the symbols for the UMi stars and uncertainties. The symbol key for sources of data for Galactic halo field stars is shown on the figure.

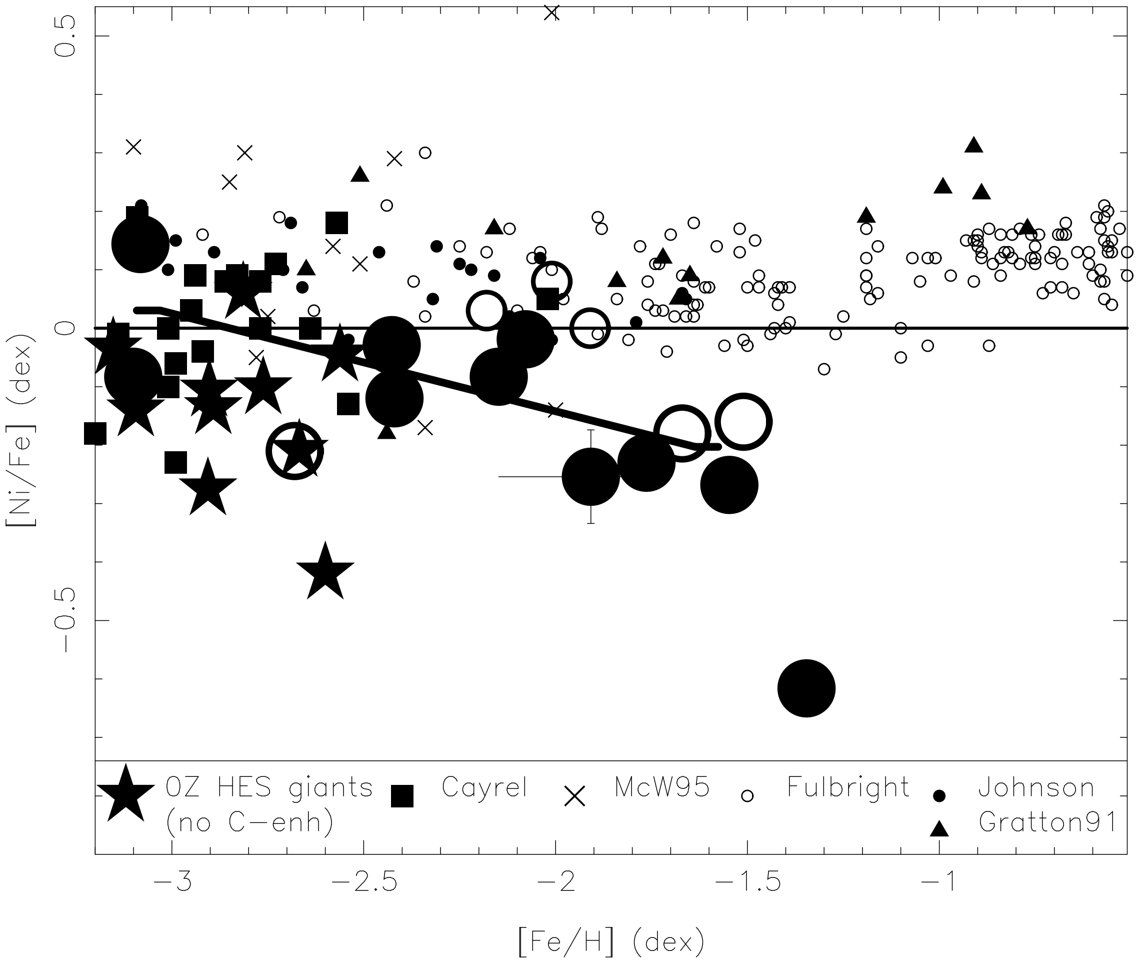

Fig. 14.— [Ni/Fe] vs [Fe/H] for UMi stars. See Fig. 5 for details regarding the symbols for the UMi stars and uncertainties. The symbol key for sources of data for Galactic halo field stars is shown on the figure. The thick line indicates the fit of the toy model described in §5.1 (see also Table 6) to the UMi data with COS171 excluded.

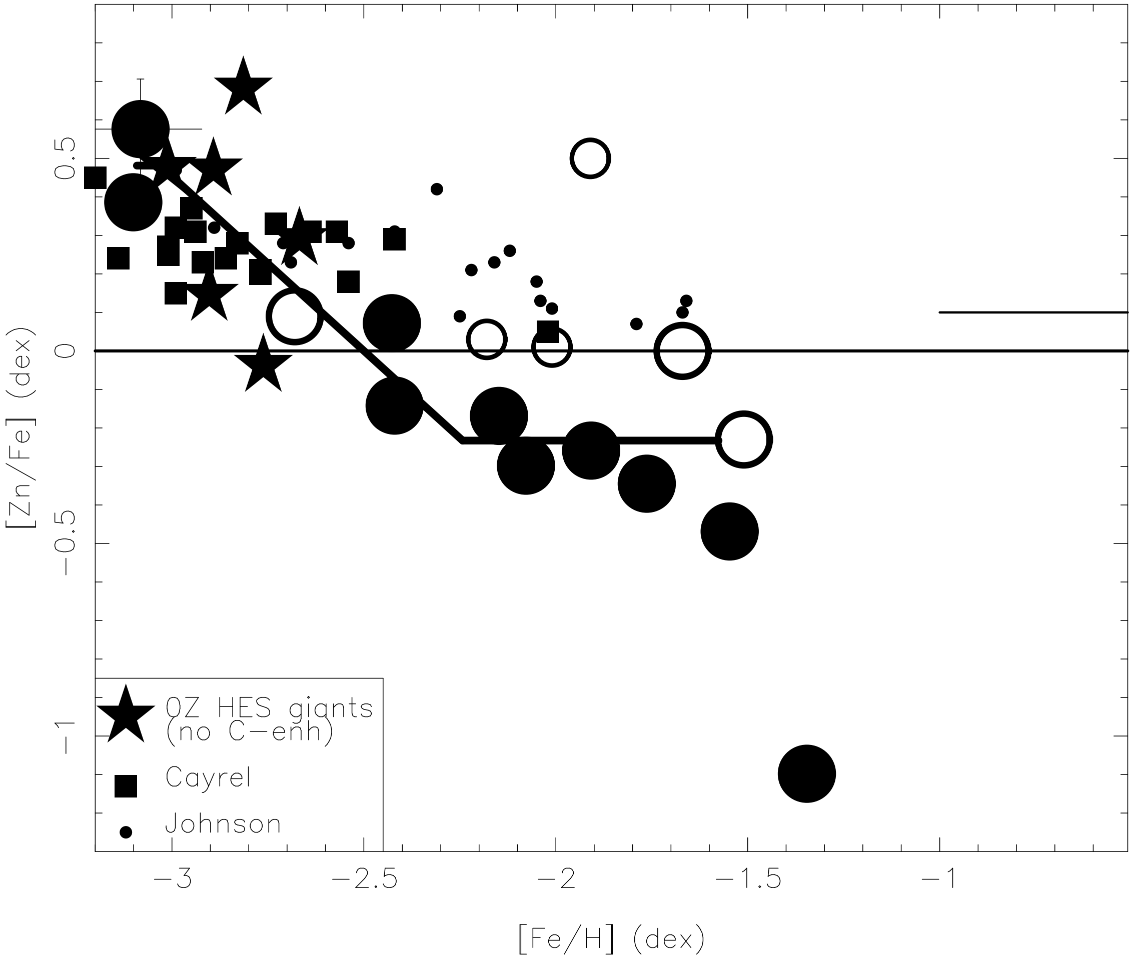

Fig. 15.— [Zn/Fe] vs [Fe/H] for UMi stars. See Fig. 5 for details regarding the symbols for the UMi stars and uncertainties. The symbol key for sources of data for Galactic halo field stars is shown on the figure. The thick line indicates the fit of the toy model described in §5.1 (see also Table 6) to the UMi data with COS171 excluded. The behavior of this abundance ratio in thick disk dwarfs from Reddy, Lambert & Allende Prieto (2006) is indicated as a solid line.

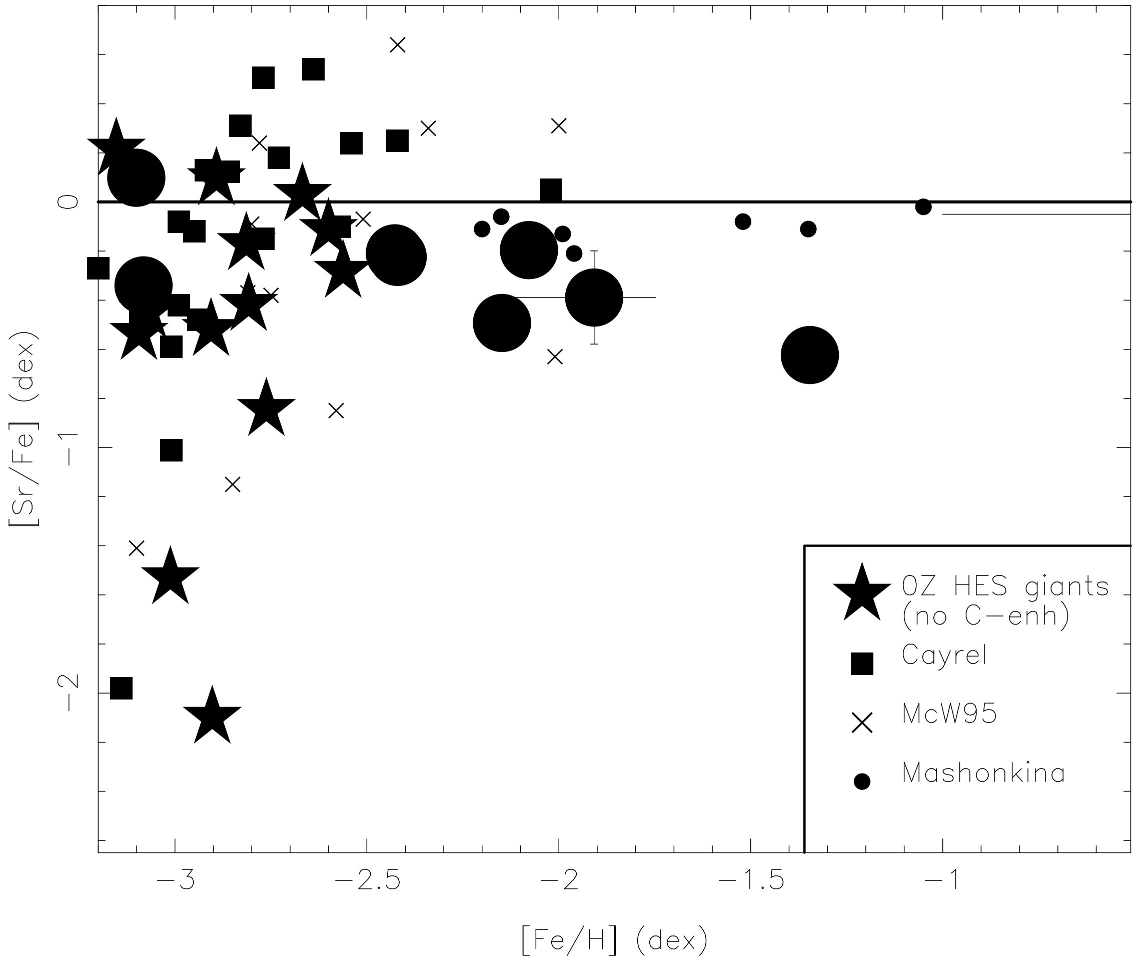

Fig. 16.— [Sr/Fe] vs [Fe/H] for UMi stars. See Fig. 5 for details regarding the symbols for the UMi stars and uncertainties. The First Stars data is from Francois et al (2007). The symbol key for sources of data for Galactic halo field stars is shown on the figure. The thick line indicates the fit of the toy model described in §5.1 (see also Table 6) to the UMi data. The behavior of this abundance ratio in thick disk dwarfs from Mashonkina & Gehren (2001) is shown as the solid line.

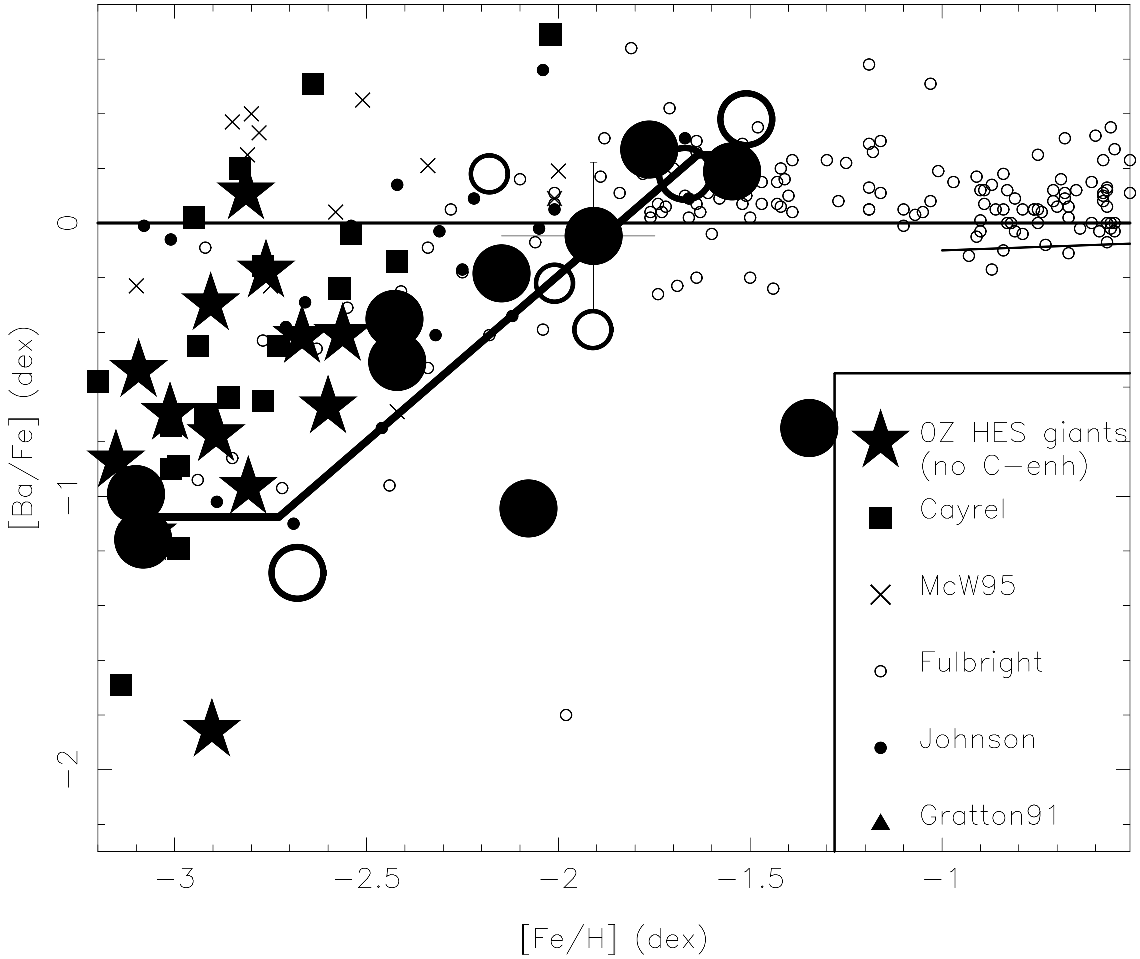

Fig. 17.— [Ba/Fe] vs [Fe/H] for UMi stars. See Fig. 5 for details regarding the symbols for the UMi stars and uncertainties. The First Stars data is from Francois et al (2007). The symbol key for sources of data for Galactic halo field stars is shown on the figure. The thick line indicates the fit of the toy model described in §5.1 (see also Table 6) to the UMi data with COS171 excluded.

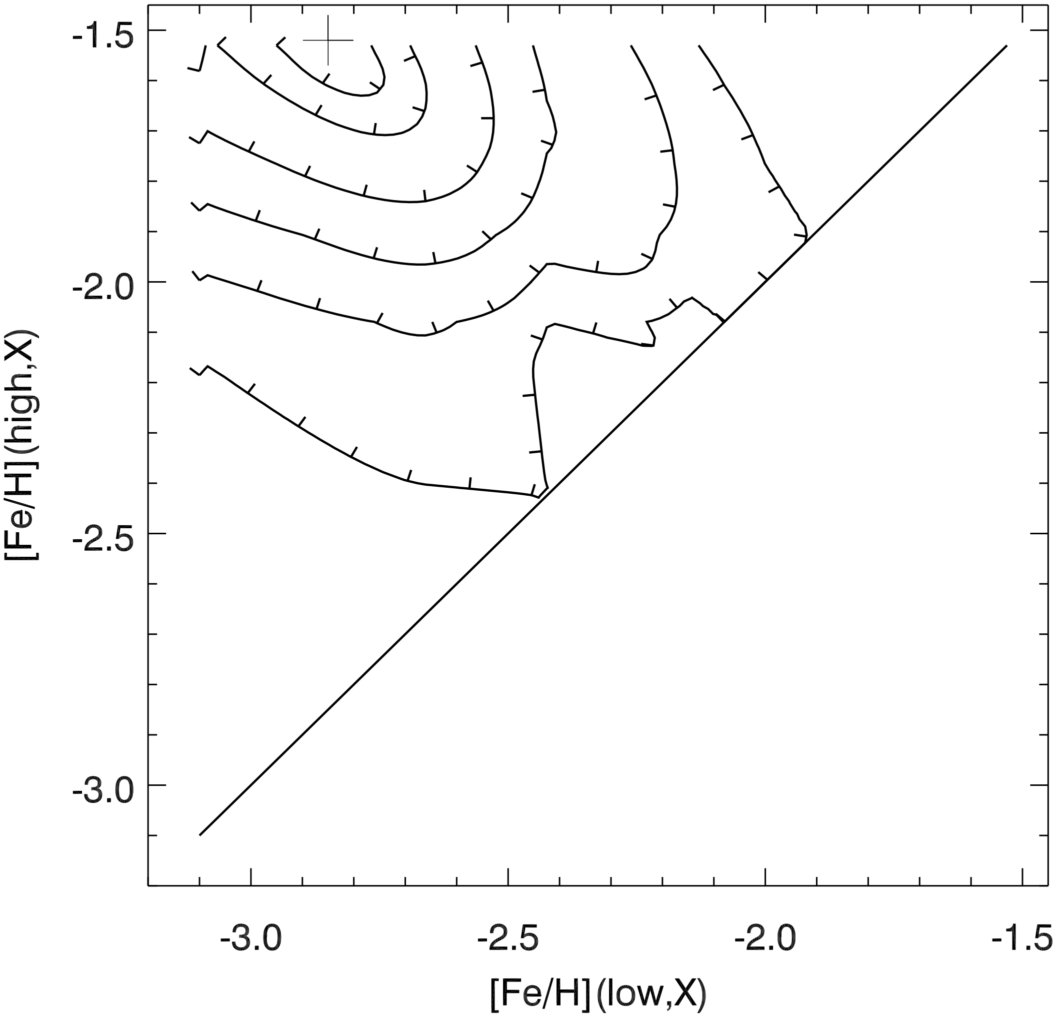

Fig. 18.— The contours of χ^2 used to estimate the uncertainties for [Fe/H](low,X) and [Fe/H](high,X) for the combined fit of the ratios of Si, Cr, Mn, Ni, and Ba with respect to Fe as a function of [Fe/H] in the UMi sample. The plus sign shows where the $\chi^2_{\rm min}$ value is reached. The contour lines are plotted around the minimum location for $(N-3)(\chi^2-\chi^2_{\rm min})/\chi^2_{\rm min}$ =1, 4, 16, 36, 64, and 100 respectively. The short, perpendicular ticks attached to each contour line show the"downhill" direction of the χ^2 "valley".

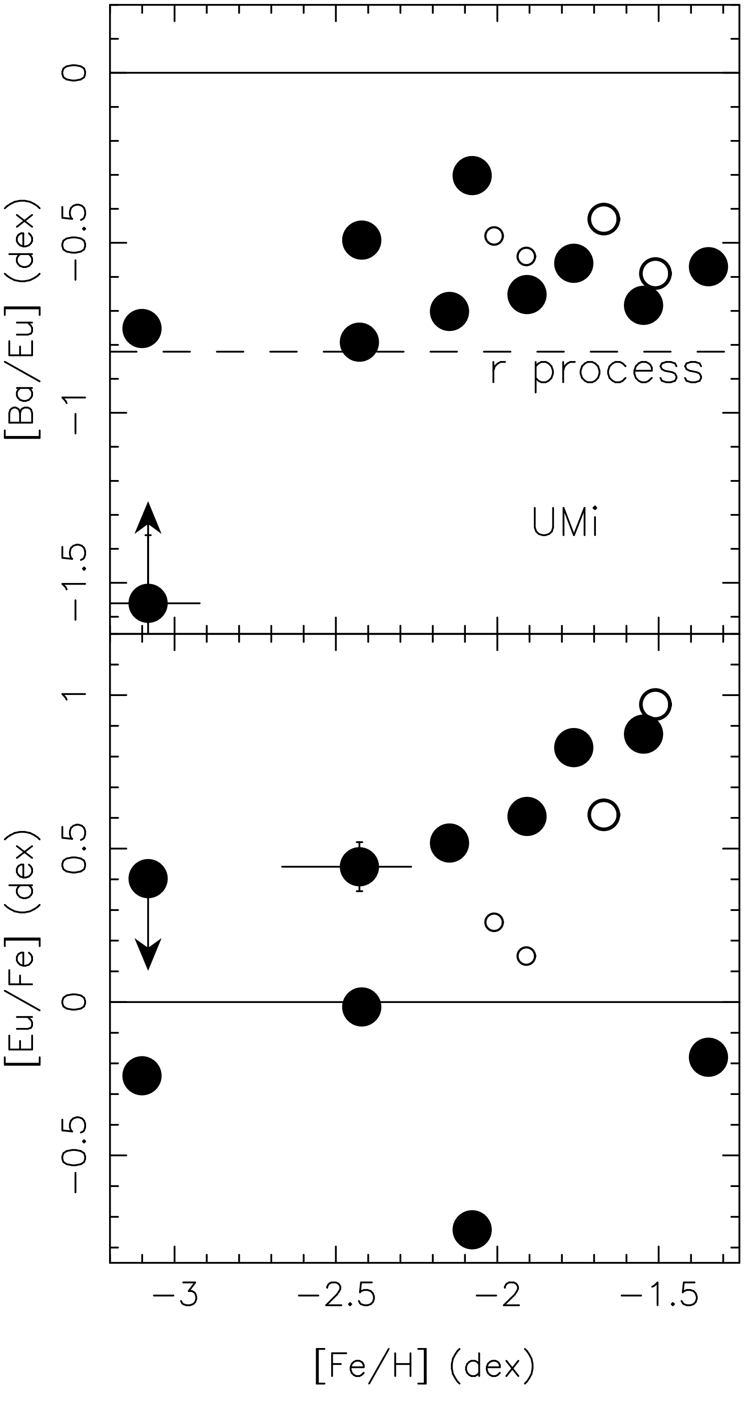

Fig. 19.— [Ba/Eu] (upper panel) and [Eu/Fe] (lower panel) vs [Fe/H] is shown for our UMi sample (large filled circles) and the two from each of Shetrone, Côté & Sargent (2001) (small open circles) and Sadakane et al. (2004) (intermediate open circles) with detected Eu. The Solar ratio is the solid horizontal line, while the dashed horizontal line is the *r*-process ratio from Simmerer et al (2004); the *s*-process ratio, +1.4 dex, is above the top of the figure. Typical uncertainties are shown for one UMi star.

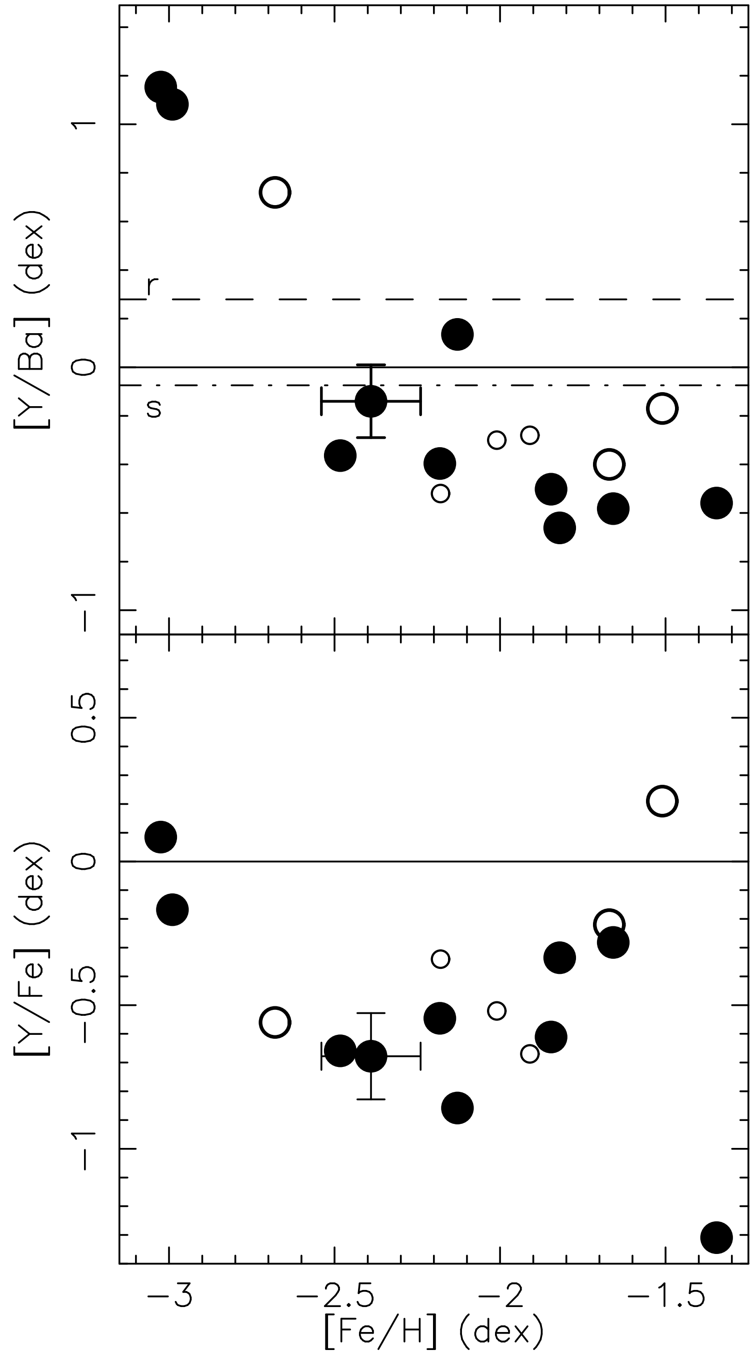

Fig. 20.— Upper panel: [Ba/Y] is shown as a function of [Fe/H] for our UMi sample. The symbols are those of Fig. 19. The Solar ratio is the lower solid horizontal line. The pure *s* and pure *r*-process ratios for the Sun from Simmerer et al (2004) are indicated. A typical error bar is shown for one star. Lower panel: [Y/Fe] vs [Fe/H] for the UMi sample.

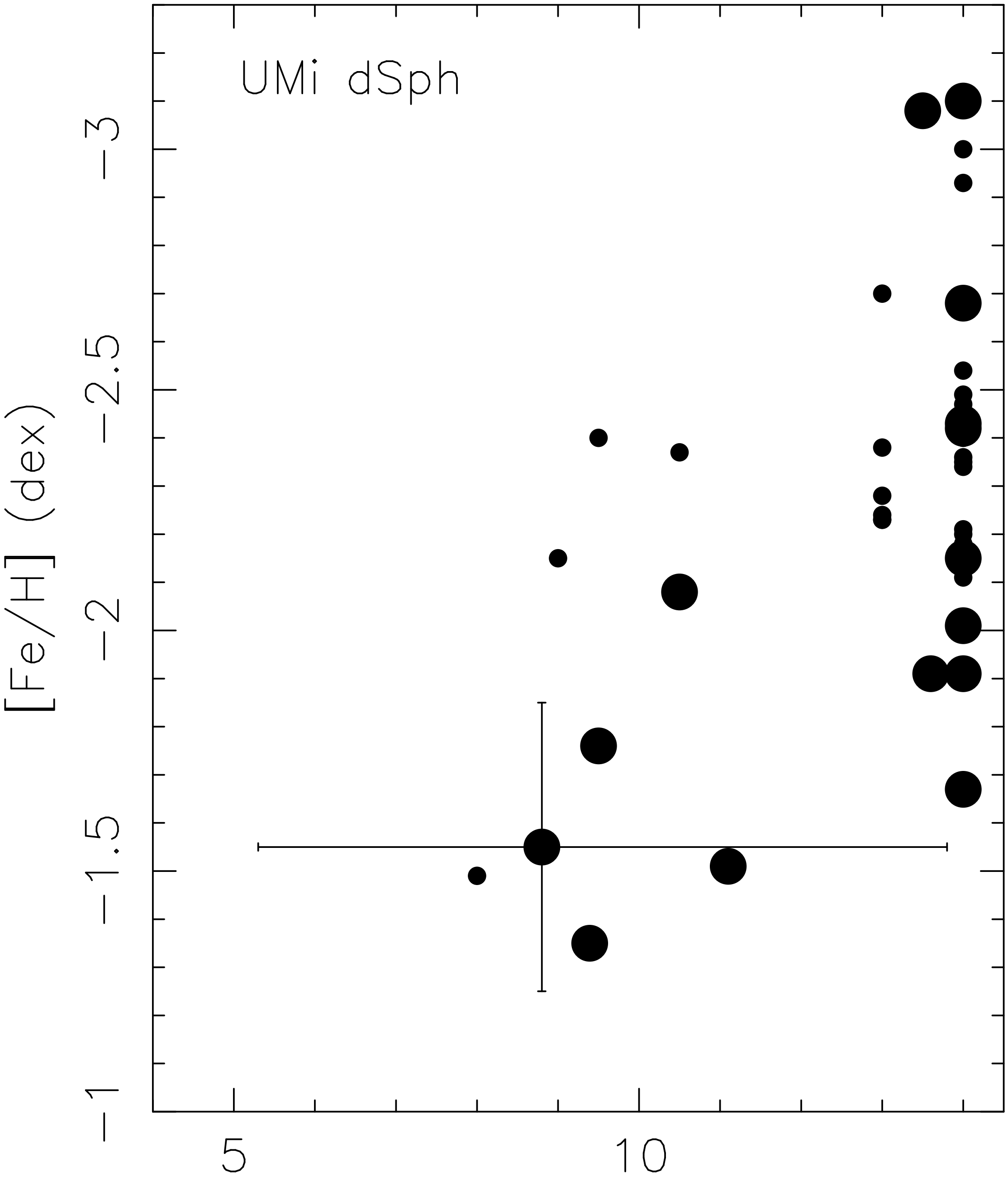

Fig. 21.— The age of each giant with $M_i < -2.0$ mag known to be a member of UMi from Table 3.6 of Winnick (2003) is shown as a function of [Fe/H]. The Dartmouth isochrones (Dotter *et al.* 2008) were used with [Fe/H] from high resolution spectra or values derived from her near-IR Ca triplet measurements. Typical error bars are shown for a single star.

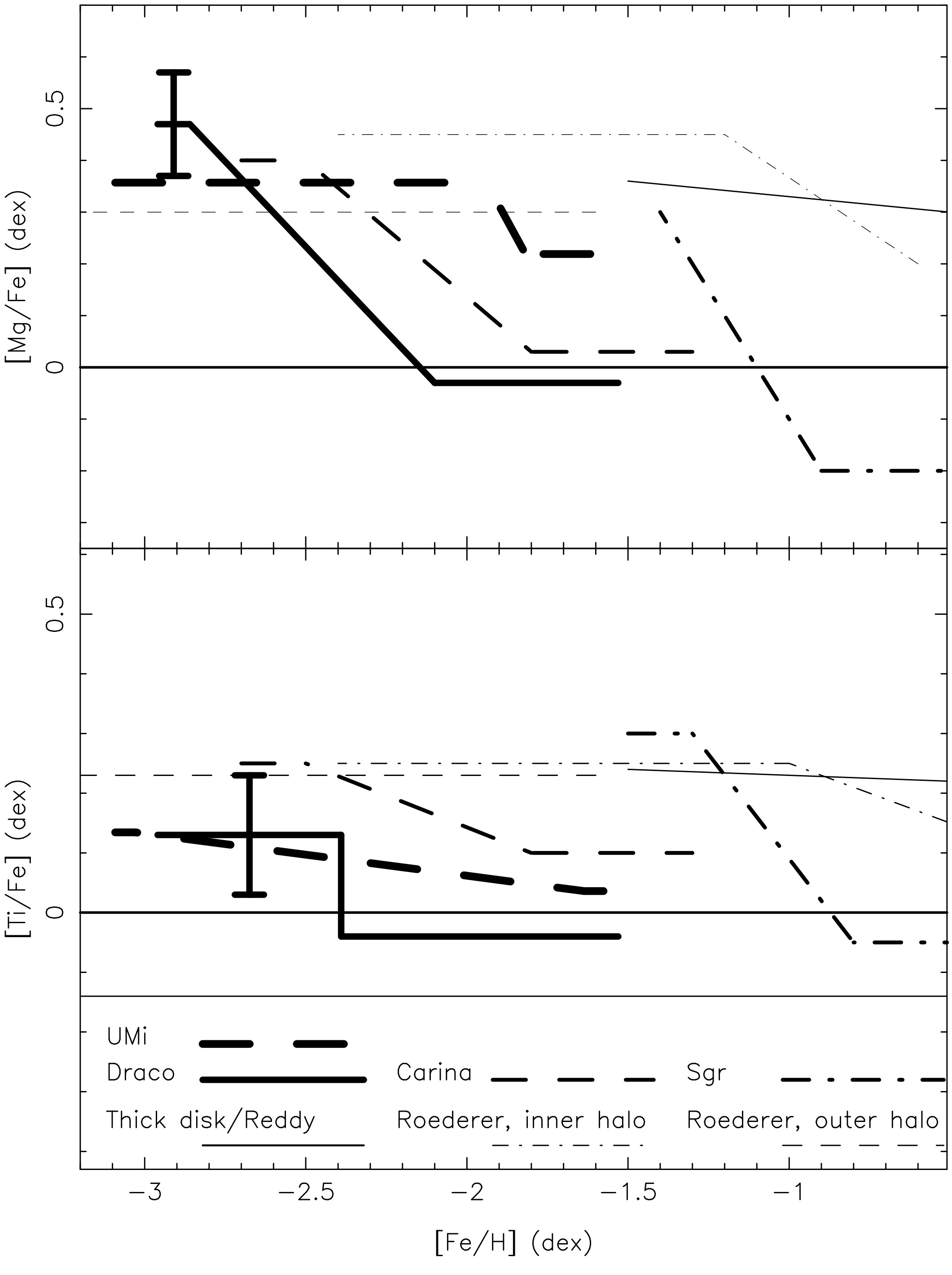

Fig. 22.— The toy model fit for [Mg/Fe] vs [Fe/H] (top panel) and for [Ti/Fe] (bottom panel) for the sample of 14 giants in each of the UMi and Draco dSph galaxies is shown together with that for the Sgr (Monaco et al 2005; Sbordone et al 2007) and Carina (Koch et al 2008a) dSph galaxies. Fits for Galactic components to data from Roederer (2008) and from Reddy, Lambert & Allende Prieto (2006) are shown as well. Typical errors in abundance ratios for the average of two stars are shown.